การปลูกและการหาลักษณะเฉพาะของฟิล์มบางคอปเปอร์อินเดียมไดซิลิไนด์แบบเอพิแทกซี
คุณภาพสูงบนแผ่นรองรับแกลเลียมอาร์เซไนด์

นายบัญชา อธิเบญญากุล

GROWTH AND CHARACTERIZATION OF HIGH QUALITY CuInSe$_2$
EPITAXIAL THIN FILMS ON GaAs SUBSTRATES

Mr. Bancha Arthibenyakul

A Dissertation Submitted in Partial Fulfillment of the Requirements

for the Degree of Doctor of Philosophy Program in Physics

Department of Physics

Faculty of Science

Chulalongkorn University

Academic year 2010

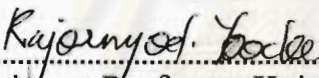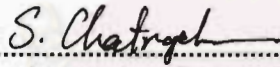|	
Thesis Title	GROWTH AND CHARACTERIZATION OF HIGH QUALITY CuInSe$_2$ EPITAXIAL THIN FILMS ON GaAs SUBSTRATES
By	Mr. Bancha Arthibenyakul
Field of Study	Physics
Thesis Advisor	Assistant Professor Sojiphong Chatraphorn, Ph.D.
Thesis Co-Advisor	Chanwit Chityuttakan, Ph.D.

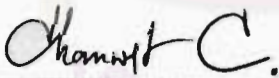Accepted by the Faculty of Science, Chulalongkorn University in Partial Fulfillment of the Requirements for the Doctoral Degree
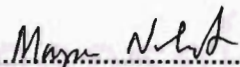
....Dean of the Faculty of Science
(Professor Supot Hannongbua, Dr.rer.nat.)
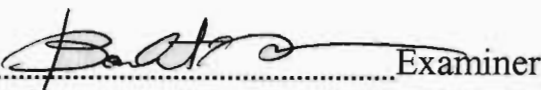
THESIS COMMITTEE
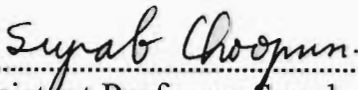
.................................Chairman
(Assistant Professor Kajornyod Yoodee, Ph.D.)

.................................Thesis Advisor
(Assistant Professor Sojiphong Chatraphorn, Ph.D.)

.................................Thesis Co-Advisor
(Chanwit Chityuttakan, Ph.D.)

.................................Examiner
(Associate Professor Mayuree Natenapit, Ph.D.)
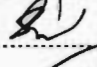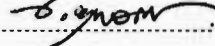
.................................Examiner
(Assistant Professor Boonchoat Paosawatyanyong, Ph.D.)

.................................External Examiner
(Assistant Professor Supab Choopun, Ph.D.)

นายบัญชา อธิเบญญากุล : การปลูกและการหาลักษณะเฉพาะของฟิล์มบางคอปเปอร์อินเดียม
ไดซิลิไนด์แบบเอพิแทกซีคุณภาพสูงบนแผ่นรองรับแกลเลียมอาร์เซไนด์. (GROWTH AND
CHARACTERIZATION OF HIGH QUALITY CuInSe₂ EPITAXIAL THIN
FILMS ON GaAs SUBSTRATES) อ. ที่ปรึกษาวิทยานิพนธ์หลัก : ผศ. ดร.โศจิพงศ์
ฉัตราภรณ์, อ. ที่ปรึกษาวิทยานิพนธ์ร่วม : อ. ดร.ชาญวิทย์ จิตยุทธการ, 111 หน้า.

สารประกอบคอปเปอร์อินเดียมไดซิลิไนด์และอัลลอยย์ของสารประกอบชนิดนี้เป็นวัสดุสำคัญ
ที่ได้ถูกใช้ทำเป็นชั้นดูดกลืนแสงในเซลล์สุริยะประสิทธิภาพสูง ความเข้าใจในคุณสมบัติทางกายภาพ
ตลอดทั้งกลไกการเตรียมสารข้างต้นมีความจำเป็นอย่างยิ่งในการพัฒนาวัสดุนี้ นอกจากนี้
ความสามารถในการทำซ้ำได้ก็มีความจำเป็นเช่นกัน ดังนั้น การเตรียมฟิล์มบางแบบเอพิแทกซีจึงได้
ถูกเลือกใช้ในงานนี้ โดยฟิล์มบางเอพิแทกซีคอปเปอร์อินเดียมไดซิลิไนด์ถูกเตรียมบนแผ่นรองรับ
แกลเลียมอาร์เซไนด์ (001) ใช้เทคนิคการเตรียมฟิล์มแบบเอพิแทกซีลำโมเลกุลในสัดส่วนของธาตุ
ต่าง ๆ กันและกระบวนการเตรียมที่แตกต่างกัน ซึ่งงานนี้ ชุดอุปกรณ์การเลี้ยวเบนอิเล็กตรอนพลังงาน
สูงแบบสะท้อนกลับและไพโรมิเตอร์ได้ถูกใช้เป็นเครื่องมือช่วยในการเตรียมฟิล์ม โดยผลการทดลอง
แสดงให้เห็นว่า ฟิล์มบางที่เตรียมแบบสัดส่วนคอปเปอร์มากและใกล้เคียงสัดส่วนธรรมชาติจะมี
รูปแบบการเลี้ยวเบนอิเล็กตรอนพลังงานสูงแบบสะท้อนกลับมีลักษณะเรียวยาวแตกต่างจากการเตรียม
แบบสัดส่วนอื่นที่มีลักษณะเป็นจุดเล็ก ๆ ซึ่งฟิล์มบางแบบคอปเปอร์มากเกิดจากการรวมตัวกันของ
สารประกอบคอปเปอร์อินเดียมไดซิลิไนด์และสารประกอบคอปเปอร์ซิลิไนด์ส่วนเกินที่สามารถถูก
กำจัดออกได้ด้วยสารละลายโพแทสเซียมไซยาไนด์และขึ้นกับอุณหภูมิแผ่นรองรับ โดยสารประกอบ
คอปเปอร์ซิลิไนด์เป็นสารประกอบสำคัญที่ทำให้ได้ฟิล์มคุณภาพสูงและเป็นสาเหตุหลักของการเกิด
ลักษณะลูกคลื่นและเม็ดสี่เหลี่ยมเล็ก ๆ บนพื้นผิวของฟิล์มบางที่เตรียมแบบสองช่วง ซึ่งสารประกอบ
นี้อยู่ทุกที่ในฟิล์มที่ถูกเตรียมและเป็นสาเหตุที่ทำให้เกิดชั้นรอยต่อคอปเปอร์แกลเลียมไดซิลิไนด์ และ
พบอีกว่าจะหายไปเมื่ออุณหภูมิแผ่นรองรับต่ำกว่า 430 องศาเซลเซียส จากงานนี้ทำให้สามารถนำเสนอ
แบบจำลองการเตรียมฟิล์มบางเอพิแทกซีแบบคอปเปอร์มากได้ โดยกลไกของกระบวนการเตรียมฟิล์ม
บางแบบสองช่วงที่วิวัฒน์มาจากฟิล์มแบบคอปเปอร์มากซึ่งแสดงตัวเป็นฟิล์มตั้งต้นคุณภาพสูง
สารประกอบคอปเปอร์ซิลิไนด์ส่วนเกินจะรวมตัวกับอินเดียมแล้วเกิดเป็นสารประกอบคอปเปอร์
อินเดียมไดซิลิไนด์ และนอกจากนี้ กลไกการเตรียมฟิล์มบางแบบสองช่วงที่ถูกดัดแปลงสามารถช่วย
ปรับปรุงคุณภาพของฟิล์มได้ โดยทั้งนี้ ฟิล์มบางแบบเอพิแทกซีที่เตรียมภายใต้สัดส่วนคอปเปอร์มาก
แสดงลักษณะของโครงผลึกที่มีคุณภาพสูง ในขณะที่ฟิล์มที่ทำการเตรียมในสัดส่วนอื่น ๆ แสดงให้เห็น
ถึงความบกพร่องในโครงผลึก

ภาควิชา ฟิสิกส์   ลายมือชื่อนิสิต

สาขาวิชา ฟิสิกส์   ลายมือชื่อ อ.ที่ปรึกษาวิทยานิพนธ์หลัก

ปีการศึกษา 2553   ลายมือชื่อ อ.ที่ปรึกษาวิทยานิพนธ์ร่วม

4672313023   : MAJOR PHYSICS

BANCHA ARTHIBENYAKUL : GROWTH AND CHARACTERIZATION OF HIGH QUALITY CuInSe$_2$ EPITAXIAL THIN FILMS ON GaAs SUBSTRATES. THESIS ADVISOR : ASST. PROF. SOJIPHONG CHATRAPHORN, Ph.D., THESIS CO-ADVISOR : CHANWIT CHITYUTTAKAN, Ph.D., 111 pp.

CuInSe$_2$ (CIS) and its alloys are the important materials that have been used as an absorber layer in high efficiency thin film solar cells. The understanding in its physical properties and growth mechanism are very essential for material improvement and the reproducibility is necessary in this study. The epitaxial growth is thus chosen for this work. The CIS epitaxial films are grown on GaAs (001) substrates by molecular beam epitaxy technique in various compositions and growth processes. Reflection high energy electron diffraction (RHEED) and pyrometer signals are applied as the *in-situ* monitoring tools in this growth. The results show that the Cu-rich and near stoichiometric films display the streaky RHEED patterns unlike the Cu-poor films. The Cu-rich films are the combination phases between the CIS compounds and the excess Cu-Se phase that can be removed by KCN aqueous solution and is dependent upon the substrate temperature. The best phase of Cu-Se that plays the important role in the high quality films is the Cu$_{2-x}$Se which is the main cause of the undulation structure and rectangular-shape protrusions in the two-stage films. The excess Cu$_{2-x}$Se can reside everywhere in the growing films and results in the presence of CuGaSe$_2$ interface layer that disappears when the substrate temperature is below 430°C. The growth model of the Cu-rich CIS epitaxial films can be proposed. The mechanism of the two-stage growth process that is evolved from the Cu-rich films which demonstrates the high quality precursor is the incorporation of In and the excess Cu-Se compounds. The mechanism of the proposed modified two-stage can enhance the structural quality of the films. The epitaxial films grown under the Cu-rich conditions present the high crystallinity whereas the other conditions reveal the many defect complexes.

Department : Physics   Student's Signature _____

Field of Study : Physics   Advisor's Signature _____

Academic Year : 2010   Co-Advisor's Signature _____

Acknowledgments

Contents

List of Tables

List of Figures

Chapter I

Introduction

1.1 Overview

At presence, the researches promoting renewable energy resources based on photovoltaic (PV) solar energy have received much more attention. The research and development efforts have been shifted gradually toward two other polycrystalline thin film materials: copper indium di-selenide ($CuInSe_2$) and cadmium telluride (CdTe) based solar cells [1]. $CuInSe_2$ (CIS) and its alloying compound e.g., $CuIn_{1-x}Ga_xSe_2$ (CIGS) have attracted considerable interest for thin film photovoltaic devices. The CIGS acts as an absorber with highest absorption coefficient compared to that of other PV materials as shown in Fig. 1.1. A band gap energy of about 1.0 to 1.7 eV (at 300K) can be adjusted by varying gallium content from 0% to 100%, which makes it possible to achieve high conversion efficiency in devices. The best CIGS thin film solar cell has reached a confirmed conversion efficiency of about 20% [2]. The CIS solar cells started with the work done at Bell laboratories in the early 1970s while its synthesis and characterization were first reported by Hahn in 1953 [3]. The single crystal growth was proposed but it was difficult to grow high quality crystals. Boeing demonstrated the thin films growth method that began to receive a lot of attention by using evaporation from separated elemental sources [4]. By this technique, the films with desired compositions and suitable electronic properties can be obtained. After that, CIS compounds were widely studied in various growth methods such as melt and metallic solution growth, molecular beam epitaxy (MBE), liquid phase epitaxy (LPE), halogen vapor phase epitaxy (VPE), hybrid sputtering and evaporation, metalorganic vapor phase epitaxy (MOVPE), chemical spray pyrolysis and etc. [5 – 11]. To improve the energy conversion efficiency, the understanding in fundamental properties of material and growth mechanism is essential. It is known that the crystallographic structure of CIS or CIGS for the best solar cells should be chalcopyrite structure. There are many growth processes and growth models proposed for growing polycrystalline CIS and CIGS of this structure. However, the polycrystalline forms are complicated to study the fundamental properties while the

bulk single crystal growth is hard to reproduce [12]. To solve this problem, the epitaxial growth is the way that can deposit the high quality films with high reproducibility.
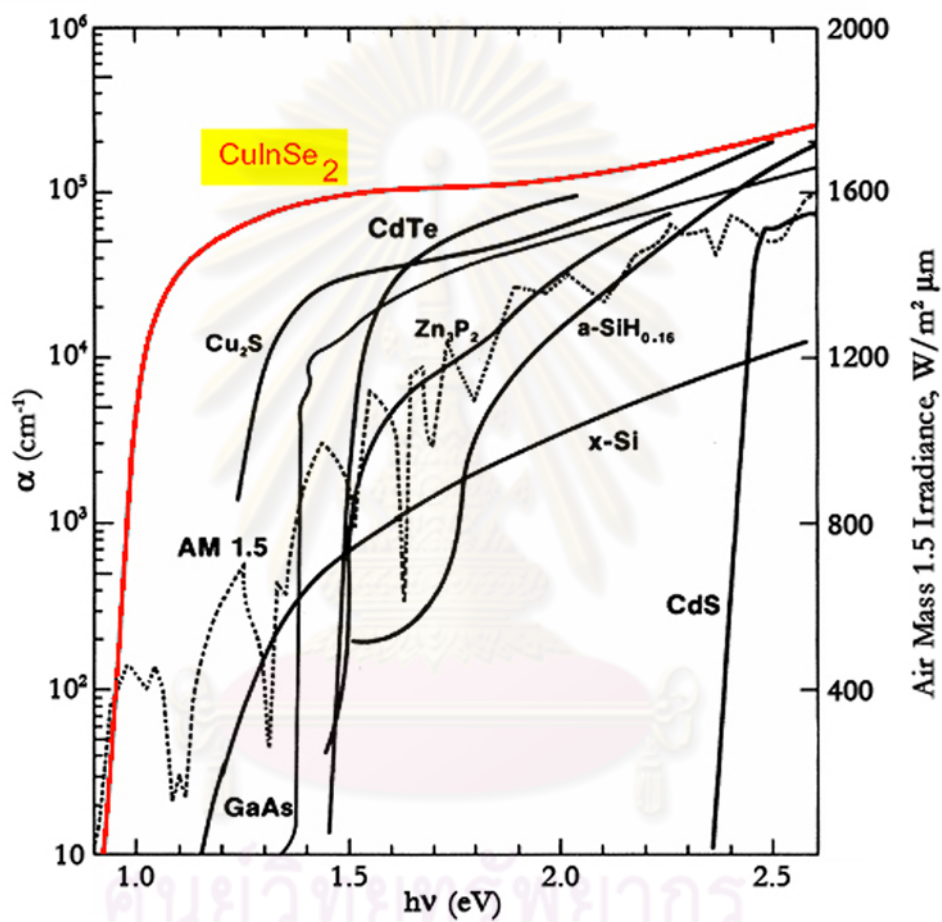
Figure 1.1: Absorption coefficient spectrum of various materials [13].

1.2 Literature Reviews

Since the CuInSe$_2$ epitaxial films can be grown by various techniques that each technique has different advantages. In 1986, Schumann *et al.* [14] grew CIS epitaxial layers on different substrates by flash evaporation, LPE and MBE. They concluded that the substrate properties under constant growth condition affected the epitaxial growth, e.g. the kind of epitaxy, the temperature range of the epitaxial growth, the occurrence of polycrystalline parts and the presence of other phases. In addition, it had been suggested that a small deviation in the c/a-ratio from ideal value led to a smaller misfit which played an important role in epitaxial growth. The effect of composition [Cu]/[In] or y ratio of the epitaxial films and substrate temperature were investigated in 1994 - 1995 by Niki and his colleagues [15 – 18]. In their work, the CIS films with y = 0.81-1.81 were grown on (001)-oriented GaAs substrates by MBE at substrate temperatures of 350 - 550°C. MBE is a thermally non-equilibrium growth process under ultra-high vacuum (UHV). The grown films were characterized in composition of the films by electron probe micro-analysis (EPMA), crystallographic structure by X-ray diffraction (XRD), structural properties by transmission electron microscopy (TEM), electrical properties by Hall measurement and optical properties by photoluminescence (PL) spectroscopy. Furthermore, the *in-situ* reflection high energy electron diffraction (RHEED) was also employed for structural investigation during the growth. They had reported that MBE was a powerful tool for investigating the intrinsic defects in CIS and there were substantial difference in chemical nature for Cu-rich (y > 1) and Cu-poor (y < 1) films. The Cu-rich films were p-type semiconductor and showed the streaky RHEED patterns and sharp PL emission lines that suggested the high quality epitaxial films. On the other hand, the Cu-poor films were highly resistive and showed dominant broad and strong emission lines that suggested the defect complexes in the films. Moreover, they had summarized that the MBE growth parameters such as substrate temperature, suggesting dominant defects in CIS epitaxial films could be controlled by varying the growth conditions. Normally, the lattice mismatch between CIS films and GaAs substrate is about 2.2% that results in a large number of misfit dislocations. So, the pseudo-lattice-matched substrates were proposed in the CIS epitaxial growth for the lattice mismatch reduction in 1996 [19]. The results showed the narrower linewidth of

CIS (008) in comparison between the normal substrate and the pseudosubstrate. Besides, it indicated that the reduction in the misfit strain by using pseudosubstrate was made possible for the growth of high quality CIS epitaxial films which was verified by the strong free exciton emissions and the decrease in the intensity of the defect-related emission lines. In 1997, the high purity CIS heteroepitaxial layers were successfully grown by low-pressure MOVPE technique [20]. The samples showed the near-band-edge PL spectra that could be observed until the room temperature. The alternate-feeding physical vapor deposition (AF-PVD) was one choice of technique that could grow the high optical quality CIS epitaxial films which was presented by Chichibu *et al.* in 1998 [21]. The results demonstrated the importance of stabilized CIS solute and $Cu_{2-x}Se$ solvent concentrations to obtain the improved film quality. In addition, it was proposed the meltback of the substrate that because of the existence of liquid-phase $Cu_{2-x}Se$. The effect of $Cu_{2-x}Se$ phase in Cu-rich CIS epitaxial films was directly observed in 1998 and 1999 [22, 23]. It was concluded that $Cu_{2-x}Se$ in the Cu-rich CIS films was an important surface impurity which played an important role in strain relief so as to obtain high quality CIS epitaxial films. Migration-enhanced epitaxy (MEE) which was a variant of MBE had been successfully employed to grow the CIS epitaxial films in 2002 [24]. There were two essential features distinguished from the conventional MBE technique: (1) sequential rather than simultaneous exposure of the substrates to cationic and anionic fluxes and (2) a fluxless "relaxation" step between each exposure. In 2003, Rega *et al.* [9, 25] studied the growth parameters and structural properties of CIS epitaxial films that were grown by horizontal reactor MOVPE. They could grow the high quality CIS epitaxial films and presented that the optimum growth temperature at a reactor pressure of 50 mbar was 500°C. For higher temperatures, Ga diffusion occurred and huge pyramidal voids appeared in the $GaAs/CuInSe_2$ interface. In addition, some polycrystalline regions could be detected at lower temperatures. The effect of Cu-Se secondary phase on CIS epitaxial films was observed again by Yoon and his colleagues in 2005 [26]. They grew the CIS epitaxial films on GaAs (001) substrates with various composition ratios using MEE technique. The results showed that films grown under Cu-poor conditions were polycrystalline, whereas the films grown with a Cu-rich composition were epitaxial. Moreover, it was proposed that a Cu–Se phase presented during the growth of Cu-rich films enhanced the mobility of adatoms on the substrate surface which was the key that allowed the films to grow epitaxially over a critical thickness. The

sputtered Cu-poor CIS epitaxial films were demonstrated in 2006 [27] to study the fundamental material properties. The Cu-poor CIS films were synthesized on different orientations of GaAs substrates by a hybrid co-sputtering Cu/In and evaporation of Se. It was found that the obtained epitaxial films had similar properties as the polycrystalline films and showed good quality single crystal films. The interdiffusion between CIS films and GaAs substrate as well as characteristic stacking fault, twin, dislocation, faceted second phase and Kirkendall void structure were also observed.

1.3 Motivation and Scope of the Research

In the recent years, the high conversion efficiency CIGS-based thin film solar cells were achieved by a two-stage growth process while a new world record of conversion efficiency CIGS-based thin film solar cells were prepared the layer using a three-stage process with multi-source evaporation technique. The two-stage process is the basis for the three-stage process. For our CIS and CIGS films, the high efficiency of approximately 14% are grown by the two-stage process and approximately 16% by the three-stage process with the y ratios just about less than unity (~ 0.9). High efficiency cell has never been achieved using a single-stage process. In order to investigate what is going on in the crystal growth process of these chalcopyrite semiconductor materials, especially CIS, one need to grow them with high quality and high reproducibility. Since a single crystal of this material is quite difficult to grow with high reproducibility compared to its form of thin films, the epitaxial CIS (no gallium) films on GaAs (001) substrates by MBE technique using a single-stage process and a two-stage process are performed to observe its physical properties, e.g. surface morphology, optical response and crystal structure of the CIS epitaxial films. In the preliminary works, the CIS epitaxial thin films up to about 1.5 micron thick could be grown indicating that the survival of epitaxy (confirmed by RHEED pattern) which was very surprising despite the lattice mismatch of 2.2%. It is noted here that the pseudo-lattice-matched substrate was not used to grow the epitaxial thin films as in others' work. Thus, I am interested in trying to understand and explain the nature of the growth mechanism for this material. I proposed to grow the CIS epitaxial thin films by varying the ratios of Cu to In both in the single-stage and two-stage

processes. Finally, I will propose the growth model and a modified two-stage growth process that can be used to improve quality of the films.

1.4 Objective of the Work

The objectives of this research are:

o To grow CuInSe$_2$ epitaxial thin films on GaAs (001) substrates by MBE technique using in-situ monitoring systems and RHEED.

o To obtain key parameters and growth conditions in order to explain growth mechanisms of high quality CuInSe$_2$ epitaxial thin films on GaAs (001) by MBE technique.

o To determine physical properties of the obtained CuInSe$_2$ epitaxial thin films on GaAs (001).

1.5 Dissertation Outline

This dissertation is composed of five chapters. In Chapter I, I introduce the overview, motivation and scope of this research and the objectives of this work. In Chapter II, a literature survey is presented on the theoretical relevance of CuInSe$_2$ material, Cu-Se compounds and CuGaSe$_2$ material. The meaning of epitaxy and the fundamental principle of MBE system which is the main tool used to deposit the epitaxial films as well as the apparatuses equipped in the MBE system are described. In Chapter III, the experimental procedures of sample preparation comprising the substrate preparing procedure, the calibration of the molecular constituents and the films composition and the deposition technique of epitaxial films, for example, single-stage process, two-stage process and etc., are discussed in details. The details of characterization technique used in this work for physical investigation are mentioned in fundamental principle. In Chapter IV, the experimental results of each deposition technique are shown and discussed. In the first section, the results of near stoichiometric films and Cu-rich films grown by single-stage process are investigated for their crystallographic structure, surface morphology and optical responses using XRD, AFM, UV-VIS-NIR spectrophotometer and PL measurement, respectively. The effect of substrate temperature is also introduced and the growth model of Cu-rich

films that are the precursor for two-stage process is proposed in this section. The characterization and growth mechanism of two-stage process are discussed in the following section. In the next section, the results and discussions of the newly proposed growth process are demonstrated and the summary of the growth is described in the last section. Finally, in Chapter V, the most significant results are summarized and the conclusions are drawn including the suggestions for the future work.

Chapter II

Theoretical background

This chapter begins with the background knowledge of the properties of the materials, especially CuInSe$_2$, Copper-selenide and CuGaSe$_2$ which can be found in the Cu-rich films are also introduced. The meaning and the category of the epitaxial films are defined in the next section. Finally, the details of molecular beam epitaxy and other accessories that used to prepare the sample in this work will be described at the end of this chapter.

2.1 Copper-indium-diselenide (CuInSe$_2$)

2.1.1 Crystallographic properties of CuInSe$_2$

CuInSe$_2$, or abbreviated calling as CIS, is one type of $A^{I}B^{III}C^{VI}_2$ ternary semiconductor which normally crystallizes in a chalcopyrite (CH) structure where A = Cu, B = In and C = Se. The CH structure is a superlattice of cubic zincblende (ZB) structure which can be systematically constructed starting from a face centered cubic structure. The ZB structure which has the space group symmetry $F\bar{4}3m$, consists of two interpenetrating face centered cubic lattices. The two sublattices are displaced by one quarter of a body diagonal line and each sublattice sites are occupied entirely by one type of atom. These types may be considered as a cation and an anion sublattice. Hence, each atom in lattice site is tetrahedrally surrounded by four atoms of the other type that depicted in Fig. 2.1(a).

In case of the CH structure, it can be obtained by doubling the ZB structure along the z-axis and filling the lattice sites according to the following: The anion sublattice is occupied by the VI-atoms while the cation sublattice is shared by the I- and III-atoms. In consequence, each C anion is coordinated by two A and two B cations and each cation is tetrahedrally coordinated by four anions. The CH structure shows the space group symmetry $I\bar{4}2d$ and its crystallographic structure is shown in Fig. 2.1(b). The observed structural features from real CH compounds are slightly

different from those obtained theoretically from this construction rules. The unique properties of the CH are related to three differences with respect to the ZB structure. First, there are two cation sublattices rather than one, leading to the existence of two basic chemical bonds A-C and B-C, with generally unequal bond lengths RAC $\neq$ RBC. Second, the unit cell is tetragonally distorted with a distortion parameter η = c/2a $\neq$ 1. Third, the anions are displaced from the ideal tetrahedral site u_0 = 1/4 by an amount u in direction of the x-axis. The structural and electronic properties of the CH are governed by the added structural (η, u) and chemical (A $\neq$ B) degrees of freedom relative to their binary analogs. The values of structural and optical band gap of CuInSe$_2$ are the cubic lattice constant a = 5.784 Å, c = 11.614 Å, the tetragonal distortion parameter η = 1.004, the anion displacement parameter u = 0.224 and the observed lowest band gap energy E_g = 1.04 eV (at T = 300 K) [28, 29], respectively.
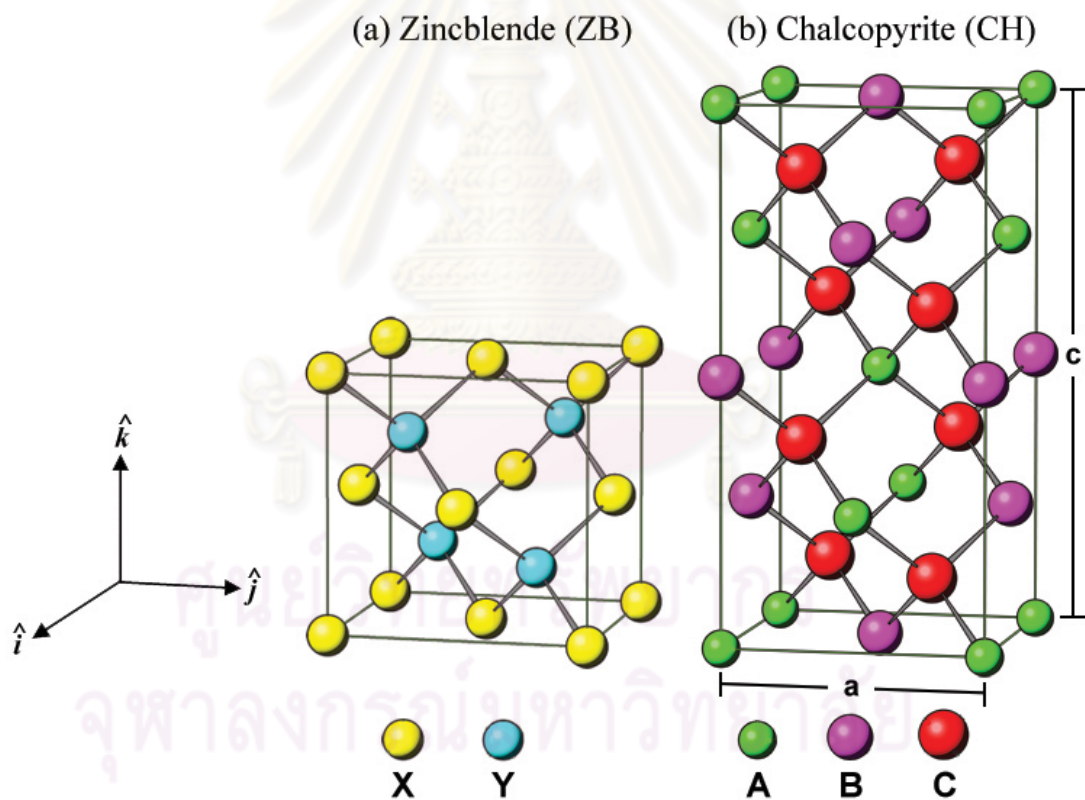
Figure 2.1: a) ZB crystallographic structure and b) CH crystallographic structure.
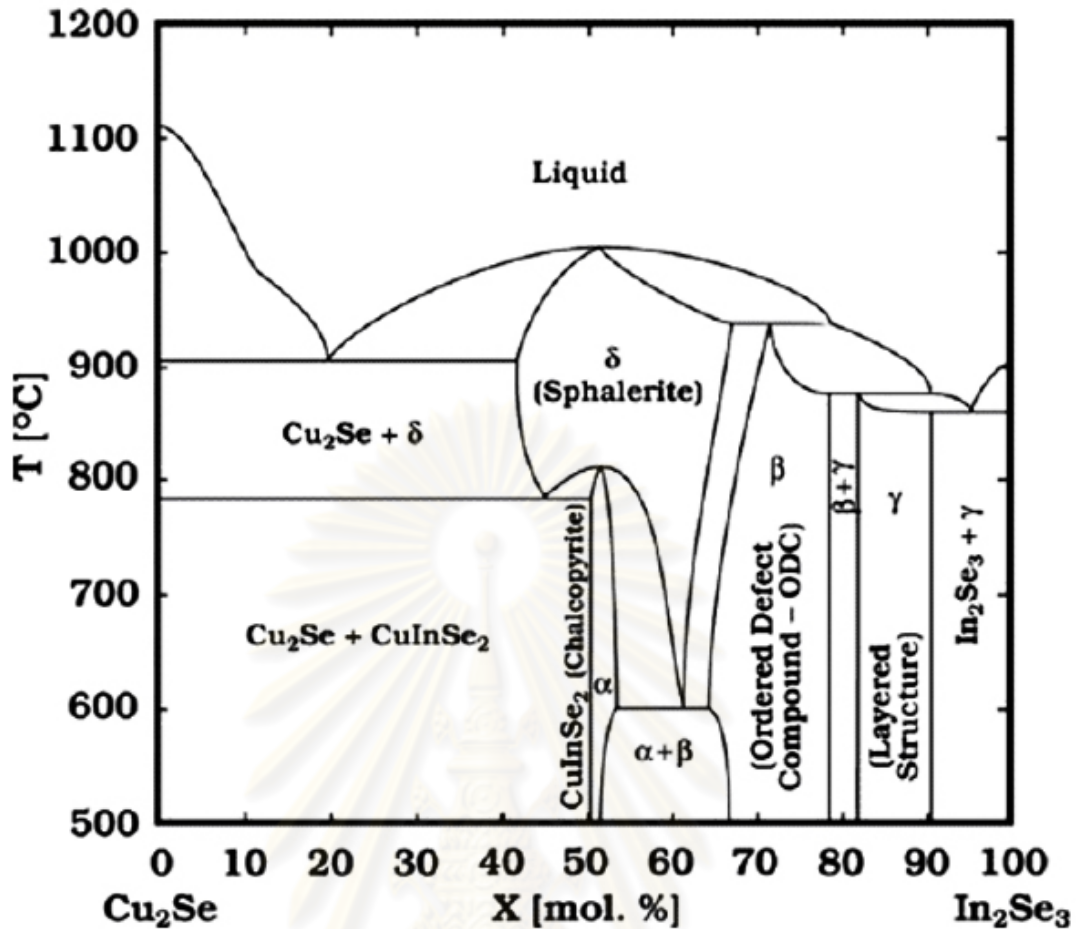
Figure 2.2: Phase diagram of the Cu_2Se-In_2Se_3 pseudobinary system [30].

2.1.2 Phase Equilibria of Cu-In-Se system

CuInSe$_2$ epitaxial thin films can be prepared by a variety of methods such as molecular beam epitaxy, hybrid sputtering and evaporation, metalorganic vapor phase epitaxy and etc. The method used in this dissertation is the molecular beam epitaxy which is a physical co-evaporation of the elements in a vacuum system. For this purpose, the phase diagram of Cu-In-Se system along the pseudobinary Cu$_2$Se and In$_2$Se$_3$ will be considered here. A schematic of the phase diagram of the pseudobinary system is shown in Fig. 2.2. The phase diagram shows that the crystal phases of Cu-In-Se material are dependent on temperature and composition. The α and δ phases belong to the chalcopyrite and sphalerite crystal structures, respectively. The β phase crystallizes in an ordered defect compound (ODC) of solid solutions within a composition range bounded by Cu$_2$In$_4$Se$_7$ and CuIn$_5$Se$_8$ [31]. The CuIn$_5$Se$_8$ compound is tentatively included in the γ phase with a layered structure. The atomic ratio of Cu to In ([Cu]/[In]) is the important parameter that relates to the composition of Cu-In-Se

system. The phase diagram exhibits that CH CuInSe$_2$ lies between a stoichiometric composition of 50 mol.% of In$_2$Se$_3$ to In-rich composition of about 53 mol.% of In$_2$Se$_3$. The corresponding value of [Cu]/[In] for this phase extends from 1.0 and 0.9. In the case of [Cu]/[In] is greater than unity or Cu-rich, the phase diagram demonstrates the mix phases of CuInSe$_2$ compound and secondary Cu$_2$Se compound. The Cu-Se compound in Cu-rich CuInSe$_2$, especially Cu$_{2-x}$Se, leads to large grain sizes and examines the high quality of structural properties [32, 33].

2.1.3 Defects in CuInSe$_2$

In the deposition process, it is difficult to obtain the intrinsic CuInSe$_2$ films due to the self-doping mechanism. When the compound is being formed as the film, it chooses to be either p- or n-type depending on the composition of the films. The defect of CuInSe$_2$ films is occurred by this mechanism. Rincon *et al.* [34] have proposed the defect chemistry model of CuInSe$_2$ for its nearly stoichiometric compound. There are two main parameters for describing the deviation of composition from the ideal and suggesting the possibility of major defect pairs. The molecularity deviation (Δm) is the first parameter that used to determine the deviation of Cu and In from the normal CuInSe$_2$. The definition of this parameter is

$$\Delta m = \frac{[Cu]}{[In]} - 1, \qquad (2.1)$$

where [Cu], [In] are the total atomic concentrations of Cu and In. There are two suggestions from this parameter. In the case of $\Delta m>0$, the composition of the compound is Cu-rich. On the other hand, the composition of the compound is In-rich when $\Delta m<0$. The stoichiometry deviation (ΔS) is another parameter that used to determine whether there is an excess ($\Delta S>0$) or deficiency ($\Delta S<0$) of selenium. This parameter can be defined as

$$\Delta S = \frac{2[Se]}{[Cu]+3[In]} - 1, \qquad (2.2)$$

where [Se] is the total atomic concentration of Se. The possible majority defect pairs and their formation energies in CuInSe$_2$ compound are shown in Table 2.1 and Table 2.2.

Table 2.1: Majority defect pairs of $CuInSe_2$ under In-rich condition ($\Delta m < 0$) [34].

Majority defect pair		Stoichiometry deviation
Acceptor	**Donor**	**(ΔS)**
V_{Cu}	In_{Cu}	<0
V_{Cu}	V_{Se}	<0
V_{Cu}	In_i	>0
Se_i	In_{Se}	>0
Se_i	In_i	>0

Table 2.2: Formation energies of intrinsic defects in $CuInSe_2$ [34].

Types of defects		Formation energy (eV)
Vacancies	V_{Se}	2.4
	V_{Cu}	2.6
	V_{In}	2.8
Interstitials	Cu_i	4.4
	In_i	9.1
	Se_i	22.4
Antisites	In_{Cu}	1.4
	Cu_{In}	1.5
	In_{Se}	5.0
	Se_{In}	5.5
	Se_{Cu}	7.5
	Cu_{Se}	7.5

2.2 Copper-selenide (Cu-Se)

Cu-Se compounds are usually found in Cu-rich $CuInSe_2$ system. It is well-known that the $CuInSe_2$ films grown under the Cu-rich condition generally yield the high crystalline quality films but the Cu-Se second phase that formed on surfaces and grain boundaries causes a short circuit during the diode fabrication when making the p-n junction of the photovoltaic devices. The phases of Cu-Se are dependent on the temperature and the percentage of Cu and Se that can be seen in Fig. 2.3. $Cu_{2-x}Se$ is the majority impurity phases in the Cu-rich $CuInSe_2$ films that grown simultaneously with $CuInSe_2$. It is a mixed ionic-electronic superionic conductor with a homogeneity range of $0 \leq x \leq 0.25$. The crystallographic structure of $Cu_{2-x}Se$ has been studied several times [35 - 39]. A structural model of α-$Cu_{2-x}Se$ is proposed by consisting of a cage of $F\overline{4}3m$ symmetry, built by Se atoms in 4(a) sites and Cu ions in 4(c) sites, and a mobile cation subsystem formed by the remaining Cu ions distributed over the interstitial sites. The β-$Cu_{2-x}Se$ phase is either described as monoclinic or tetragonal [37]. The ordering of Cu ions in the β-phase results in a complicated superstructure. However, it can be concluded that the Cu ions in the $Cu_{2-x}Se$ and the phases of them play the important role in crystalline formation and physical properties of $CuInSe_2$ films that is very sensitive to the composition, temperature and deposition techniques.

2.3 Copper-gallium-diselenide (CuGaSe$_2$)

$CuGaSe_2$, or abbreviated calling as CGS, is another type of $A^{I}B^{III}C^{VI}_2$ ternary CH semiconductor where A = Cu, B = Ga and C = Se. The values of structural and optical band gap of $CuGaSe_2$ are the cubic lattice constant a = 5.614 Å, c = 11.032 Å, the tetragonal distortion parameter η = 0.9825, the anion displacement parameter u = 0.250 and the observed lowest band gap energy E_g = 1.68 eV (at T = 300 K) [28, 29], respectively. The $CuInSe_2$ compound can be alloyed with the $CuGaSe_2$ compound as $CuIn_{1-x}Ga_xSe_2$ where x is the percentage of Ga-atom in compound. This alloying compound can vary the properties of crystallographic structure and band gap energy that increases the potential for the innovative development of solar cells [40].
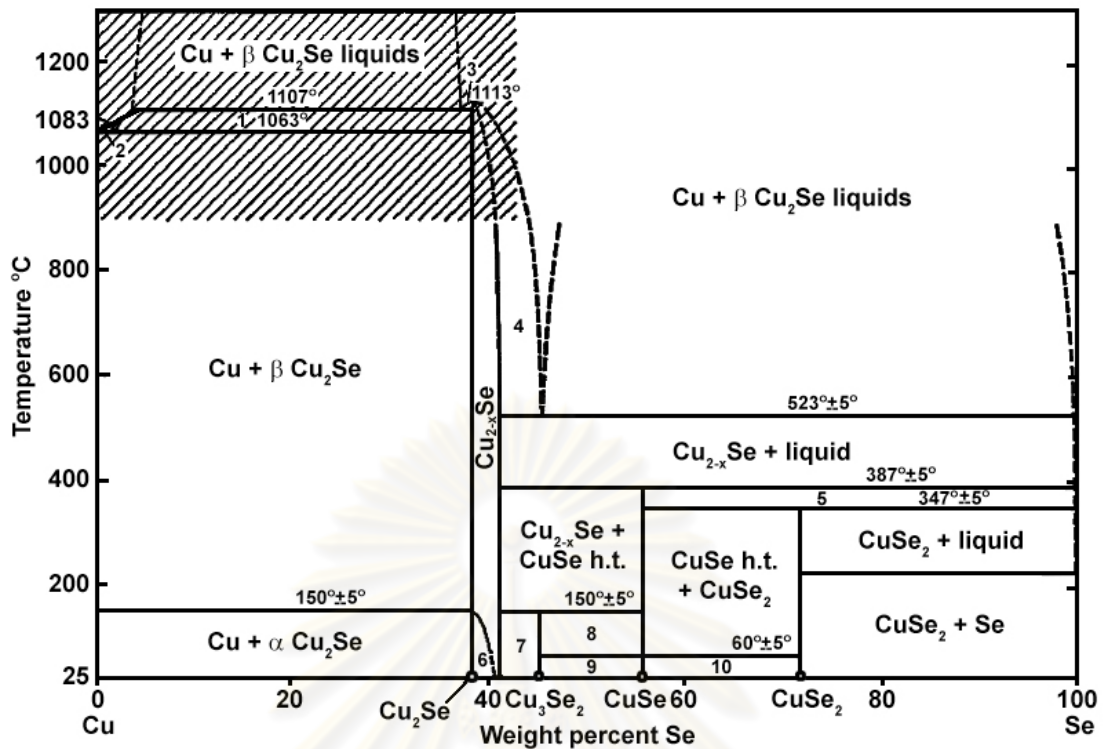
Figure 2.3: Phase diagram of the Cu-Se system : (1) liquid + β Cu$_2$Se; (2) Cu + liquid; (3) liquid + Cu$_{2-x}$Se; (4) Cu$_{2-x}$Se + liquid; (5) CuSe h.t. (high temperature) + liquid; (6) α Cu$_2$Se + Cu$_{2-x}$Se; (7) Cu$_{2-x}$Se + Cu$_3$Se$_2$; (8) Cu$_3$Se$_2$ + CuSe h.t.; (9) Cu$_3$Se$_2$ + CuSe l.t. (low temperature); (10) CuSe l.t. + CuSe$_2$ [41].

2.4 Epitaxial films

Epitaxy comes from the Greek roots which can be separated as *epi*, meaning above and *taxis*, meaning in ordered manner or to arrange upon. So, epitaxy is the word that describes the method of depositing a monocrystalline films upon a monocrystalline substrate. The deposited films are denoted as epitaxial films or epitaxial layer. The epitaxial films may be grown from gaseous or liquid precursors. The monocrystalline substrate acts as a seed crystal that controls the lattice structure and orientation of the deposited films identical to those of the substrate. Epitaxy can be classified in two kinds that examined by the materials of the deposited films on the substrate. The first kind of epitaxy is homoepitaxy that the epitaxial films and the substrate are the same as material. This technology is used to grow the films which are purer than the substrate or to fabricate layers having different doping levels. Heteroepitaxy is the second kind of epitaxy that the materials of the epitaxial films

and the substrate are different. This technology is often used to grow crystalline films of materials which single crystals cannot be obtained or to fabricate integrated crystalline layers of different materials.

Because the crystallographic structure of chalcopyrite resembles the double stack of zincblende structure and the crystallographic structure of GaAs is zincblende, so the (001)-oriented GaAs can be used as the substrate for growing the epitaxial CIS films. The important *in-situ* apparatus that uses to monitor the epitaxy is reflection high energy electron diffraction (RHEED).

2.5 Molecular Beam Epitaxy

Molecular beam epitaxy (MBE) is one type of the deposition techniques for growing high quality semiconductor materials that developed in the early 1970s [42, 43]. MBE is the physical co-evaporation techniques that the environment of the system is the ultrahigh vacuum ($\sim 10^{-10}$ Torr) and very clean for obtaining the unidirectional flow of atom or molecules. The ultrahigh vacuum (UHV) is the essential condition for the molecular beam that is related to the mean free path of the particles of the element that used to grow the epitaxial layer. The mean free path of the particle (κ) in the vacuum chamber is much larger than its dimension that is the important thing. The value of the mean free path can be estimated by [44]

$$\kappa = \frac{k_B T}{\sqrt{2}\pi\phi^2 P} = \frac{1}{\sqrt{2}\pi\phi^2 N^*}, \qquad (2.3)$$

where φ is the collision diameter of the molecule, P is the pressure, T is the temperature and N* is the molar density.

In this technique, thin films crystallize via reactions between thermal-energy molecular or atomic beams of source elements and the substrate surface, which is maintained at an elevated temperature. Each element is independent from each other which contained in the Knudsen effusion cells (K-cell). K-cell is the evaporation source which consists of a pyrolytic boron nitride (PBN) crucible used as the element container, a tantalum heater, a rotary feedthrough with molybdenum shutter and a thermocouple. The proportion-integral-deviation (PID) programmable temperature controller is used to control the precise flux of element in the K-cell. Since each element can be independently controlled, the complex structures including compounds that could not be found naturally or fabricated by other means can be

obtained. For the precise control of compositional element profiles, the epitaxial observation and reproducibility, the *in-situ* analysis tools are installed in the growth chamber such as quartz crystal thickness monitor (QCM), reflection high energy electron diffraction and pyrometer. The quartz crystal thickness monitor is the tool which used to measure the flux of source that depends on the temperature for compositional profile calculation. Reflection high energy electron diffraction tool is used to observe the evolution of the films during growth process. The crystal structural information of the films during the growth can be indicated by RHEED patterns which are the diffraction patterns of electrons that diffracted differently by periodic lattices. The pyrometer is another tool which is used to confirm compositional profile calculation and monitor the surface temperature of the sample. The schematic diagram of the MBE growth chamber is shown in Fig. 2.4.
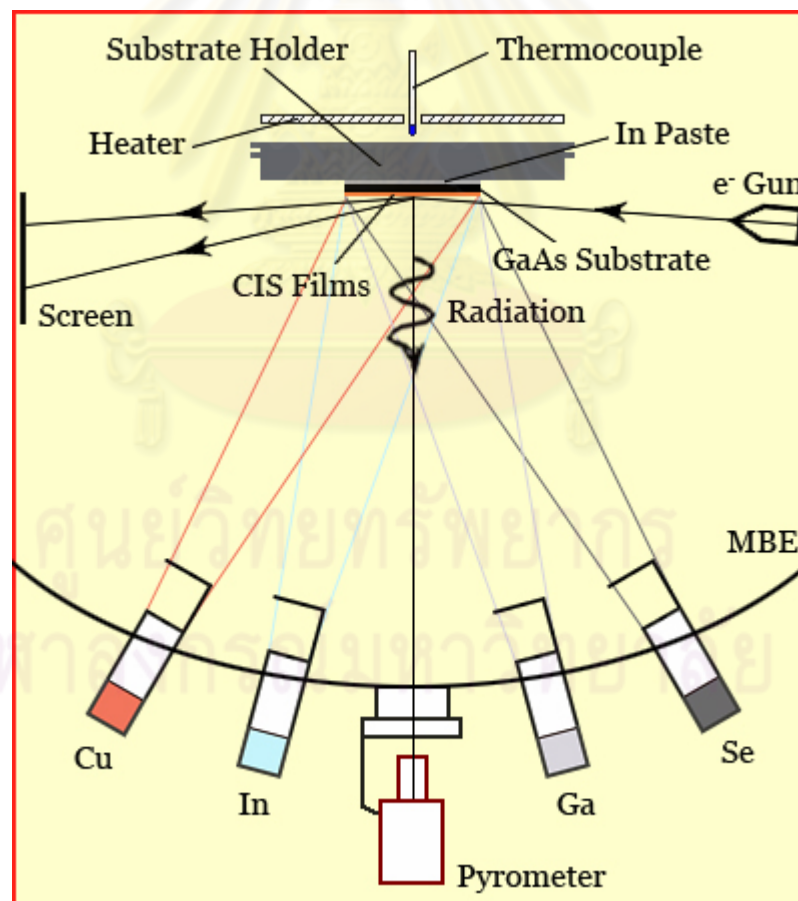
Figure 2.4: The schematic diagram of MBE growth chamber.

2.6 Quartz Crystal Thickness Monitor

Quartz crystal thickness monitor (QCM) is the essential tool which is used to measure the rate of the elements for film growth. The change in frequency of a quartz crystal resonator that is sensitive to additional mass can be used to determine the deposition rate and the final thickness of the deposited film. In principle, quartz is one member of a family of crystals that experiences the piezoelectric effect. When a material is deposited onto the surface of the acoustic resonator, the resonant frequency decreases from the initial value. This frequency change can be quantified and correlated precisely to the mass change using Sauerbrey's equation [45]. Since the sensor and the sample generally cannot be in the same direction from the deposition source and may not even be at the same distance from it. Therefore, the rate at which the material is deposited on the sensor may not equal the rate at which it is deposited on the sample. The ratio of the two rates is called the tooling factor that represents the different geometrical arrangement. In practice, the radiative heating of the quartz detector via the heat from the effusion cells must be minimized by cooling water because the change of quartz temperature results in an erroneous reading.

2.7 Reflection High Energy Electron Diffraction

Reflection high energy electron diffraction (RHEED) is the important analytical tool for characterizing thin films during sample preparation by molecular beam epitaxy, since it is very sensitive to surface structure and morphology. It is widely used to monitor removal of oxides from the surface and epitaxial growth of the films. RHEED system is very simply which required, at the minimum, only an electron gun, a phosphor screen and a clean surface that is shown in Fig. 2.5. The high energy electron ranging from about 8 to 100 keV directly goes to the surface of the film at grazing incident angle. Because of its small penetration depth, RHEED is sensitive to the atomic structure of the first few planes of a crystal lattice. Diffraction from a periodic structure underlies the patterns on phosphor screen. The diffraction patterns that emerge on the screen are called RHEED patterns which can be explained by the basic theory of Ewald construction. In the reciprocal space, the curvature of big Ewald sphere compared to the dimensions of the unit cell of the surface reciprocal net which determined by the conservation of energy is nearly flat. The intersection of the

Ewald sphere and the reciprocal lattice points determines the RHEED patterns which diffraction conditions are allowed. The picture of the Ewald sphere construction is shown in Fig. 2.6. The feature of RHEED patterns is dependent on the ordered crystallinity and the surface morphology. Figure 2.7(a) shows the diffraction spots from a highly flat ordered crystalline or ideal surface which appear along the Laue circles. In realistic growth, the ideal surface is difficult to obtain but the smooth surface (a little roughness) can be possible. Because the small roughness introduces the two-dimensional reciprocal lattice rods, the diffraction patterns become the streaks patterns that can be seen in Fig. 2.7(b). When the surface of the films becomes rough, the incident electrons will pass through the crystalline islands on the surface and the reciprocal net becomes the three-dimensional lattice points, RHEED patterns then exhibit the spot patterns as shown in Fig. 2.7(c). Finally, Fig. 2.7(d) shows the polycrystalline ring, diffraction pattern from polycrystalline surface, which caused by the randomly oriented single crystals.
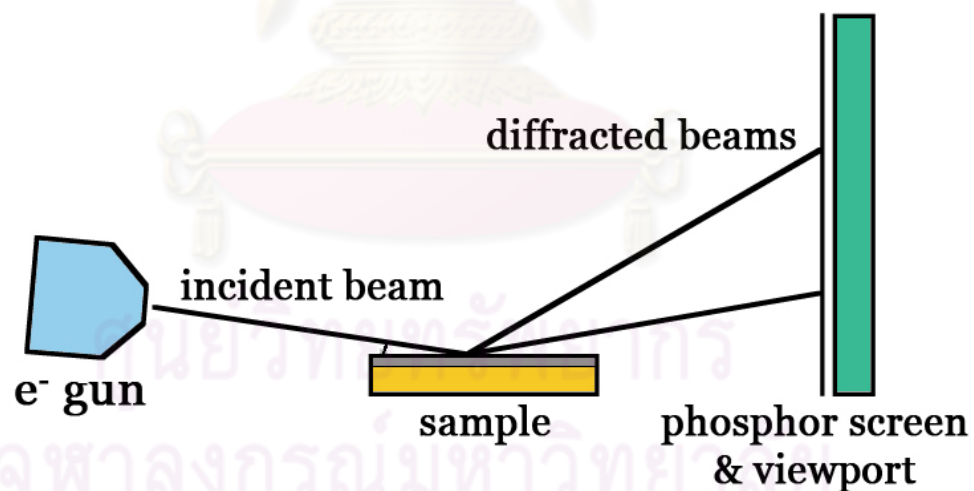
Figure 2.5: The schematic diagram of RHEED apparatus.
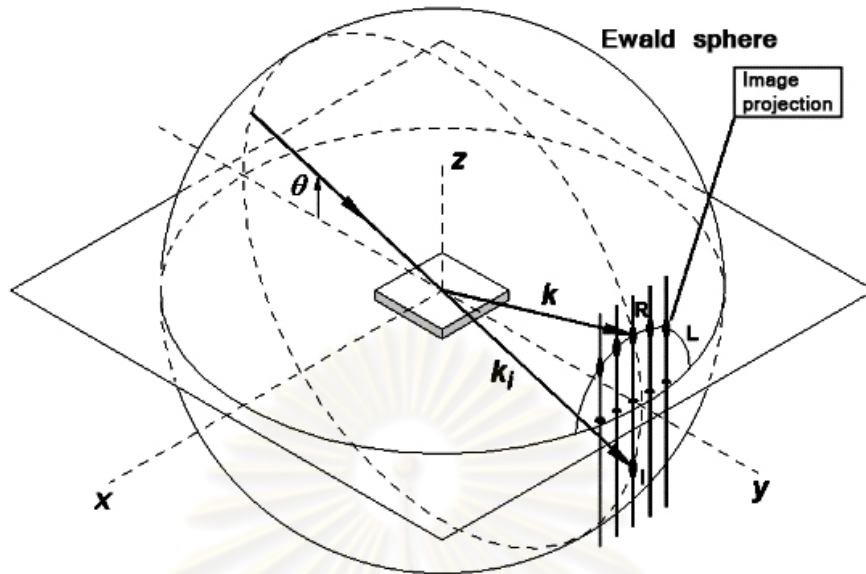
Figure 2.6: The schematic diagram of Ewald construction which used to explain RHEED patterns.
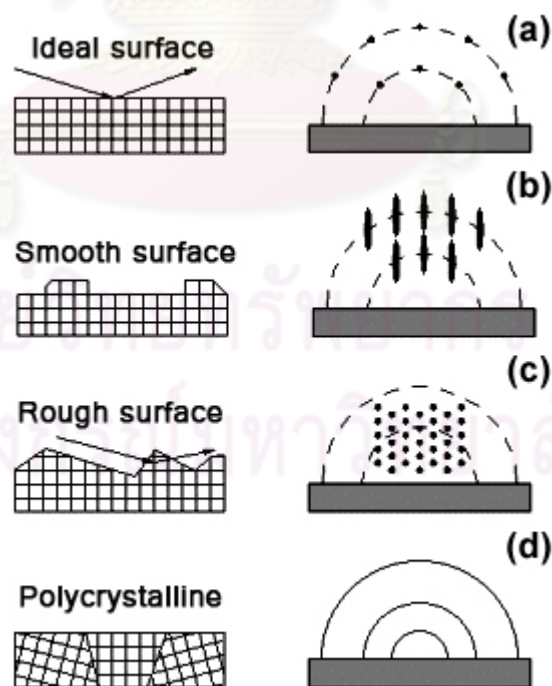
Figure 2.7: RHEED patterns from the different surface morphologies and polycrystalline.

2.8 Pyrometer

Pyrometer is another type of *in-situ* apparatus which is used to calibrate the composition of the films. It is a non-contact device that measures thermal radiation. The optical system is combined to focus thermal radiation onto the detector. The detected radiation intensity signal is then converted into a temperature by Stefan–Boltzmann law

$$j^* = \varepsilon\sigma T^4,\qquad\qquad(2.4)$$

where j* is the intensity of thermal radiation or irradiance, ε is the emissivity of the grey body, σ is the Stefan–Boltzmann constant and T is the object's temperature. Emissivity is defined as the ratio of the energy radiated by an object at a given temperature to the energy emitted by a perfect blackbody (ε = 1) at the same temperature. The emissivity is the necessary value in order to compensate the precise temperature for different material that ranges from 0.0 to 1.0. For all material, the interaction of energy exchange is characterized by the total of reflection, transmission and absorption that is equal to unity. From Kirchhoff's law of thermal radiation, the absorption factor of the material is related to emissivity. In realistic case, the emissivity is also dependent on the wavelength.

Chapter III

Sample Preparation and Characterizations

The epitaxial CuInSe$_2$ films are deposited on the GaAs (001) substrates by the MBE technique. The most important factors to get high quality thin films are the substrate preparation and precise control of the molecular constituents. In this section, I will explain how to prepare the samples that start from the GaAs substrate preparation and then the deposition processes which consist of the molecular constituents and the films composition calibration as well as the deposition technique of CuInSe$_2$ epitaxial films will be explained. After that, all of samples will be characterized by various techniques whose fundamental operation principles are described in the next section. The experimental procedures of this work can be schematically described in Fig. 3.1.
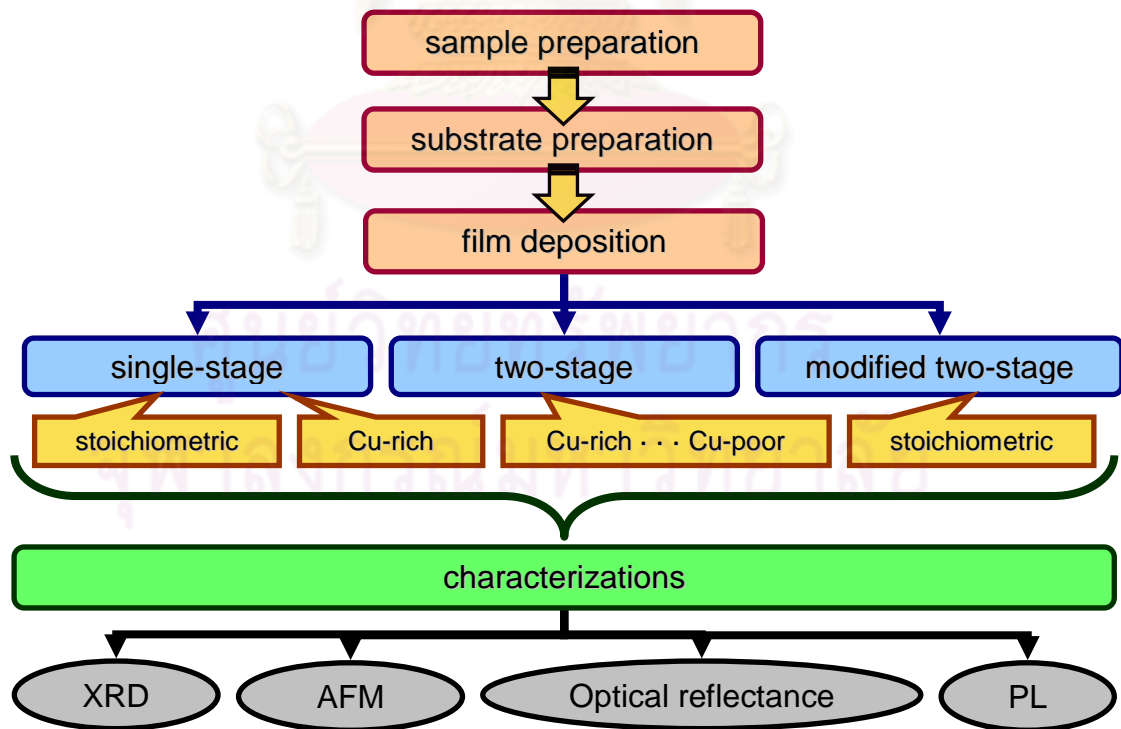
Figure 3.1: Schematic diagram of experimental procedures.

3.1 GaAs Wafer Preparing Procedure

The clear and pure surface of GaAs wafer is the important subject in substrate preparation. Cleaning procedures will remove contaminations from the surface and prepare the smooth surface of the GaAs wafer. The contaminants such as grease, organic compounds and dust are removed from the surface. Steps for cleaning contaminations are as followed:

1. Blow the compress nitrogen gas through the surface of GaAs wafer to remove coarse dust particles.

2. Clean the substrate for 5 minutes in Trichloroethylene (TCE) in an ultrasonic bath to remove organic contamination that might be left on the surface from the substrate production.

3. Clean the substrate for 5 minutes in acetone in an ultrasonic bath to further remove organic contamination and residual TCE.

4. Clean the substrate for 5 minutes in methanol in an ultrasonic bath to further remove organic contamination and remaining acetone.

5. Thoroughly rinse in de-ionized (DI) water to remove any residual methanol. Then blow dry with compress nitrogen gas.

Next steps of cleaning procedure are the chemical etching that taken when one needs to prepare smooth surface of GaAs wafer. This step will generally be taken before putting the substrates into the deposition chamber. Etchants are the mixture of 98 weight percent sulfuric acid, 30 weight percent hydrogen peroxide, and DI water. The volume ratios of these agents are $(5)H_2SO_4 : (1)H_2O_2 : (1)H_2O$ [46]. The sulfuric acid converts organic compounds to elemental carbon. The peroxide then oxidizes the carbon to carbon dioxide and water. To etch the GaAs wafer, the following steps are taken:

1. Mix the etchant, H_2SO_4: H_2O_2: H_2O with the ratio 5:1:1 in ice bath for controlling the mixture temperature.

2. Dip the wafer for 1 minute in the etchant and agitating every 15 seconds to remove metal ions and to oxidize the surface.

3. Dip in DI water pool and rinse in running DI water for 2-3 minutes to remove etchant.

4. Blow dry with compress nitrogen gas.

After the surface preparation of GaAs substrate is finished, the sample is bound on the molybdenum sample holder (Mo block) by using a small amount of high pure In solder. The Mo block is placed on the hot plate and kept at 160 – 180°C. The GaAs substrate is put on the melted In that covered on Mo block and slid back and forth along the surface, thus the substrate can be mounted firmly with the surface tension. It is important to wet the entire surface to ensure uniform heating and to prevent inclusion of gas between the wafer and the Mo block. After cooling down, it is ready to be installed in the deposition chamber.

3.2 Calibration of Molecular Constituents

Calibration of the effusion cells should be done periodically to check the effusion rate of each constituent for getting the desired material. The calibration measures the rate as a function of the effusion cell temperature that is read by temperature controller. The measurement of the effusion rate is done by measuring the deposition rate using the quartz crystal thickness monitor (QCM) located on the retractable arm under the substrate. In our MBE machine, the incident angles of all beams impinging on the substrate are designed to be about 15 degrees. The thickness of the metal film is evaluated from the change of the frequency of the quartz crystal and the known parameters of density and acoustic impedance of the source elements, according to Eq. 3.1 [45];

$$d = N_q \frac{\rho_q}{\rho_m} \left[\frac{\gamma_q - \gamma_2}{\gamma_2^2} - \frac{\gamma_q - \gamma_1}{\gamma_1^2} \right] \left(\frac{l_q}{l} \right)^2, \qquad (3.1)$$

where   d is the thickness of the evaporated film,

ρ_q is the density of the quartz (2.20 gcm^{-3}),

ρ_m is the density of the evaporated film,

γ_q is the resonant frequency of the uncoated crystal (6MHz),

γ_1 is the resonant frequency of the crystal before the evaporation,

γ_2 is the resonant frequency of the crystal after the evaporation,

l_q is the distance between source and crystal,

l is the distance between source and substrate,

N_q is the frequency constant for a quartz crystal vibrating in the thickness shear mode (1.668×10^{-5} cm/s).

For the QCM, I usually open the shutter and wait for a few minutes before measuring due to an initial transient. Each evaporation source is calibrated at six or more different temperatures in the range of working temperature to find the deposition rate as a function of the effusion cell temperature. The relationship between the deposition rate and the effusion cell temperature is given by

$$\ln(r) = a\frac{1}{T} + b, \tag{3.2}$$

where r is the deposition rate (Å/s), T is the effusion cell temperature (°C) and a and b are fitting parameters that can be determined by the least-square fit method.

3.3 Calculation of the Film Depositions

After checking the deposition rate of all sources, the calculation of the film deposition is necessary before the growth process. For the CuInSe$_2$ films, the chemical composition is commonly defined by the atomic ratio of Cu to In (y = [Cu]/[In]). This main parameter highly affects the films morphology and quality. The desired total thickness of the films is another parameter which is used to assign the thickness of Cu and In. Since Se vapor spreads overall the growth chamber, so the deposition rate of Se is typically set to overpressure. The composition and the thickness can be calculate from these equations

$$y = \frac{N_{Cu}}{N_{In}} = \frac{d_{Cu} \times \rho_{Cu} \times M_{Cu}^{-1} \times A \times N_A}{d_{In} \times \rho_{In} \times M_{In}^{-1} \times A \times N_A}, \tag{3.3}$$

and

$$d_i = r_i \times t_i, \tag{3.4}$$

where N_i is the number of atoms of specie i accumulated in the growing film at time t,

d_i is the thickness of the metal i at time t,

ρ_i is the density of the metal i,

M_i is the mass per mole of the metal i,

A   is the unit area of the metal,

N_A is Avogadro's number,

r_i is the deposition rate of the metal i,

and t_i is the total time that the metal i is deposited.

The numerical values of the parameters are given in Table 3.1.

Table 3.1: Density and mass per mole values of the materials.

Material	ρ (g/cm^3)	M (g/mole)
Cu	8.96	63.55
In	7.31	114.82
Se	4.79	78.96
CuInSe$_2$	5.89	336.29

To simplify the expression in Eq. 3.3, the new parameter α_i is defined as $\alpha_i = \rho_i \times M_i^{-1}$. The area of Cu and In are the same as the area of the growing films and Avogadro's number is a constant. From these parameters, the relationship of the corresponding metal films thickness is

$$d_{In} = \frac{1}{y} \cdot \frac{\alpha_{Cu}}{\alpha_{In}} \cdot d_{Cu} .$$ (3.5)

Table 3.2: α parameter of the elements.

Material	α (mole/cm^3)
Cu	0.1410
In	0.0637
Se	0.0607
CuInSe$_2$	0.0175

According to Eq. 3.4 and the deposition time of In is equal to Cu, thus Eq. 3.5 can be rewritten in the term of the deposition rate as

$$r_{In} = \frac{1}{y} \cdot \frac{\alpha_{Cu}}{\alpha_{In}} \cdot r_{Cu} .$$ (3.6)

Due to the deposition rates of Cu and In are assigned by the total thickness of CuInSe$_2$ (d_{CIS}) and the value of y, the thickness of CuInSe$_2$ layer and the thickness of Cu layer are related by the Cu content of CuInSe$_2$ film, and can be calculated from

$$\frac{d_{Cu}}{d_{CIS}} = \frac{N_{Cu} \times M_{Cu} / \rho_{Cu}}{N_{CIS} \times M_{CIS} / \rho_{CIS}} .$$ (3.7)

The ratio of N_{Cu} and N_{CIS} is equal to unity. From Table 3.1 or Table 3.2, it can be shown that

$$d_{Cu} = 0.124 \cdot d_{CIS}. \qquad (3.8)$$

Before starting the deposition process, the composition and the total thickness of CuInSe$_2$ films are defined and then Eqs. 3.8, 3.4 and 3.6 are used to calculate the deposition rates of Cu and In elements. After that, the Eq. 3.2 is used to determine the temperature of constituents that is set during deposition process. To confirm the calculation, the composition of the films is checked again by the two-stage growth process technique that is described in section 3.4.2.

3.4 Deposition Techniques of CuInSe$_2$ Epitaxial Films

Before starting growth process, GaAs substrate is loaded into the growth chamber. The substrate temperature is ramped up to 600°C for about 5 - 10 minutes as a thermal treatment and then it is heated up or cooled down to the set-point. The temperatures of all constituents are ramped up to the set-point at the same time. In this work, the key parameters and growth mechanisms in the single-stage growth process and the two-stage growth process are to be determined. The modified two-stage growth process is then proposed for improving the quality of the epitaxial films. The details of these processes are described as the following.

3.4.1 Single-stage Growth Process

The single-stage growth process is a one shot growth process. The composition of the films is set to a constant value throughout the deposition time. In the growth process, the flux or rate of the effusion cells and the substrate temperature are kept constant. The rate of the effusion cells can be determined using Eqs. 3.8, 3.4 and 3.6. When the substrate temperature reaches to the set-point, the shutters of all constituents are opened simultaneously. The growth process is started and allowed until the thickness of the films is achieved. After that, the shutters of all constituents are then shut off simultaneously. The growth profile of the process and the composition evolution can be seen in Fig. 3.2.
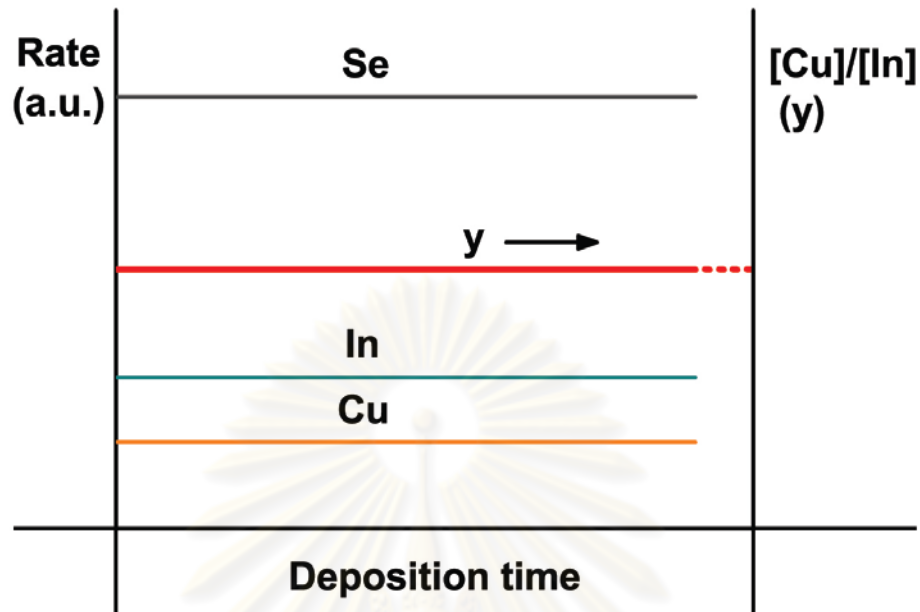
Figure 3.2: Schematic diagram of the growth profile and composition evolution of the films in the single-stage process.

3.4.2 Two-stage Growth Process

The two-stage growth process is generally known as "bilayer process" or "Boeing recipe". The name of this process indicates that there are two stages in the growth process. In the first stage, the growth profile is the same as the single-stage growth process until the deposition time goes to t_1 and then the Cu flux is terminated and maintained only In and Se fluxes in the second stage. The growth profile of this process is shown in Fig. 3.3. The significant feature of this technique is that the composition of the films in the first stage must be set greater than unity or Cu-rich condition in order to obtain the bigger grain size. After the shutter of Cu is closed, the composition of the films decreases and the value of the composition is dependent upon the deposition time t_2 in the second stage. The total thickness of the Cu-content in the end of the second stage is equal to the end of the first stage. From the following feature of the Cu-content and Eqs. 3.4 and 3.6, it can be obtained that the composition of the films in the first stage and the second stage as

$$y(t_1) \cdot t_1 = y(t_2) \cdot t_2 . \qquad (3.9)$$

The evolution of the composition of the films according to Eq. 3.9 can be seen in Fig. 3.3. At the end of the growth process (at $t = t_2$), the final desired composition, $y(t_2)$, can also be used as the *in-situ* monitoring signal. The *in-situ* signals consist of (i) the temperature of the surface of substrate read by pyrometer (T_{pyro}) and (ii) the output power of substrate temperature controller (OP). Moreover, end point detection (EPD) technique which has been introduced by T. Nishitani *et al.* [47] in 1995 is an *in-situ* method to predict when the growth process should be finished. In this work, the *in-situ* monitoring signals of the two-stage process are followed by the work of P. Chinvetkitvanich [48] that grew the $CuIn_{1-x}Ga_xSe_2$ films on the SLG substrate using molecular beam deposition (MBD) technique. The example of the *in-situ* monitoring signals of the two-stage as a function of deposition time is illustrated in Fig. 3.4. The composition at the end point detection of these signals is equal to 0.9 which is the certain value that can be used to calculate back to check the composition of the films in the first stage using Eq. 3.9.
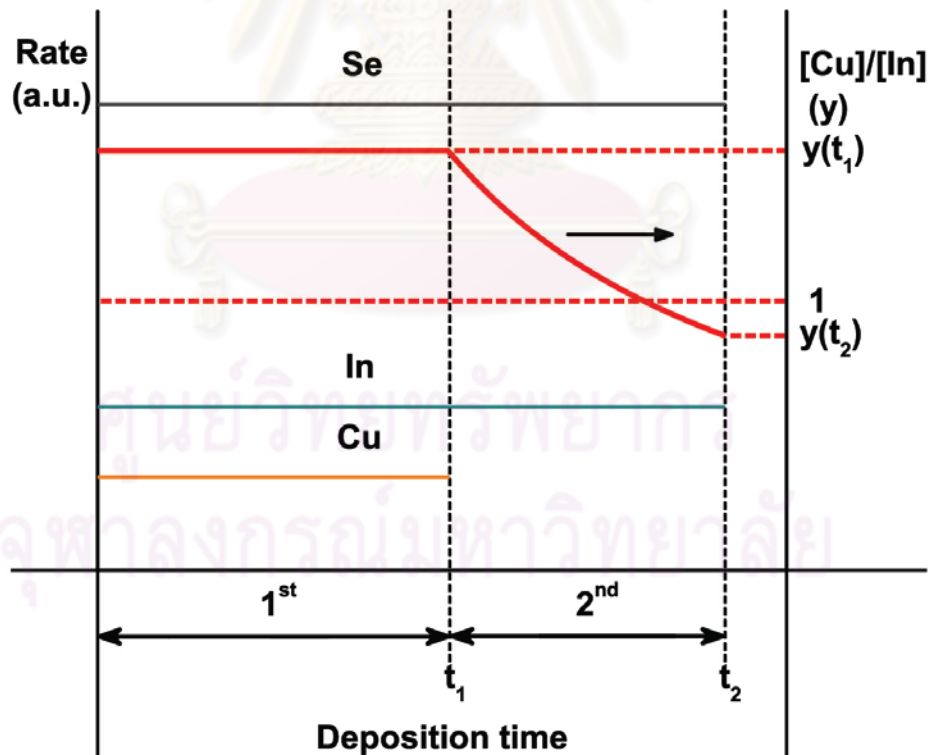
Figure 3.3: Schematic diagram of the growth profile and composition evolution of the films in two-stage process.
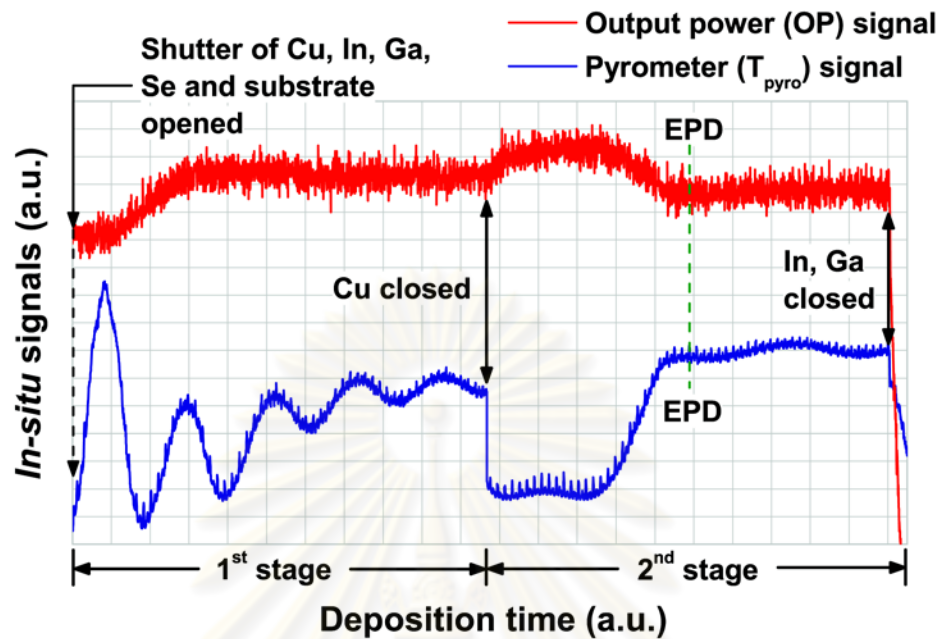
Figure 3.4: *In-situ* monitoring signals of the $CuIn_{1-x}Ga_xSe_2$ films grown with the two-stage growth process as a function of deposition time.

3.4.3 Modified Two-stage Growth Process

The modified two-stage growth process is proposed for improving the Cu-deficiency in the normal two-stage growth process. The process starts with the single-stage growth process with Cu-rich condition for a short time and then the temperature of effusion cell of In is ramped up linearly. In this technique, the flux of Cu source is still allowed throughout the deposition time. From Eq. 3.2, the rate of In source increases exponentially and results in the decrease of the composition in the second stage. The growth profile of the process and the composition evolution can be seen in Fig. 3.5.
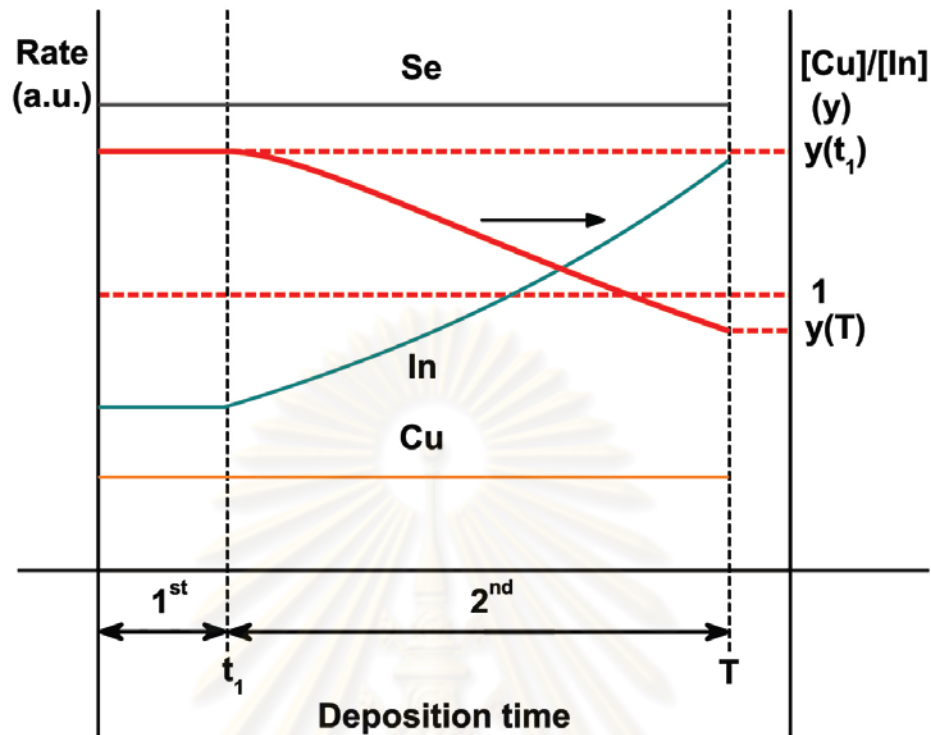
Figure 3.5: Schematic diagram of the growth profile and composition evolution of the films in modified two-stage process.

At the end of the growth process ($t = T$), the final composition of the films can be determined from Eq. 3.3. The total number of Cu-atom that accumulated in the growing film is

$$N_{Cu} = r_{Cu} \times T \times \alpha_{Cu}.$$ (3.10)

From Fig. 3.5, it can be seen that the total number of In-atom relates to the area under the curve of the In-rate. So that,

$$N_{In} = \left[r_{In1} \cdot t_1 + \int_{t_1}^{T} r_{In2} dt \right] \times \alpha_{In}.$$ (3.11)

The rate of In source is kept constant in the first stage (r_{In1}) of the growth process and then it is increased exponentially in the second stage (r_{In2}). Suppose the rate of In source in the second stage is

$$r_{In2} = r_{In1} \cdot e^{\upsilon(t-t_1)},$$ (3.12)

where υ is the ramping rate and t is the deposition time. Substituting Eqs 3.10, 3.11 and 3.12 into Eq. 3.3 yields

$$y = \frac{r_{Cu}T\alpha_{Cu}}{\left[r_{In1}t_1 + \int_{t_1}^{T} r_{In1}e^{\upsilon(t-t_1)}dt\right]\alpha_{In}} = \frac{r_{Cu}\alpha_{Cu}}{r_{In1}\alpha_{In}} \frac{T}{\left[t_1 + \frac{1}{\upsilon}\{e^{\upsilon(T-t_1)}-1\}\right]} . \qquad (3.13)$$

Consider the term $\frac{r_{Cu}\alpha_{Cu}}{r_{In1}\alpha_{In}}$ in the Eq. 3.13, it is the composition of the film (y_1) in the first stage. So, it can be rewritten as

$$y = \frac{y_1 \cdot T}{\left[t_1 + \frac{1}{\upsilon}\{e^{\upsilon(T-t_1)}-1\}\right]} . \qquad (3.14)$$

From Eq. 3.14, it is found that the composition of the films at the end of the growth process is dependent on the ramping rate parameter. To find the value of the ramping rate, Eq. 3.14 can be rearranged as

$$\frac{1}{\upsilon}\left[e^{\upsilon(T-t_1)}-1\right] - \left[\frac{y_1 \cdot T}{y} - t_1\right] = 0 . \qquad (3.15)$$

In the calculation, the value of the composition of the film and deposition time in the first stage and the desired composition of the film and deposition time at the end of the growth process are set and substituted into Eq. 3.15. The numerical technique is performed to solve this equation. When the value of the ramping rate is obtained, it is then substituted into Eq. 3.12 in order to define the temperature of effusion cell of In at the end of the growth process.

3.5 Characterization of CuInSe$_2$ Epitaxial Thin Films

After the sample preparation, several characterization techniques are used to evaluate the quality of the epitaxial films. The morphology of the films is observed by atomic force microscopy (AFM). X-ray diffraction (XRD) technique is used to study the crystallographic phase and structure. The composition of the films is determined by energy dispersive X-ray spectroscopy (EDS). Finally, the optical response of the films is characterized by UV-VIS-NIR spectrophotometer and photoluminescence (PL) technique. The details of each technique are briefly described in the following subsections.

3.5.1 Atomic Force Microscopy (AFM)

The atomic force microscope is one type of high-resolution scanning probe microscopy which is powerful tool for studying surface science. It is used to measure various local properties of the sample such as surface morphology, grain size evaluation, the roughness of the films and etc. The resolution of the scanner which made from piezoelectric material is in the order of fractions of a nanometer. In general, AFM system consists of a PZT tube scanner, a laser with position-sensitive photo detector and a cantilever with a sharp tip located at the free end. The basic setup of AFM apparatus is shown in Fig. 3.6. When the tip is moved down close to the sample surface, the cantilever is bent by the interaction force between the tip and the sample according to Hooke's law.

In basic principle, during the tip scan over the surface of the sample in x and y directions by scanner, a constant force between the tip and the sample is maintained. The changes in surface topography result in a deflection of the cantilever. The deflection of the cantilever is measured using a laser spot reflected from the top surface of the cantilever into an array of photodiodes and then generates a map of surface topography. For imaging mode, the operation can be divided into a static or contact mode and a dynamic or non-contact mode. In the static mode operation, the contact cantilever is dragged across the surface of the sample keeping a constant force between the tip and the surface. The static tip deflection is used as a feedback signal. The contours of the surface are measured directly using the constant deflection of the cantilever. In the non-contact mode operation, the tip of the cantilever does not touch the surface of the sample. The cantilever is externally oscillated slightly above its fundamental resonance frequency. The oscillation amplitude, phase and resonance frequency are modulated by tip-sample interaction forces. These changes in oscillation with respect to the external reference oscillation provide information and construct a topographic image of the sample surface. Another operation mode of the AFM is the tapping mode which the cantilever operates intermittently between the dynamic and contact modes. A tapping image is therefore produced by imaging the force of the intermittent contacts of the tip with the sample surface.
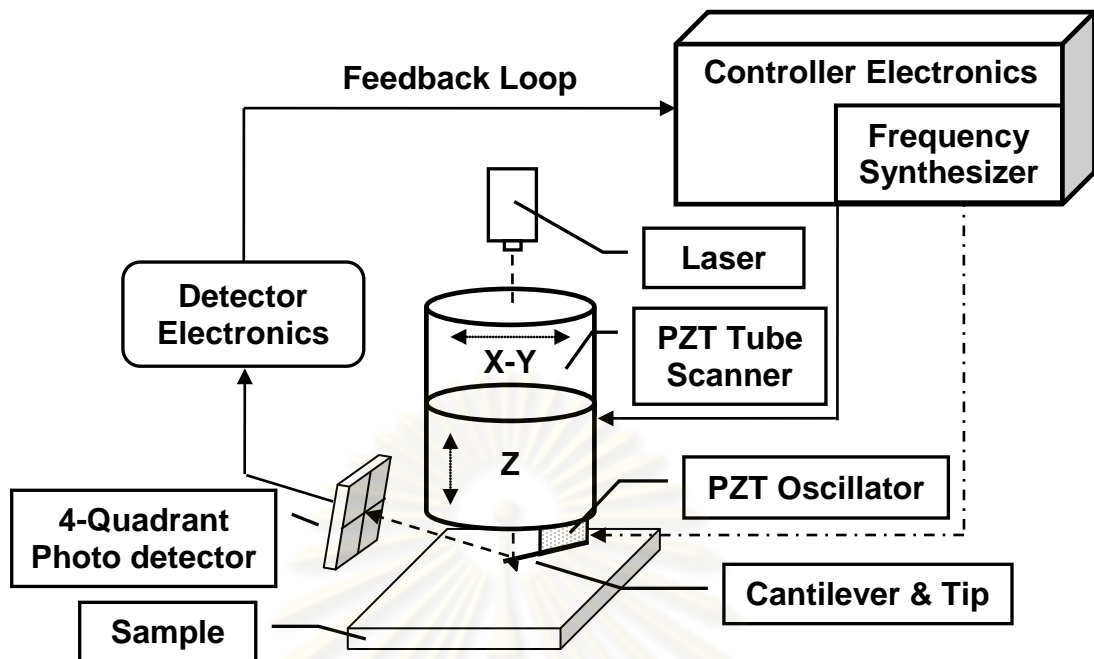
Figure 3.6: The basic atomic force microscope setup.

3.5.2 X-ray Diffraction (XRD)

X-ray diffraction is a non-destructive technique to identify the crystallographic phases and analyze the structure properties. In this work, Bruker model D8 Advance X-ray powder diffractometer is used to analyze all epitaxial samples. The X-ray source of this machine generates Cu-$K_{\alpha 1}$ radiation with the wavelength of 1.5406 Å and Cu-$K_{\alpha 2}$ radiation with the wavelength of 1.5444 Å. The XRD spectra are collected in the 60° – 70° of 2θ range with a measurement step of 0.01° for most samples in order to carry out phase analysis. Since the axis of samples is tilted around 2° toward <111> direction, so the scanning mode is chosen as unlocked couple for this correction. X-ray diffraction from an electromagnetic wave (the X-ray) impinging on a regular array of scatterers (the repeating arrangement of atoms within the crystal) is shown in Fig 3.7. The diffraction peaks in XRD spectra are the constructive waves which are satisfied by Bragg condition.
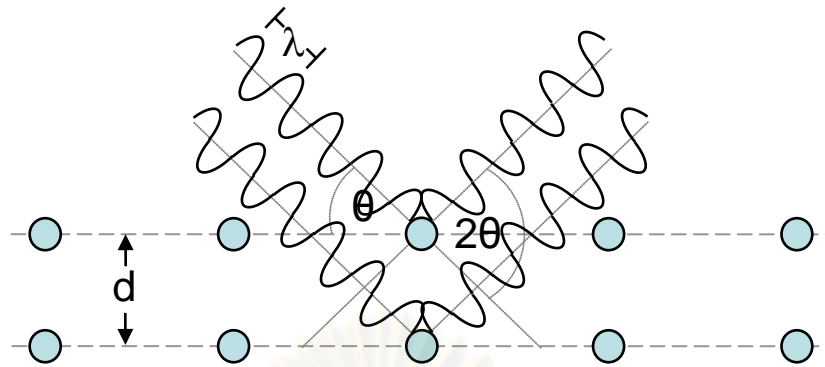
Figure 3.7: Diffraction of X-ray from parallel planes in the crystal.

Identification of the lattice parameters of the epitaxial films from XRD results is done using Bragg's law

$$2d \sin \theta = n\lambda \,, \tag{3.16}$$

where d is the interplanar spacing, θ is the Bragg angle and λ is the wavelength of X-ray source. In the case of the tetragonal system, the lattice parameters of the chalcopyrite structure of the samples can be determined by this equation,

$$\frac{1}{d^2} = \frac{h^2 + k^2}{a^2} + \frac{l^2}{c^2} \,, \tag{3.17}$$

where h, k, l are the Miller indices of the diffraction planes, a and c are the lattice parameters. The experimental XRD peak positions can be determined by Guassian fitting method. In addition, the Joint Council for Powder Diffraction Studies (JCPDS) files is the important database which is used to identify the crystallographic phases of the films.

3.5.3 Energy Dispersive X-ray Spectroscopy (EDS)

Energy dispersive x-ray spectroscopy (EDS or EDX) is an analytical technique which is equipped with scanning electron microscope (SEM) or transmission electron microscope (TEM). The principle of this apparatus is based on the x-ray fluorescence spectroscopy for inspecting the elemental composition or chemical characterization of the specimen. The samples being analyzed are mounted on the holder in the vacuum

system. The high energy beam of charged particles such as electrons or protons or a beam of x-rays are impinged and focused on the samples. The emission of characteristic x-rays is stimulated and then the number and energy of them can be measured by an energy-dispersive spectrometer as shown in Fig. 3.8. Generally, the EDS has an effective probe depth of ~ 1 μm, and may be limited to detection of elements with Z > 11 when a Beryllium window is used at the detector. In this work, the samples are analyzed by JEOL TEM model JEM-2100 using acceleration voltage of 200 kV. A typical EDS spectrum of CuInSe$_2$ thin films is shown in Fig. 3.9. The characteristic peak of x-rays from the sample can be fitted by Gaussian function, according to Eq. 3.18, to find the area under the peak of each element which infers the atomic weight percent of such element in the sample. The Gaussian function applied in the fitting process is

$$G(E) = I \times \exp\left[-\frac{1}{2} \times \left(\frac{E-C}{W} \right)^2 \right], \qquad (3.18)$$

where I is the amplitude of the peak, E is the energy, C is the energy at the center of the peak and W is the width of the peak. The area under the peak (A) is the integration of Gaussian functions over the entire energy,

$$A = \int_{-\infty}^{\infty} G(E)\,dE = I \times W \times \sqrt{2\pi}. \qquad (3.19)$$

After the fitting process, the area under the peak of each element can be obtained, and used to determine the value of the composition ratio ([Cu]/[In]) of the films.
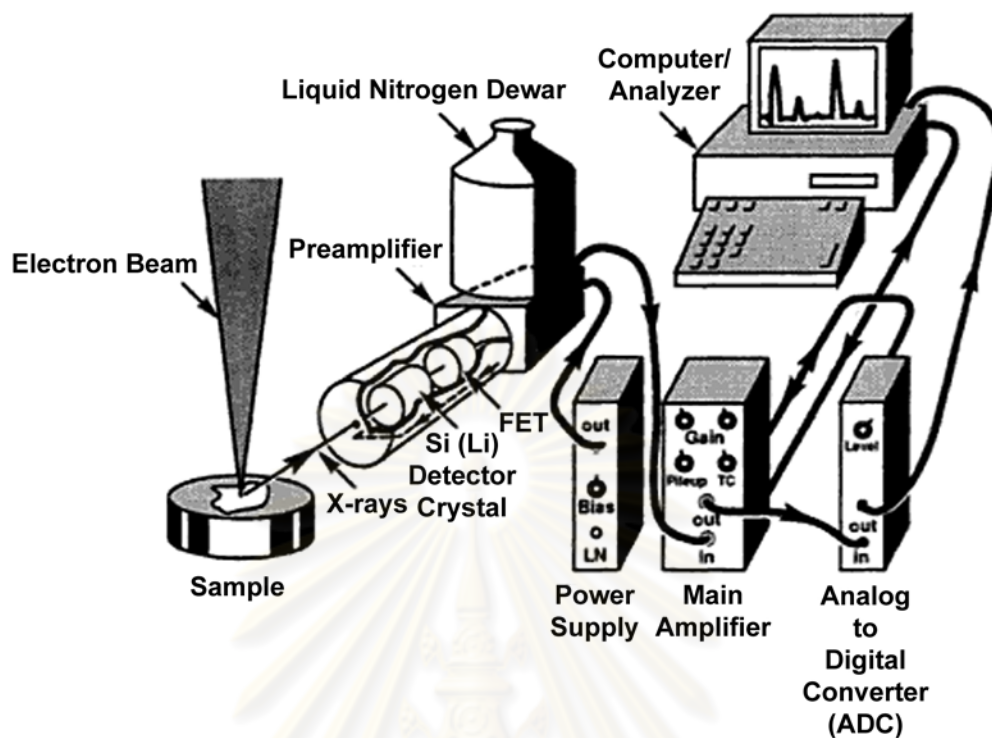
Figure 3.8: Schematic representation of an energy-dispersive spectrometer and associated electronics [49].
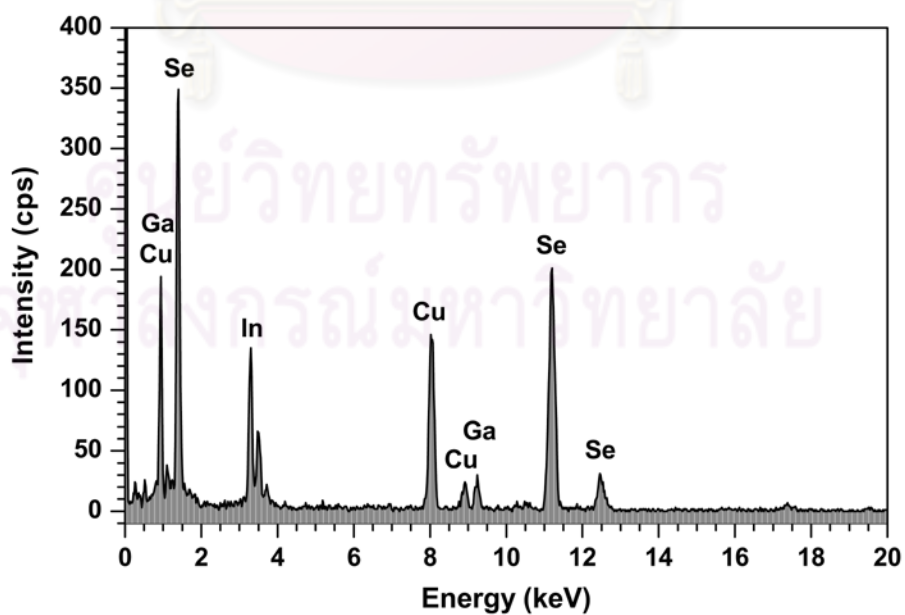
Figure 3.9: Example of EDS spectrum from $CuInSe_2$ epitaxial thin films.

3.5.4 Optical Reflectance Spectroscopy

Optical reflectance is the measurement of the optical response of the sample that measures the fractional intensity of the reflected electromagnetic field. In this work, the reflectance spectra are measured by a Perkin Elmer Lambda 900 spectrometer. The working spectral range is from 400 nm to 2600 nm that covers the ultra-violet (UV), visible and near-infrared (NIR) spectrum. The halogen lamp is used as the light source for visible and IR radiation and then automatically changes to deuterium lamp for UV radiation. In the process of the measurement, the auto-zero process is required before by measuring standard mirror as a reference. For the thin films, the interference fringe oscillations occur from the superposition of the reflected coherent light waves at the top surface and the interface between the film and the substrate that is illustrated in Fig. 3.10.
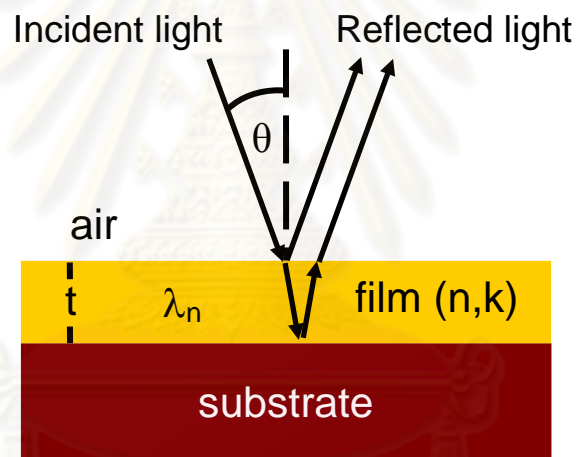
Figure 3.10: Demonstration of the optical path for light reflected from the top surface and the interface between the film and the substrate.

The degree of constructive or destructive interference between the two light waves is dependent upon the difference in their phase. This difference is also dependent on the thickness of the films layer, the refractive index of the films, and the angle of incidence of the original wave on the films. In this measurement setup, the angle of incident light is zero or normal to the surface of the films. From this relation, the thickness (*t*) of the film can be found from

$$t = \frac{1}{2n\left(\frac{1}{\lambda_{m+1}} - \frac{1}{\lambda_m} \right)}, \tag{3.20}$$

where n is the refractive index of the film and λ_m is the mth wavelength of light that is constructive interference.

3.5.5 Photoluminescence (PL) Spectroscopy

Photoluminescence is the phenomena of spontaneous photo emission which the substance absorbs photon and then re-radiates photons. The PL spectroscopy is an important technique which is used to identify the purity and crystalline quality of semiconductors. In the process of the measurement, a light source with sufficient energy such as laser incidents on the sample. The photons are absorbed and electronic excitations occur. When these excitations relax and the carriers return to the ground state, the electromagnetic radiations will be emitted. The radiative light is collected by lenses to the monochromator and then measured by a photo-detector. The conventional setup of the PL spectroscopy is shown in Fig. 3.11. In this measurement, He-Ne laser with a wavelength of 632 nm and a power of 40 mW is used as an excitation source. The PL spectra are carried out with a SPEX 750m single-pass monochromator together with a liquid nitrogen-cooled Ge detector (Edinburgh Instruments: Model EI-L). All samples are examined for temperature dependence from 10 K up to 290 K in a cryostat (Leybold: Model RDK 10-320).
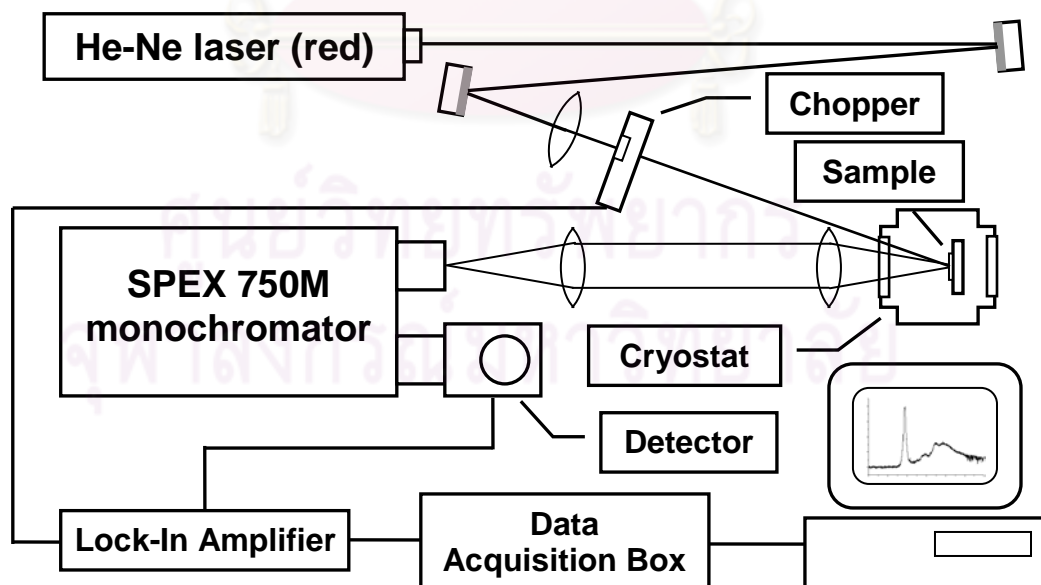
Figure 3.11: Conventional experimental setup for PL spectroscopy.

In a substance, defects and impurities lead to an imperfection of crystallinity that causes the perturbation in the band structure. Typically, the degeneracy states of the defect or impurity act as a donor or acceptor of excess electrons in the crystal. The PL measurement is the method for observing these states that lie within the band gap. The peak position of PL spectra represents photon energy of electrons or holes that emit after state recombination occurrence. The possible evidences of radiative recombination can be seen in Fig. 3.12.
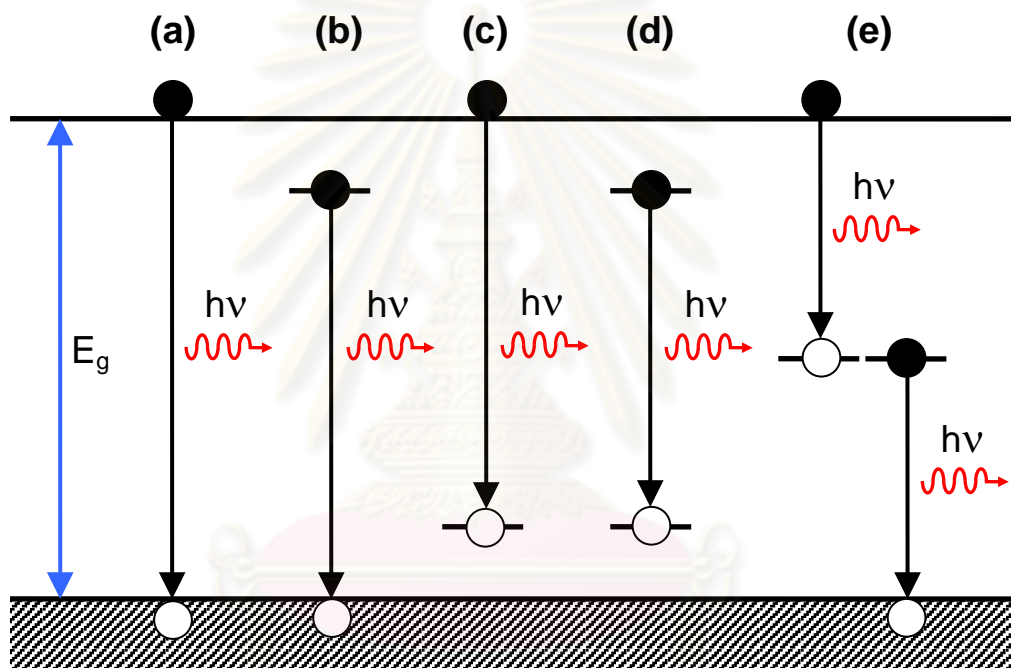
Figure 3.12: Radiative recombination paths: a) interband transition, b) donor to valence band transition, c) conduction to acceptor band transition, d) donor to acceptor band transition and e) conduction to intermediate band or intermediate to valence band transition.

3.6 Potassium-cyanide (KCN) Etching Process

For the Cu-rich CIS films, etching process with KCN aqueous solution is applied to remove the excess $Cu_{2-x}Se$ compounds [23, 26]. The composition of the films after etching process is near stoichiometric [23]. After the as-grown films are etched with KCN aqueous solution, they will be re-characterized again in order to compare and investigate the changes between before and after etching process. Steps of etching process are as followed:

1. Dissolve the KOH tablet in DI water for adjusting the pH level of DI water to about 8.
2. Measure and dissolve the KCN powder in the prepared DI water for making etchant aqueous solution with concentration of 5 wt %.
3. Dip the sample for 1 minute in KCN aqueous solution and shake the sample holder every 15 seconds to remove the residue Cu-complex.
4. Dip in DI water pool and rinse in running DI water for 2-3 minutes to remove etchant.
5. Blow dry with compress nitrogen gas.

Caution: KCN is the well-known as the extremely poison and lethal compound. It is a colorless compound with smell of almonds, similar in appearance to sugar and highly soluble in water. If it is consumed more than 3 – 4 mg, the consciousness will be lost within one minute and may be fatal. It can be inhaled or absorbed through skin. It is very stable in dry environment. When it contacts with the acids or moisture, it can release the poisonous hydrogen cyanide gas. So, the fume hood is a necessary requirement for operating with KCN.

Chapter IV

Results and Discussion

The results of this work are presented in this chapter. The results are ordered by the respective studies and they will be discussed as the following. Firstly, the growth and characterizations of CuInSe$_2$ epitaxial thin films with Cu-rich and near stoichiometric composition under various substrate temperatures using the single-stage growth process will be presented. Secondly, the results of the films grown by the normal two-stage growth process with various final compositions will be shown. Next, the modified two-stage growth process epitaxial films will be exhibited. Finally, the growth model and the mechanisms of the growth process are discussed and proposed in this chapter.

4.1 Results and Discussion of the CuInSe$_2$ Epitaxial Films Grown by Single-stage Growth Process

The single-stage CuInSe$_2$ epitaxial films are grown on GaAs (001) substrate by setting compositions of the films as Cu-rich, near stoichiometric and Cu-poor. During the growth process, RHEED apparatus is employed to check the epitaxial films and observe the evolution of the growing films. RHEED patterns of GaAs substrate, as shown in Fig. 4.1, exhibit the raindrop-like patterns due to the roughness of surface after surface preparation. The major characteristics of the patterns have two types that are dependent upon the direction of interception between the reciprocal rods and the Ewald surface as shown in Fig. 4.2 and 4.3. After growth process is started, the characteristic of RHEED patterns will be changed by the films growing on the surface. The RHEED patterns of the Cu-rich and the near stoichiometric CIS films seen in Fig. 4.4 and 4.5 show the streaky patterns indicating that the surface of the films is very smooth. Whereas the surface of the Cu-poor CIS films, as shown in Fig. 4.6, is rougher which are indicated by spotty RHEED patterns. Moreover, it can be observed the reconstruction pattern along [$\overline{1}\,\overline{1}0$] direction that is the specific pattern

of the Cu-rich CIS films [17] and cannot be found in the near stoichiometric CIS films. From these results, it can be concluded that the high quality epitaxial films from Cu-rich and near stoichiometric conditions can be obtained. In contrast, the highly Cu-poor CIS films demonstrate the low quality films [17] that are out of range of our purpose in this works. So the only Cu-rich and near stoichiometric CIS films are characterized both before and after etching with KCN aqueous solution.
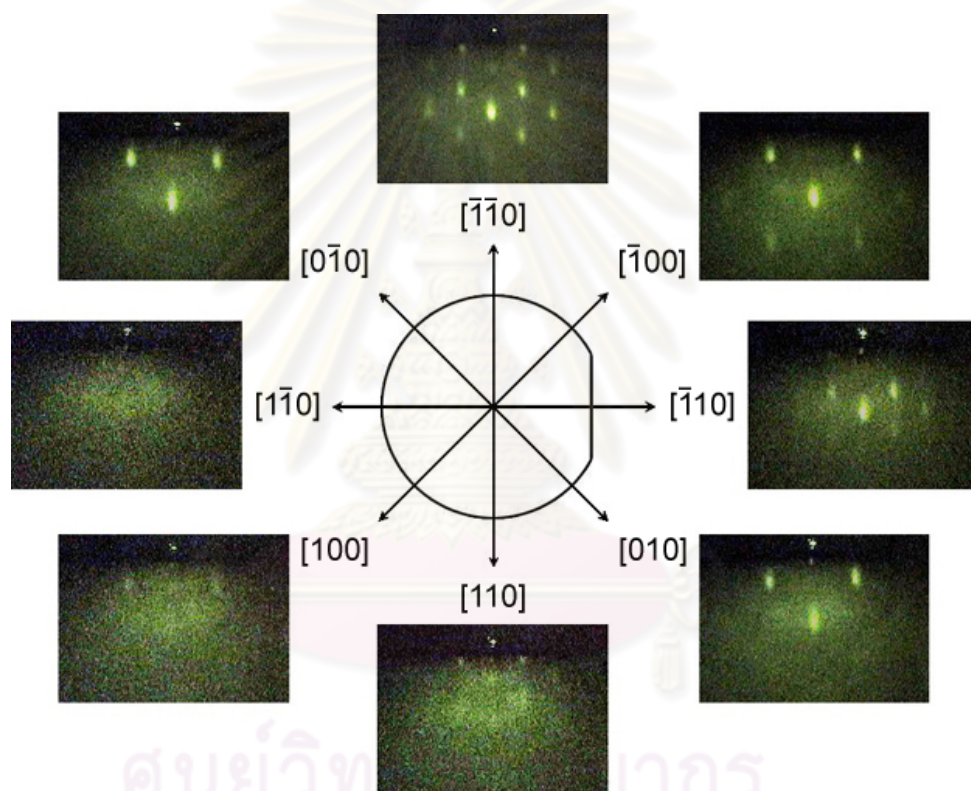
Figure 4.1: RHEED patterns of the GaAs substrate after thermal treatment along different directions.
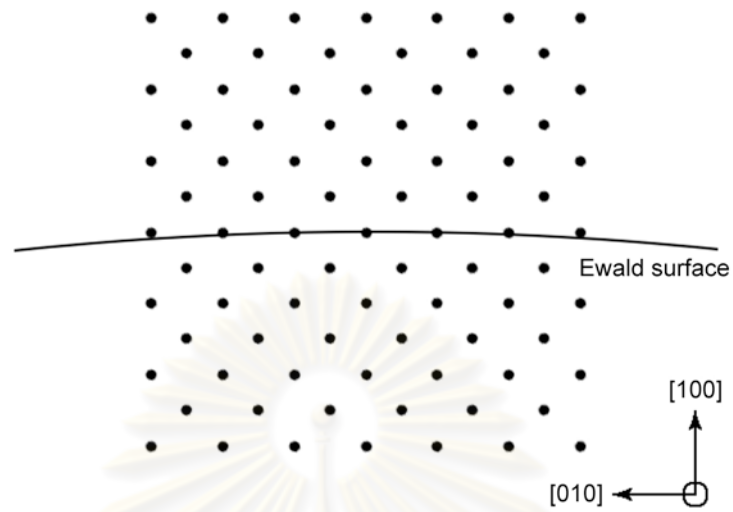
Figure 4.2: Schematic diagram of reciprocal rods of GaAs substrate intercept with Ewald surface along [100] direction.
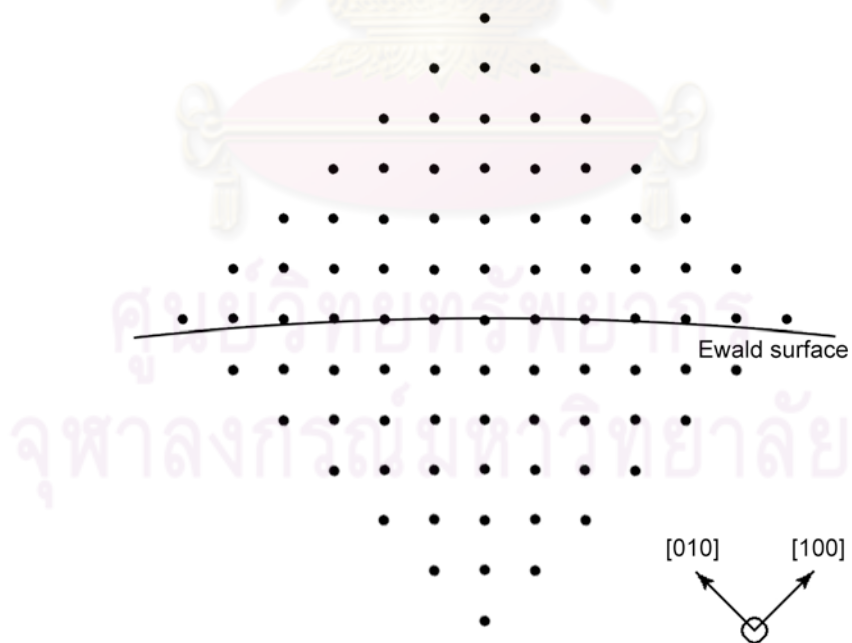
Figure 4.3: Schematic diagram of reciprocal rods of GaAs substrate intercept with Ewald surface along [110] direction.
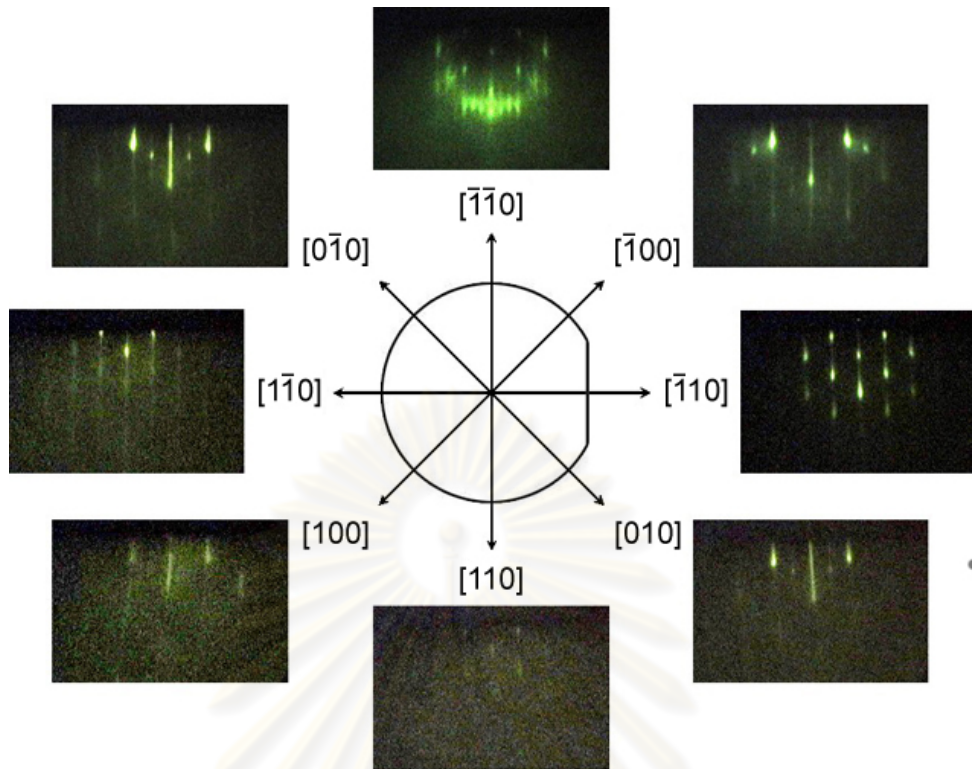
Figure 4.4: RHEED patterns of the Cu-rich CIS epitaxial films along different directions of the GaAs substrate.
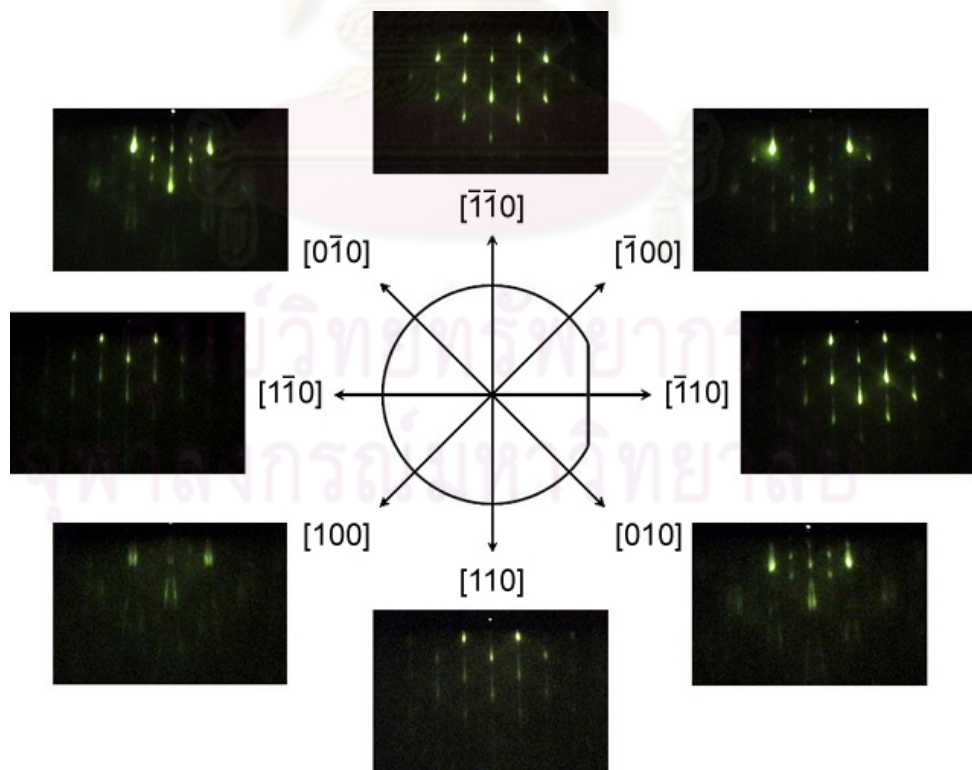
Figure 4.5: RHEED patterns of the near stoichiometric CIS epitaxial films along different directions of the GaAs substrate.
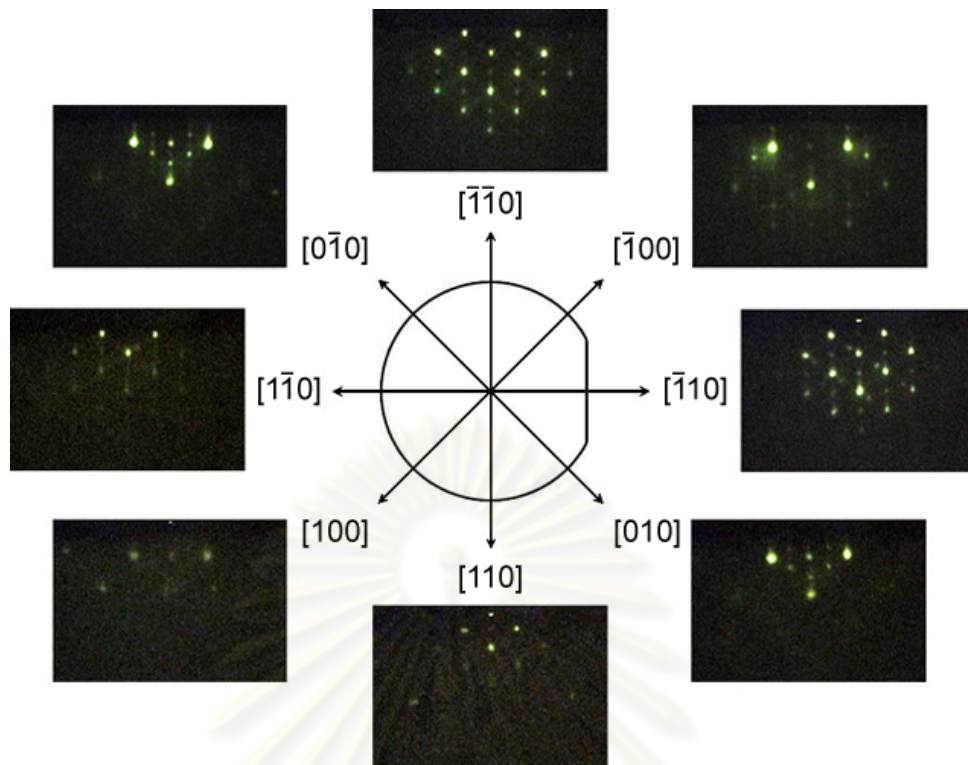
Figure 4.6: RHEED patterns of the Cu-poor CIS epitaxial films along different directions of the GaAs substrate.

4.1.1 Near Stoichiometric CuInSe$_2$ Epitaxial Films

The near stoichiometric CIS epitaxial films are grown by setting y ~ 1.0 throughout the deposition time. The substrate temperature during the deposition process is set at 600°C which the smooth surface due to the diffusion are expected. The deposition time is allowed for 3 hours in order to obtain the thickness more than 1.5 μm. In the growth process, the pyrometer signals and the output power of the temperature controller are collected at all times and used as the *in-situ* monitoring signals. Figure 4.7 shows the pyrometer signal of the near stoichiometric films. The oscillations of the pyrometer signal occur from the interference of reflection of the black body radiation between back and front surfaces of the growing films. The period of the interference oscillations refers to the thickness and the growth rate of the films. The decreasing of oscillation amplitude is due to the decrease of the transmission of the IR radiation through the substrate when the film thickness is increasing. After the growth process is finished, the as-grown films are examined for their crystallographic phase, morphology and optical response both before and after etching with KCN aqueous solution.
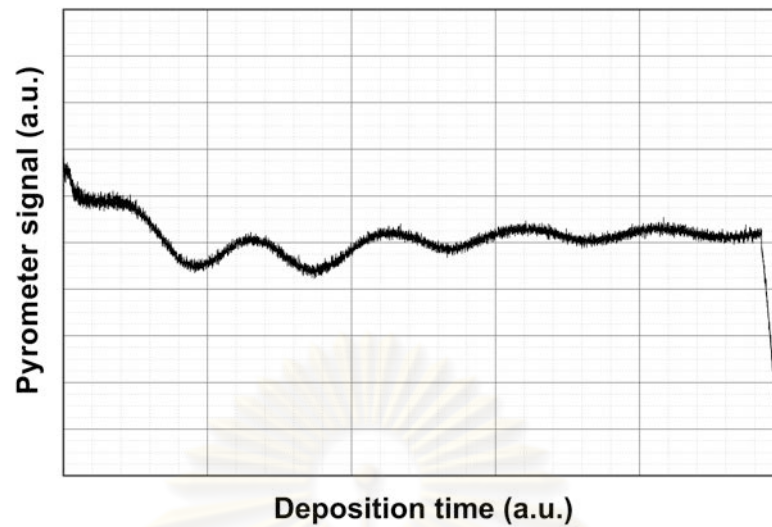
Figure 4.7: Pyrometer signal of single-stage near stoichiometric CIS epitaxial films.

The crystallographic phases of the samples are examined by the XRD. The (004) peak of GaAs is observed with the highest intensity at 2θ about $66.06°$. Figure 4.8 exhibits the XRD spectra of the near stoichiometric CIS (008) epitaxial films before and after etching with KCN solution compared with the bare GaAs substrate. The XRD result shows that the well-resolved peaks of Cu-$K_{\alpha 1}$ and Cu-$K_{\alpha 2}$ radiations of CIS (008) at 2θ about $64.23°$ and the crystallographic structure of the grown films is not changed after KCN-etching. This suggests that the MBE technique can be used to grow the high crystallographic quality CIS epitaxial films and there are no excess Cu-Se compounds on the top surface or between the grain boundaries which is generally found in the Cu-rich CIS films [26]. The AFM image shows the rectangular and step-like structure that can be seen in Fig. 4.9. Furthermore, the big holes and the small grains on the surface can be observed. The rectangular shape of the grains is due to the side plane of crystallographic structure of CIS in (001) plane. The cross-section SEM image illustrated in Fig. 4.10 demonstrates the dense CIS epitaxial films. Any hole or void cannot be observed inside the CIS layer except the voids at the surface of the substrate. The optical reflectance in Fig. 4.11 shows the interference fringes in the range of energy below the band gap that disappear about 1.04 eV. By this result, it can be used to preliminarily confirm that the grown films are the CIS films. Moreover, the unchanged results of optical reflectance before and after KCN-etching can be seen

similar to the results from XRD spectra. It confirms that there is no excess Cu-Se compound in the CIS films. The low-temperature PL spectroscopy is another type of optical characterization that is used to observe the intrinsic property. The result of PL spectrum depicted in Fig. 4.12 shows the conduction band to acceptor transition (c,A) as the dominant emission line. This strong defect-related emission line indicates the presence of a large number of point defects in the films especially the acceptor-type defects due to effect of the misfit strain [50]. This result agrees with Yu's work [51] that grows p-type bulk CIS under stoichiometric melt. Besides, the emission line accounted as the donor to acceptor band transition (D,A) can be also seen but rather weak. The fluctuation in the spectrum line at wavelengths from 1350 nm to 1450 nm is the absorption structures due to the water vapor in the air [16].
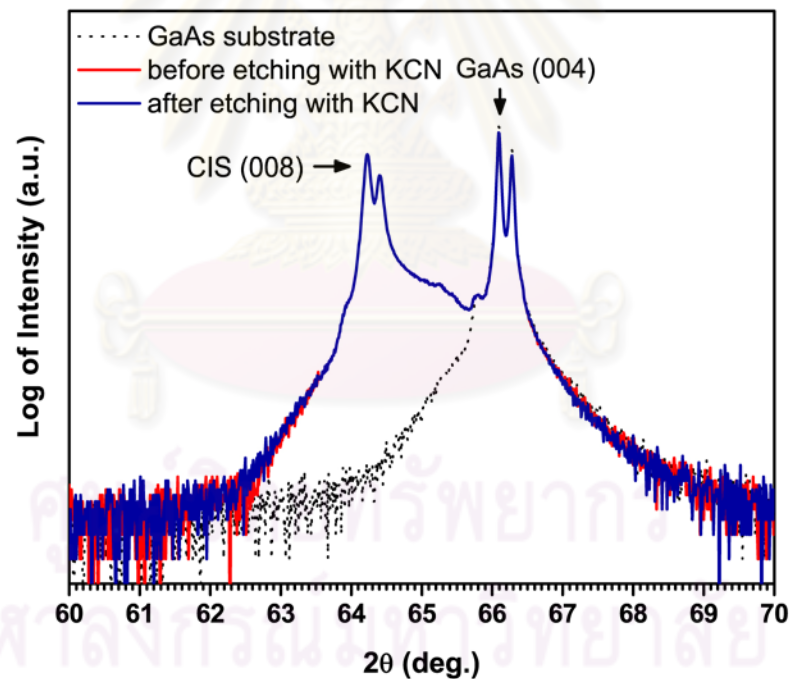
Figure 4.8: XRD spectra of single-stage near stoichiometric CIS epitaxial films before and after etching with KCN solution, compared with bare GaAs substrate.
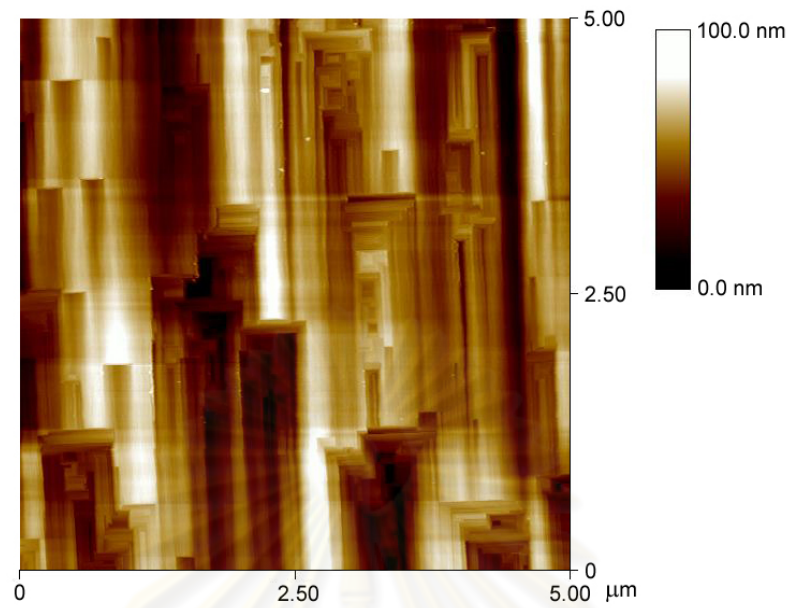
Figure 4.9: AFM image of single-stage near stoichiometric CIS epitaxial films.
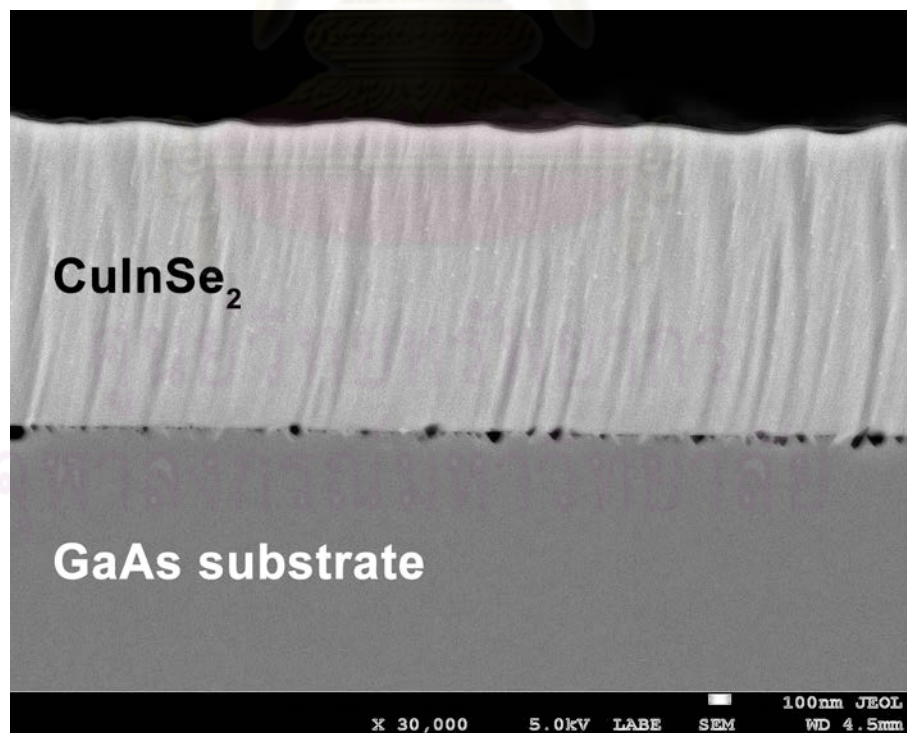
Figure 4.10: SEM cross-section image of single-stage near stoichiometric CIS films

after etching with KCN.
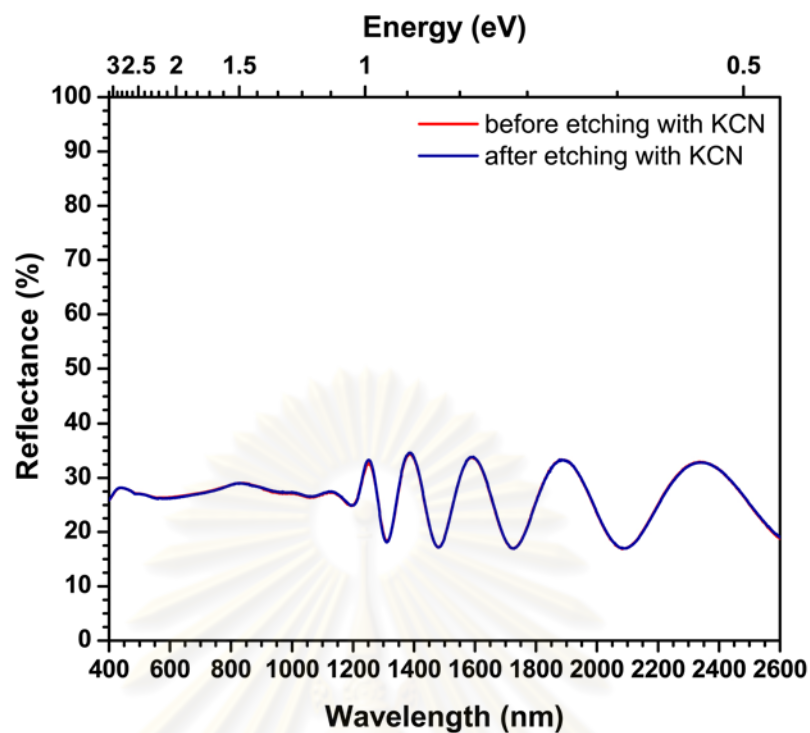
Figure 4.11: Optical reflectance spectra of single-stage near stoichiometric CIS epitaxial films.
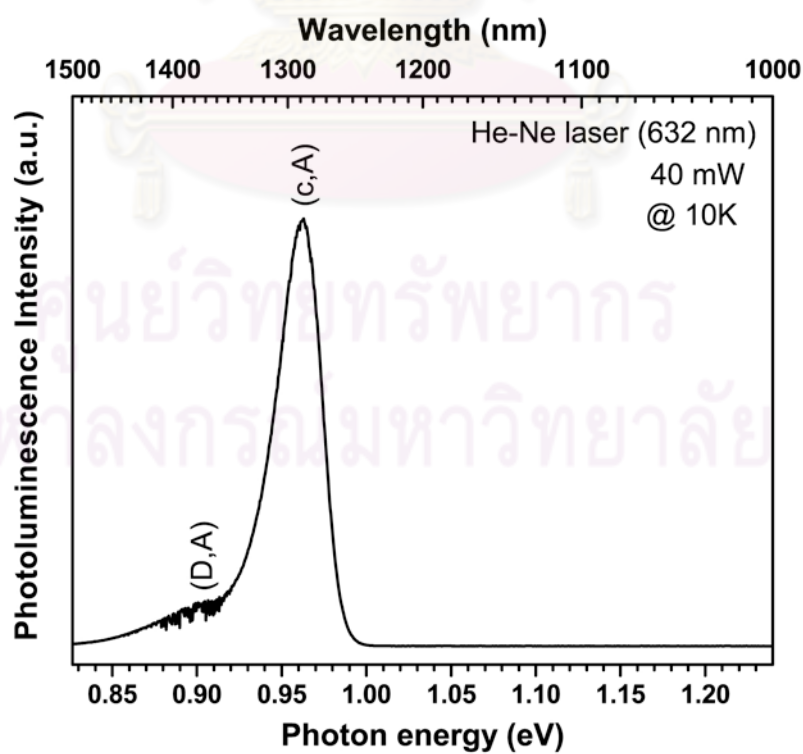
Figure 4.12: Photoluminescence spectrum of single-stage near stoichiometric CIS films at 10 K.

4.1.2 Cu-rich CuInSe$_2$ Epitaxial Films

The Cu-rich CIS epitaxial films are grown by setting y ~ 1.6 throughout the deposition time. This composition is used as the precursor in the first stage of two-stage growth process. In this work, the effect of the substrate temperature to the excess Cu-Se compounds in the Cu-rich films are studied by setting the substrate temperature at 600°C, 500°C, 450°C and 400°C. The pyrometer signals and output power of the temperature controller are stored and used as the *in-situ* monitoring signals during the deposition process. The pyrometer signal as shown in Fig. 4.13 displays the interference fringe due to the thickness of the growing film. The characteristic of the pyrometer signal decays as a function of the deposition time unlike the pyrometer signal from the near stoichiometric films which is rather constant. The as-grown films are characterized for their crystallographic phase, morphology and optical response and then they are etched with KCN solution in order to remove the excess Cu-Se compounds before the examination once again.
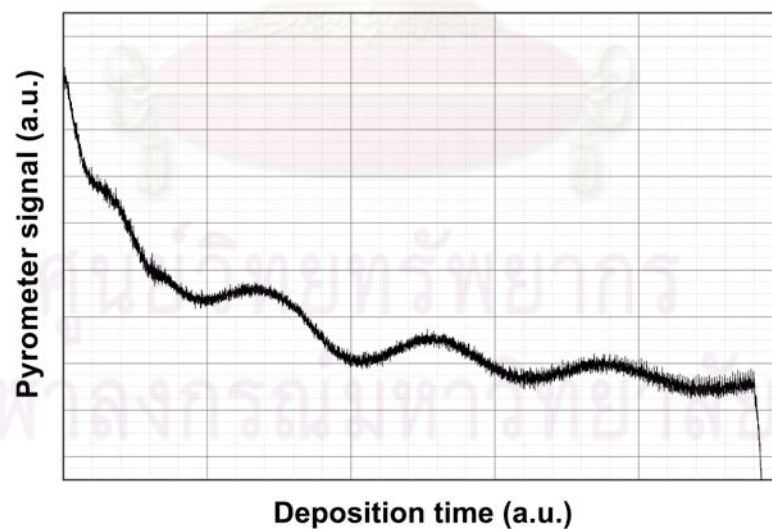
Figure 4.13: Pyrometer signal of single-stage Cu-rich CIS epitaxial film.

4.1.2.1 The characterization of Cu-rich CIS epitaxial films

The XRD spectra in Fig. 4.14 show the crystal structure of the Cu-rich CIS epitaxial films on GaAs (001) substrate at the substrate temperature of 600ºC before (red line) and after (blue line) etching with KCN. The red broadening spectrum between CIS (008) and GaAs (004) peaks in Fig. 4.14 shows the combination of CIS (008) at 2θ around 64.08º [52] and $Cu_{2-x}Se$ (004) at 2θ around 64.98º [53]. The $Cu_{2-x}Se$ is not observed after etching the film with KCN [54] and left with CIS (008) phase. The composition of KCN-etched CIS sample becomes near stoichiometric [23]. It has been found that the crystal structure of the KCN-etched Cu-rich CIS films is a well-resolved spectrum and qualitatively similar to that of the near stoichiometric CIS (008) films except the additional of unknown elevated signal above background and the peak at 2θ between 67° and 69°. This peculiar crystal structure is stable, cannot be removed by the KCN and can also be observed in $Cu_{2-x}Se$ epitaxial films grown on GaAs (001). From the database of crystallography, they are in the vicinity of the (008) crystal plane of the $CuGaSe_2$ (CGS) [55]. The AFM images of Cu-rich CIS epitaxial films before and after etching with KCN solution are shown in Figs. 4.15 and 4.16, respectively. The morphology of the as-grown Cu-rich films displays the undulation surface aligned along the $[\bar{1}\bar{1}0]$ direction. In addition, there are many rectangular shaped protrusions distributed all over the surface. Fons *et al*. have indicated that these undulations are related to heteroepitaxial strain [22] and the presence of a $Cu_{2-x}Se$ layer on the surface which may act as a surfactant. The protrusions on the surface disappear after etching with KCN and leave the numerous holes that are believed to be the residence of $Cu_{2-x}Se$ grains [56]. The optical reflectance of the as-grown films (the red line) in Fig. 4.17 shows the superposition of metallic behavior and the oscillations due to the CIS layer. The decreasing intensity of reflectance in range of near infrared is the property of metal that is believed to be the effect of Cu-Se surface [23]. This metallic phenomenon disappears after etching with KCN. The characteristic of optical reflectance after etching process (the blue line) in Fig. 4.17 is quite similar to the near stoichiometric CIS film. The disappearance of metallic behavior in optical reflectance is consistent with the disappearance of the protrusions seen in AFM image and $Cu_{2-x}Se$ (004) structure in the XRD spectrum. It can be confirmed that the protrusions on the surface which act as the metallic layer are the $Cu_{2-x}Se$ epitaxial compounds.
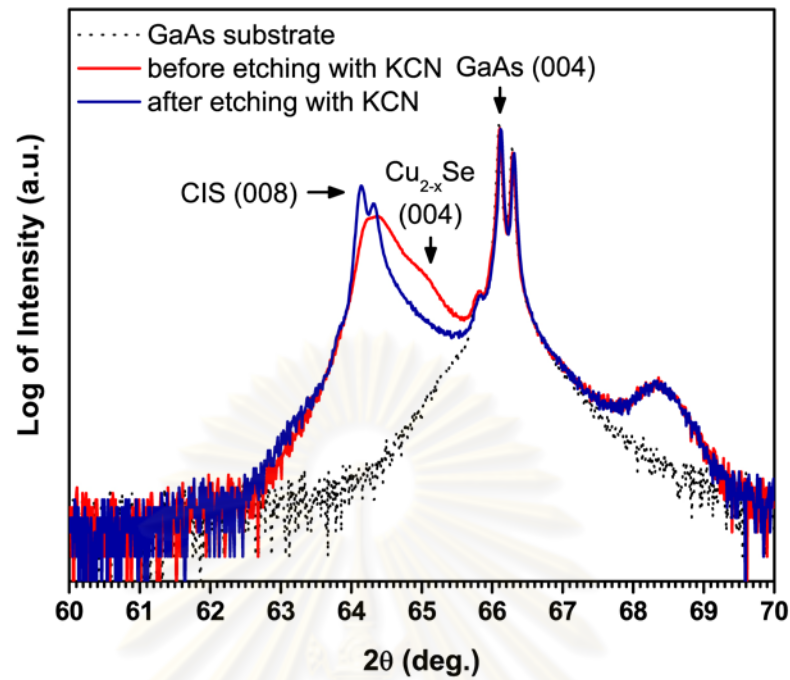
Figure 4.14: XRD spectra of single-stage Cu-rich CIS epitaxial film before and after etching with KCN solution, compared with bare GaAs substrate.
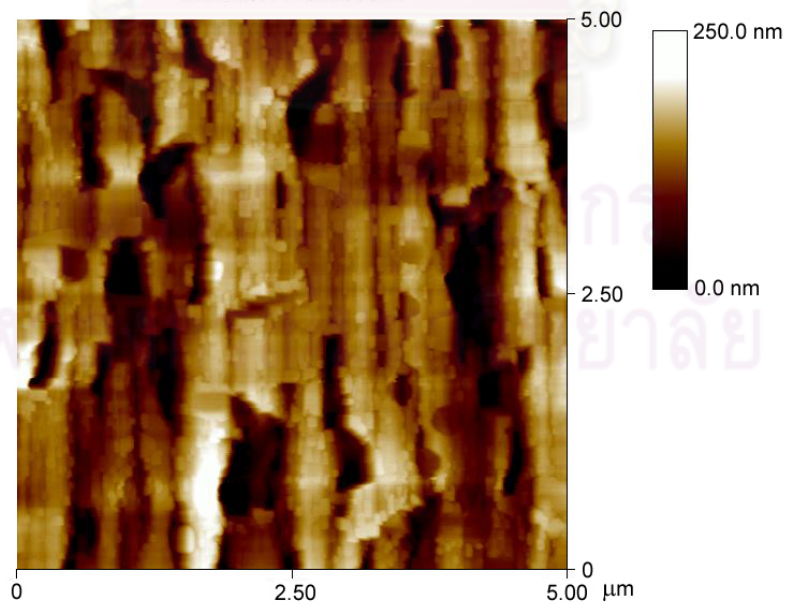
Figure 4.15: AFM image of single-stage Cu-rich CIS epitaxial film before etching with KCN.
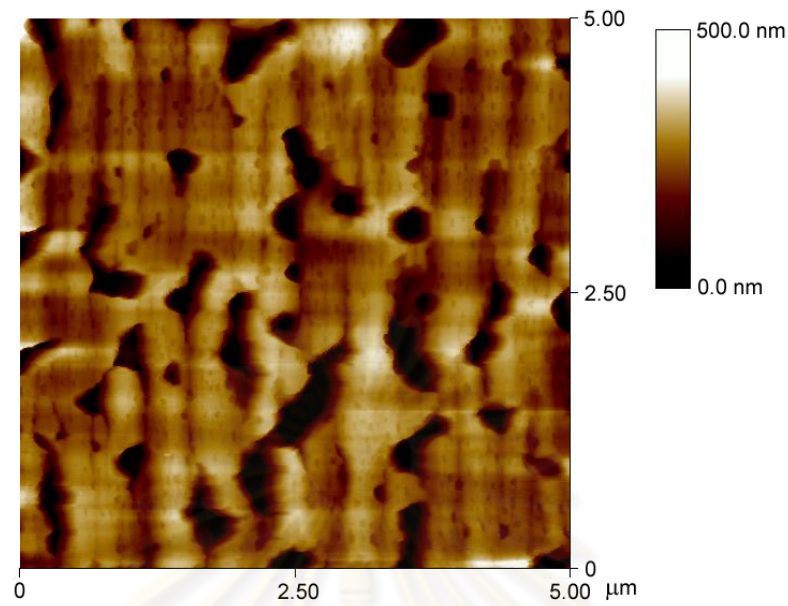
Figure 4.16: AFM image of single-stage Cu-rich CIS epitaxial film after etching with KCN.
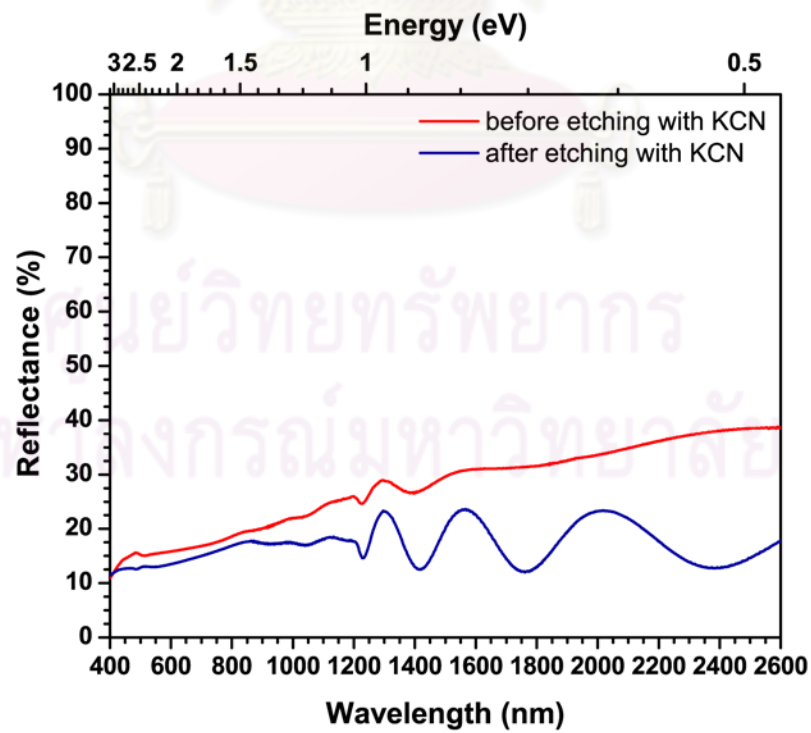
Figure 4.17: Optical reflectance spectra of single-stage Cu-rich CIS epitaxial film.

4.1.2.2 Photoluminescence of Cu-rich CIS epitaxial films

The PL spectra obtained from the Cu-rich CIS epitaxial films at temperature of 10 K are shown in Fig. 4.18. The red line is the PL spectrum of the film before etching with KCN and the blue line is the PL spectrum after etching process. It can be seen that the characteristics of the PL spectrum before and after etching process are distinguishable and different from the work reported by Niki *et al.* [23]. Both spectra have the same emission lines but the PL intensities are different. A donor to valence band transition is dominant in the as-grown film while a conduction band to acceptor transition and near-band-edge exciton (E_x) emission is predominantly observed in the KCN-etched CIS films. It is believed that the main cause of difference is due to the effect of crystal structure from the combination of the excess $Cu_{2-x}Se$ and CIS epitaxial films. After the excess $Cu_{2-x}Se$ is removed, the donor-type defects are reduced and show the perfect crystallinity of CIS epitaxial structure that can be indicated by the occurrence of near-band-edge exciton emission line. Moreover, we find the conduction band to acceptor emission line which relate to the acceptor-type defects in the films that are naturally found in the near stoichiometric and the Cu-rich CIS films [50]. The main cause of acceptor-type defect is the Cu-vacancy (V_{Cu}) [57]. The self-healing mechanism is a result of the mobility of Cu and reactions involving Cu-related defects and defect complexes [58]. The CIS epitaxial films which are grown under the excess Cu-atoms can reduce the self-healing mechanism in crystal structure from Cu-deficiency and then get the perfect crystallinity. In addition, it plays the important role in lateral growth mechanism giving rise to the high quality films. The position of sharp peak of near-band-edge exciton emission is about 1.039 eV. The PL emissions of the sample can be observed up to room temperature. Figure 4.19 shows the temperature dependence PL spectra of the KCN-etched CIS films. The blue-shifts and the increase of line width of near-band-edge exciton emission with increasing temperature are often found in I-III-VI_2 semiconductors [51]. The band gap of CIS, E_g, can be approximated from the energy of the near-band-edge exciton emission (E_x) using the relation $E_g = E_x + E_a$ [18], where E_a is the activation (binding) energy of the exciton obtained from empirical relation:

$$I = \frac{I_0}{1+C\,exp\left(-\dfrac{E_a}{k_B T}\right)}. \tag{4.1}$$

The activation energy of the exciton is determined by fitting the intensity of the PL peaks of near-band-edge exciton emission and the reciprocal temperature using Eq. (4.1), where I_0, C and E_a are fitting parameters, k_B is the Boltzmann constant and T is the temperature in Kelvin [59]. From the fitting result shown in Fig. 4.20, the activation energy of the exciton is about 6 meV. The band gap energy of the KCN-etched near stoichiometric CIS film is about 1.045 eV at 10 K which is slightly different from the band gap energy of the near stoichiometric CIS epitaxial films (1.046 eV) [18].
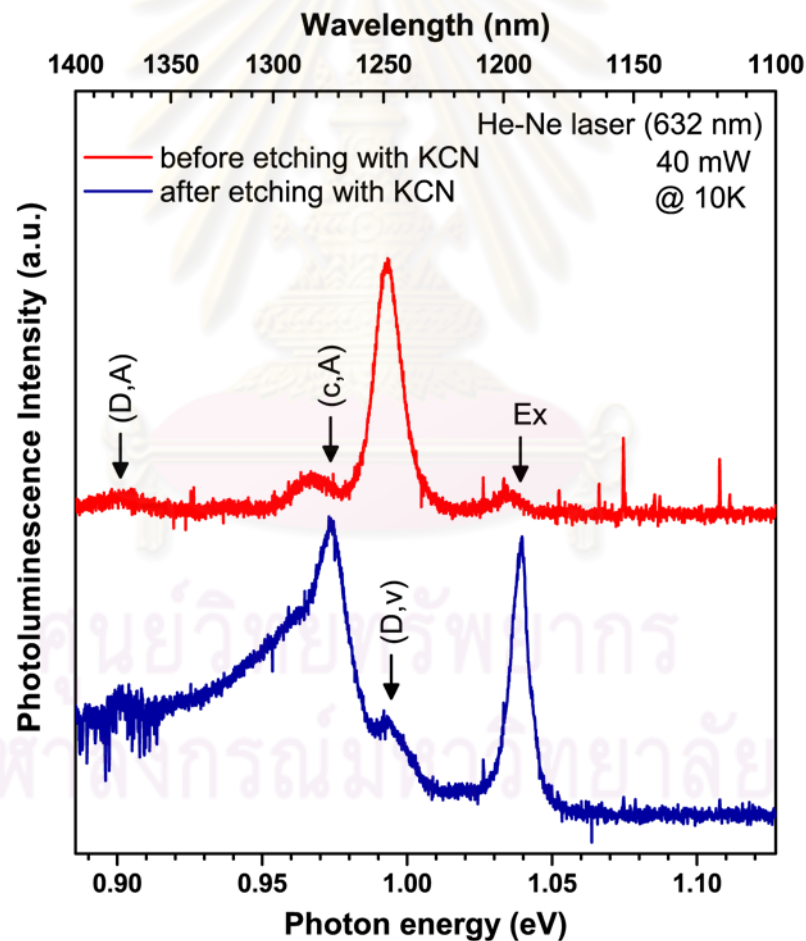
Figure 4.18: Photoluminescence spectra of single-stage Cu-rich CIS epitaxial films before and after etching with KCN at 10 K.
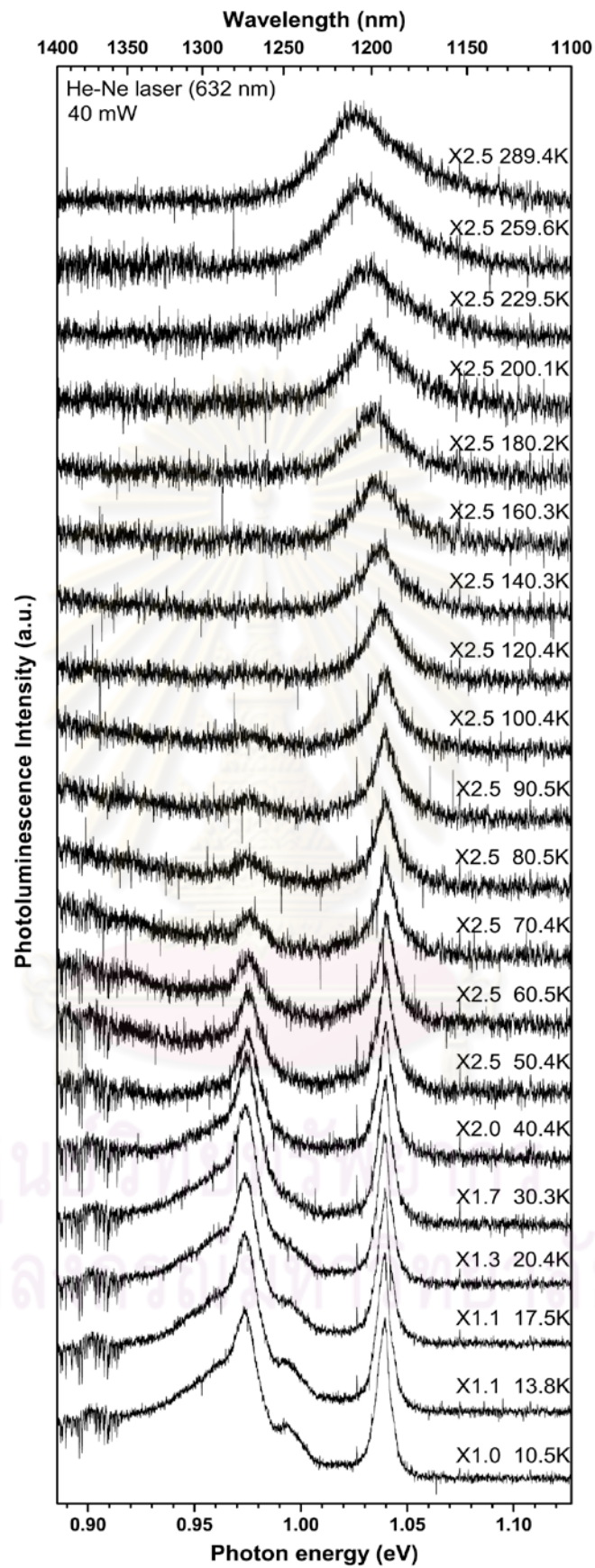
Figure 4.19: Temperature dependent photoluminescence spectra of single-stage Cu-rich CIS epitaxial films after etching with KCN.
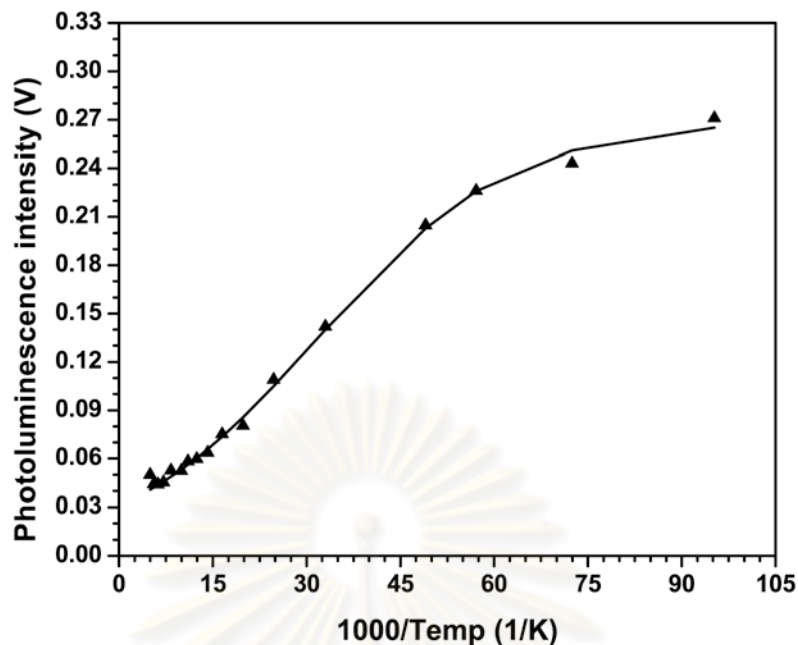
Figure 4.20: The intensity of exciton peak as a function of reciprocal temperature.

4.1.2.3 The effect of substrate temperature

The substrate temperature is the important key parameter for the growth of epitaxial films [14, 17]. Figure 4.21 shows the optical images from optical microscope with the magnification of 45x. It can be seen that the homogeneity of the grown films is significantly dependent upon the substrate temperature. The films that are grown under the substrate temperature at higher than 500°C reveal the higher surface uniformity as can be seen in Fig. 4.21(a) and (b). When the substrate temperatures are reduced below 500°C, the films' surface is slightly changed to the rougher surface that is shown in Fig. 4.21(c) and (d). The crystallographic structure which is characterized by the XRD measurement demonstrates that the substrate temperature also significantly influences the quality of the grown films. Figure 4.22 illustrates the results of XRD spectra before (red line) and after (blue line) etching with KCN. The broadening spectrum in all samples is attributed as the Cu-rich CIS films. In addition, it is found that there are some differences in the crystallographic phase of the excess Cu-Se compounds in the as-grown films and becomes more distinguishable. From the phase diagram of the Cu-Se system, it indicates that the phase of Cu-Se compounds is very sensitive to the temperature and the composition between Cu and Se constituents. Moreover, the shifts of broadening spectrum are observed when the

substrate temperatures are decreased. After etching with KCN, the XRD spectra show the well-resolved peak of CIS (008) but they are different in details. The residual excess Cu-Se structure cannot be found in all samples. The details of XRD spectra of CIS (008) peak such as peak position, c-axis and full width at half maximum (FWHM) that determines the crystal deviation are listed in Table 4.1. The results reveal the fact that the decrease of substrate temperature affects the quality of crystallographic structure that can be indicated by the higher deviation in crystal structure. Furthermore, it can be found that the great shift of CIS (008) spectral line is in the samples grown with the substrate temperature below 450°C. This shift is related to the strain in the films. From these results, it can be concluded that the phase of excess Cu-Se compounds plays the important role in strain relief and must rely on the substrate temperature.
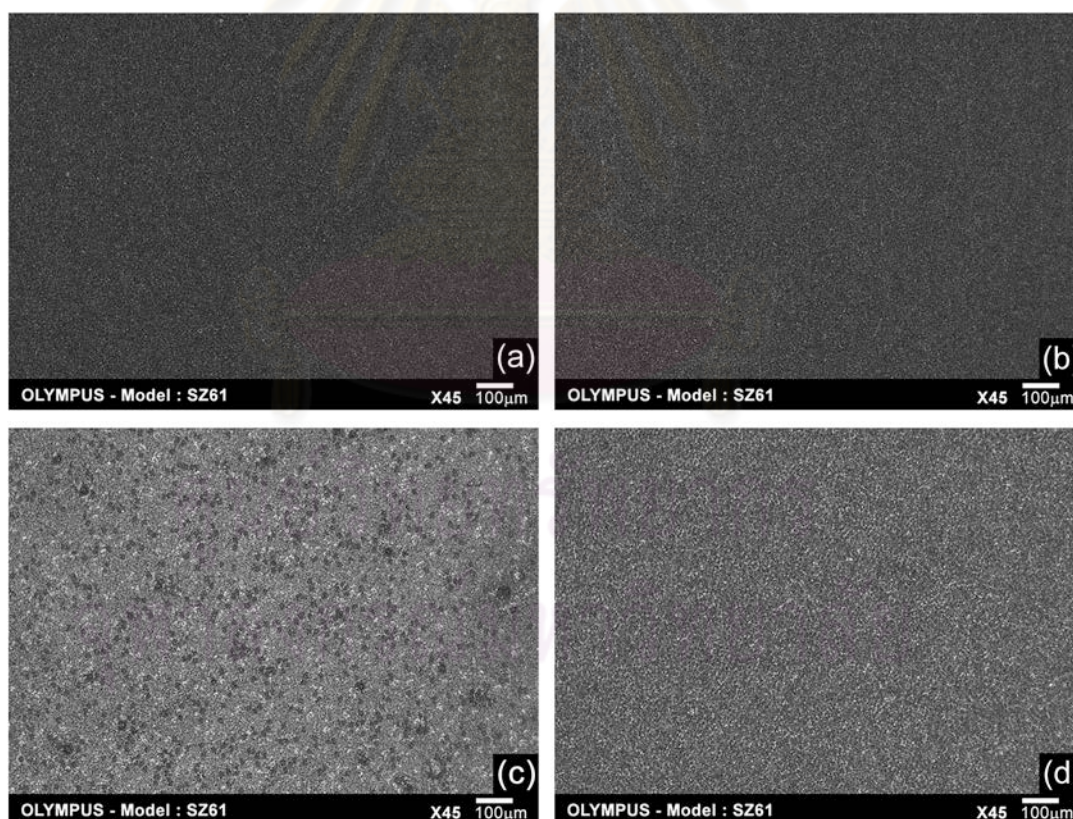
Figure 4.21: Optical micrographs of CIS epitaxial films at substrate temperatures (a) 600°C, (b) 500°C, (c) 450°C and (d) 400°C.
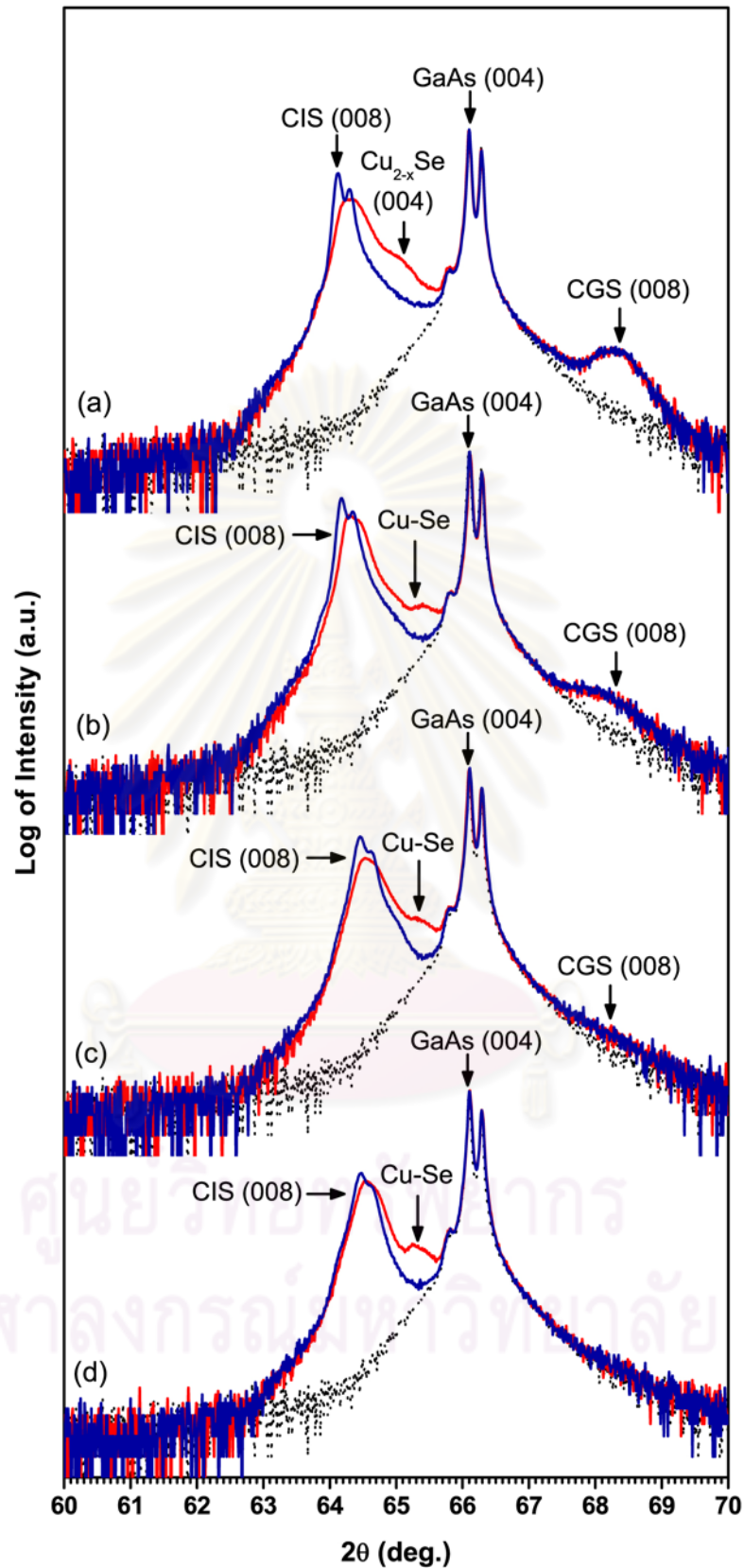
Figure 4.22: XRD spectra of CIS epitaxial films before (red line) and after (blue line) etching with KCN solution at substrate temperatures (a) 600°C, (b) 500°C, (c) 450°C and (d) 400°C, compared with GaAs substrate.

Table 4.1: The position of XRD spectrum, c-axis and full width at half maximum (FWHM) of CIS (008) at various substrate temperatures.

Tsubstrates	2θ	c-axis (Å)	FWHM
600°C	64.12°	11.609	0.120
500°C	64.18°	11.600	0.129
450°C	64.45°	11.554	0.169
400°C	64.46°	11.553	0.195

4.1.2.4 The presence of CuGaSe$_2$ interfacing layer [60]

The Cu-Se epitaxial films are also deposited on the GaAs (001) substrate. Figure 4.23 shows the XRD spectra of the Cu$_{2-x}$Se films before and after etching with the KCN. The inset shows the RHEED patterns at the end of the deposition process verifying that the Cu$_{2-x}$Se can be formed as an epitaxial layer on GaAs(001) substrate. The XRD spectrum shows the well-resolved Cu$_{2-x}$Se (004) peaks due to Cu-Kα_1 and Cu-Kα_2 lines. After etching with KCN, the (004) peak of Cu$_{2-x}$Se disappeared and leaving with only the trace of the peculiar peak at 68º < 2θ < 69º similar to those found in the Cu-rich CIS films. This broad peak is not accounted for any phases of Cu$_{2-x}$Se compound and suggests that this structure is stable. However, this broad peak is in the vicinity of the (008) crystal plane of the CGS even if the Ga flux is not allowed during the deposition. The results in Fig. 4.24 exhibit the optical reflectance of the bare GaAs substrate and the Cu-Se films before and after etching with KCN solution. The optical response of Cu$_{2-x}$Se films before etching with KCN in Fig. 4.24 (red) shows the high reflection in range of infrared spectrum and decrease in range of visible light and ultraviolet spectrum. This phenomenon is the characteristic of metal and semi-metal films. It can be confirmed that the metallic-like phenomenon in the as-grown of Cu-rich CIS films is the effect of Cu$_{2-x}$Se surface. After etching with KCN, the optical reflectance in Fig. 4.24 (blue) is not the same as optical behavior of bare GaAs substrate in Fig. 4.24 (black). This evidence suggests that there is some layer remains at the surface of GaAs substrate after the etching process. This result is consistent with the result of XRD spectra. They are further postulated that the peculiar structure may be CGS (008) that exists at the interface between the grown films and the substrate.

To verify the existence of the CGS layer, the Cu-rich CGS epitaxial films are directly grown on GaAs (001) substrate. Figure 4.25 shows the comparison of XRD spectra of (a) the near stoichiometric CIS film, (b) the $Cu_{2-x}Se$ film, (c) the Cu-rich CIS film and (d) the Cu-rich CGS film. It can be seen that the peculiar spectrum can be found only in the $Cu_{2-x}Se$ films and the Cu-rich CIS films but it cannot be observed in near stoichiometric films. The position of the peculiar spectra of the $Cu_{2-x}Se$ in Fig. 4.25(b) and the Cu-rich CIS in Fig. 4.25(c) resemble the position of crystallographic phase of CGS (008) as identified in Fig. 4.25(d). This suggests that there is a formation of the CGS at the interface of the Cu-rich CIS or the $Cu_{2-x}Se$ films and the GaAs substrate due to the diffusion of Ga atoms from the GaAs substrate and the excess $Cu_{2-x}Se$ that reside everywhere in the growing films. In this mechanism, the substrate temperature should be the key parameter for this role which the effect of the substrate temperature to CGS formation is exhibited in Fig. 4.26. The reductions in the XRD intensity can be observed, i.e. thinner interface layers at lower substrate temperatures. The thickness of the CGS interface layer is indirectly determined from the interference fringes of optical reflectivity oscillations after etching the as-grown Cu-rich CIS films with the KCN and deduced from the area under the curve of the XRD spectrum after the elimination of the background from the GaAs substrate. From this relation, the thickness of the CGS interface layers grown with the substrate temperatures at 600ºC, 500ºC, 450ºC and 400ºC are found to be approximately 16, 7, 1 and 0 nm, respectively, as shown in Fig. 4.27. Using the linear fit, it suggests that the excess $Cu_{2-x}Se$ is inactive in forming the CGS interface layer when the substrate temperature is below 430ºC. It is worth to note here that all substrates are first heated to 600ºC for 10 minutes to eliminate the residual oxides on the surface before reducing to the deposition temperatures.
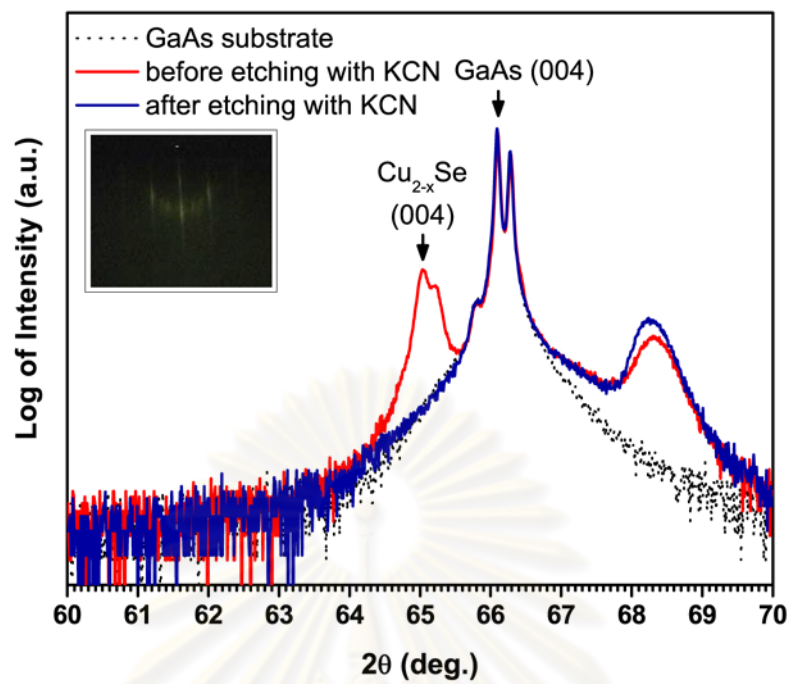
Figure 4.23: XRD spectra of Cu-Se epitaxial films before and after etching with KCN solution, compared with bare GaAs substrate. Inset shows RHEED pattern of Cu-Se epitaxial films at the end of deposition process.
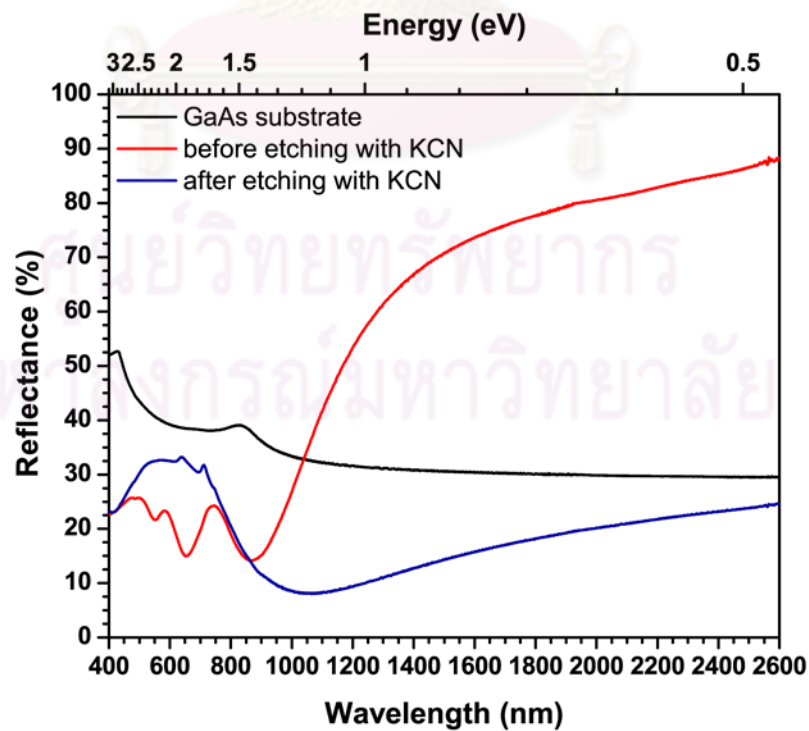
Figure 4.24: Optical reflectance spectra of GaAs substrate and Cu-Se epitaxial films.
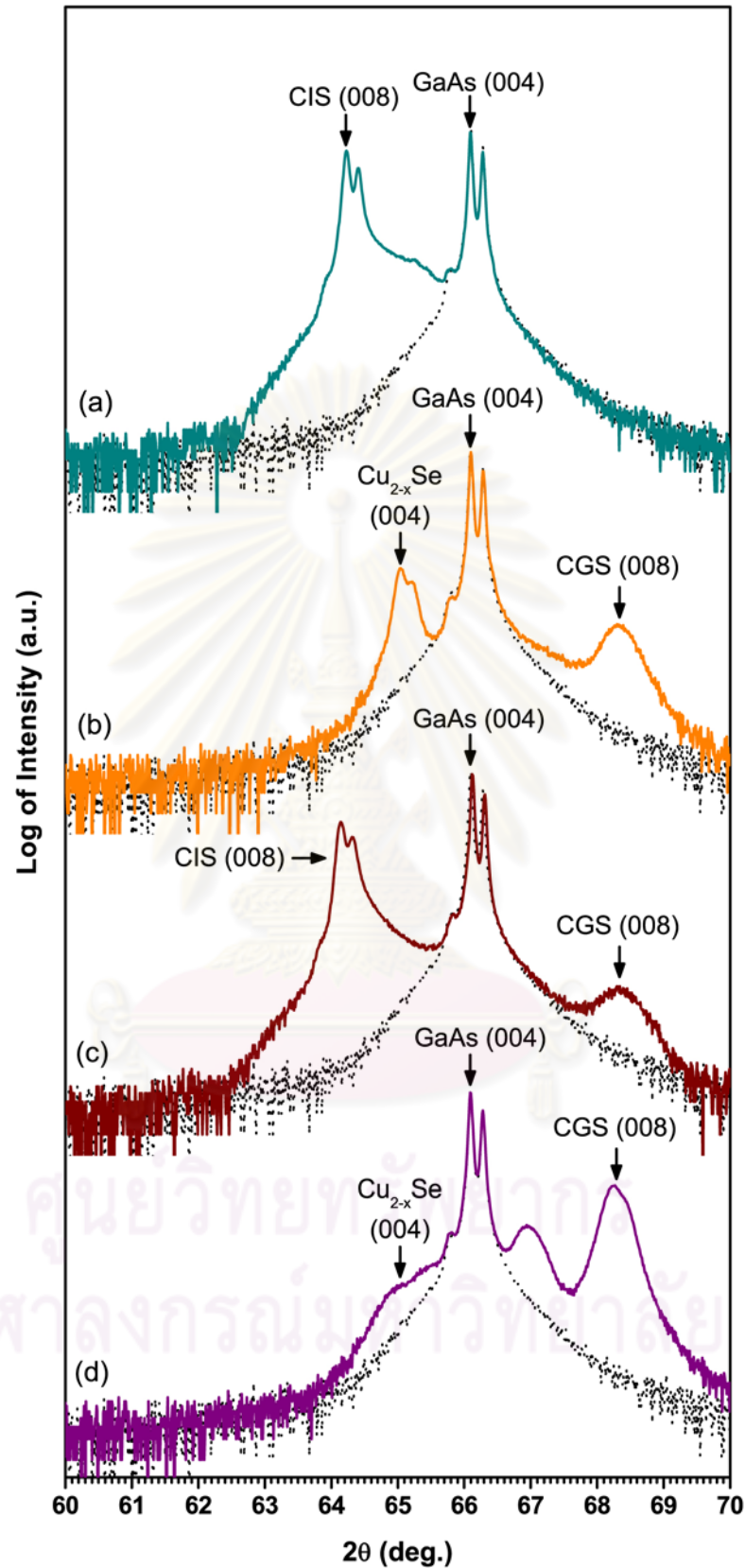
Figure 4.25: XRD spectra of (a) near stoichiometric CIS epitaxial films, (b) Cu-Se epitaxial films, (c) Cu-rich CIS epitaxial films after etching with KCN and (d) Cu-rich CGS epitaxial films, compared with GaAs substrate.
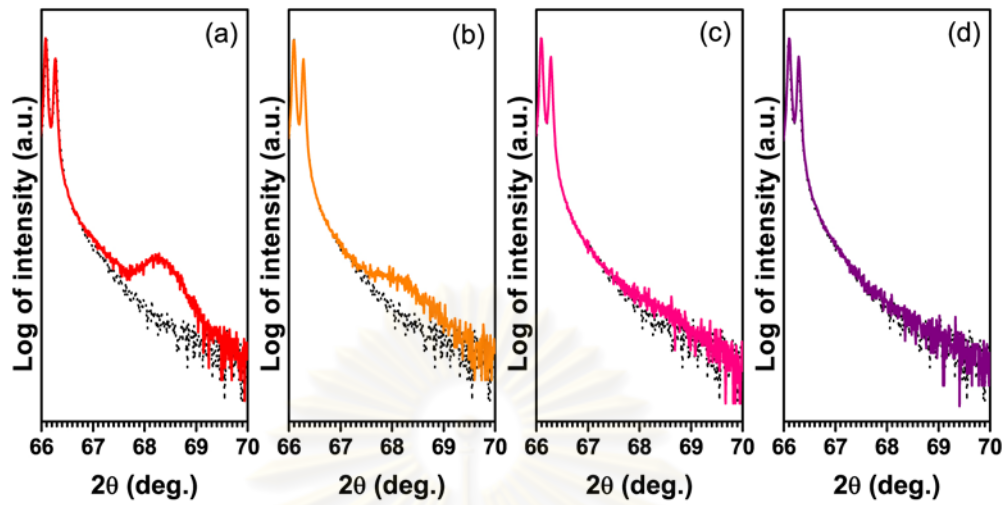
Figure 4.26: XRD spectra of the interface layers in the Cu-rich CIS films after etching with KCN at substrate temperatures (a) 600°C, (b) 500°C, (c) 450°C and (d) 400°C. The dotted line is the structure of GaAs substrate.
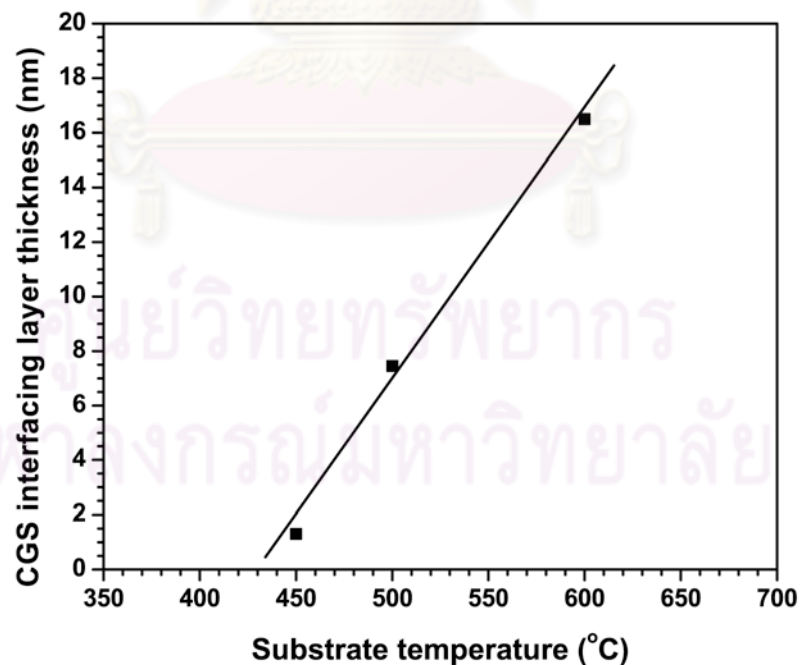
Figure 4.27: Relationship between the thickness of the CGS interface layer and the substrate temperature.

The direct investigation methods such as the cross-section SEM and the cross-section STEM imaging are used to prove the existence of the CGS interface layer. For the cross-section SEM imaging, the KCN-etched Cu-rich CIS film is cut and then its cross-section surface is polished by ion milling. The specimen is examined in back-scatter image (BEI) mode that could resolve the layer in the films. The SEM image of the KCN-etched Cu-rich CIS films is illustrated in Fig. 4.28. It shows many deep holes that have been the dwelling of $Cu_{2-x}Se$ compounds prior to removing by KCN. This trace is very important which can be used to indicate where the excess $Cu_{2-x}Se$ dwells. Furthermore, the thin layer between the CIS film and the GaAs substrate can be observed that confirms the existence of the interface layer. This layer can also be clearly seen in the high resolution STEM image. The sample is cut in a narrow stripe and then thinned down by ion slicer in order to avoid the electron interaction with the below material when analyzing the composition of the film using EDS. The high angle annular dark field (HAADF) image obtained from the STEM is shown in Fig. 4.29 including spot EDS spectra at the locations; (a) grown films, (b) interface and (c) GaAs substrate. The examination results of the EDS measurement are demonstrated in Fig. 4.30. From the STEM image, the Kirkendall voids [60] are clearly seen near the interface due to imperfection of the substrate surface and can be observed in the area of the interface layer. The EDS spectra show that region (a) is the CIS layer and region (b), as interface layer, is composed of the Cu, Ga and Se elements with the composition ratio Cu : Ga : Se of approximately 1.1 : 1.0 : 2.0. No trace of In could be observed in the interface layer. These results verify that the interface layer is the CGS sandwiched between the CIS and the GaAs substrate. It is worth to note here that there is a slight diffusion of Ga into the CIS layer as seen in the EDS spectrum in region (a).
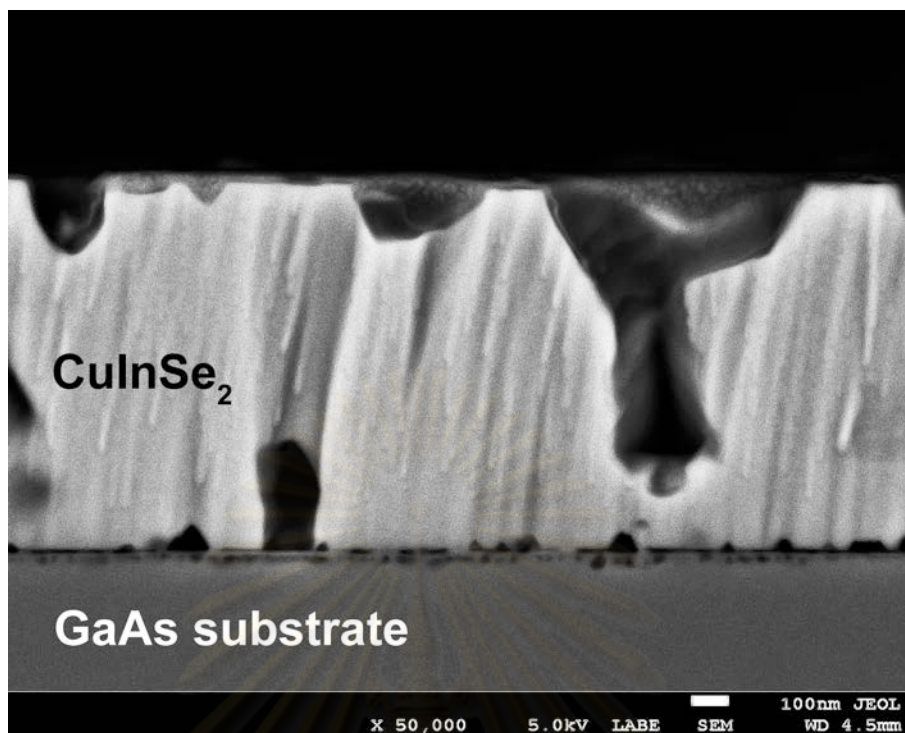
Figure 4.28: SEM cross-section image of Cu-rich CIS films after etching with KCN.
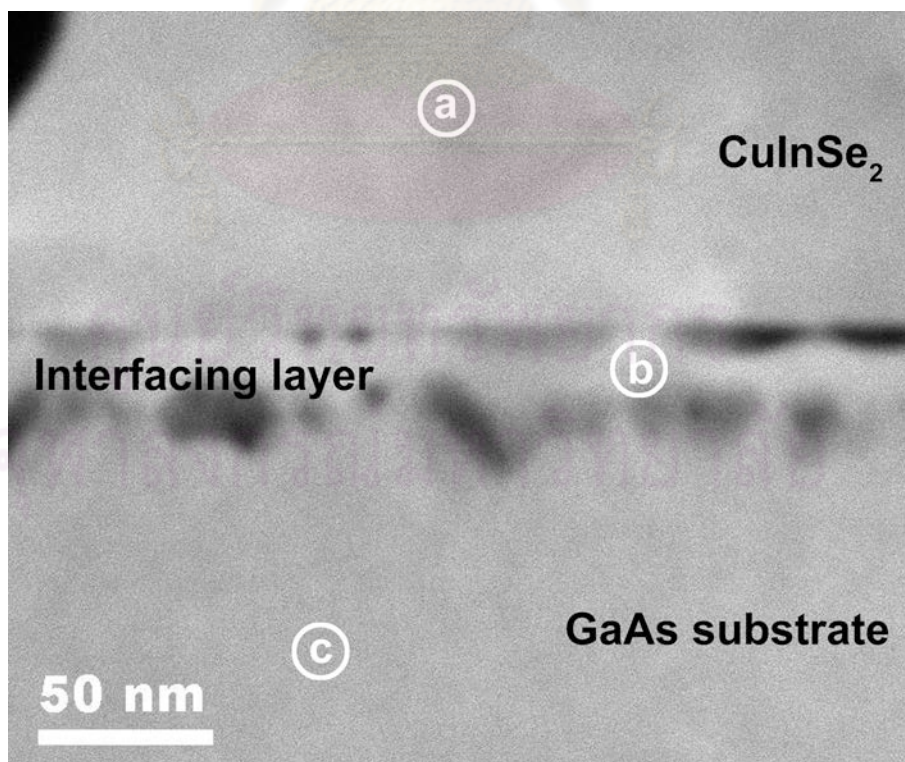
Figure 4.29: Cross-section STEM micrograph of Cu-rich CIS epitaxial films after etching with KCN.
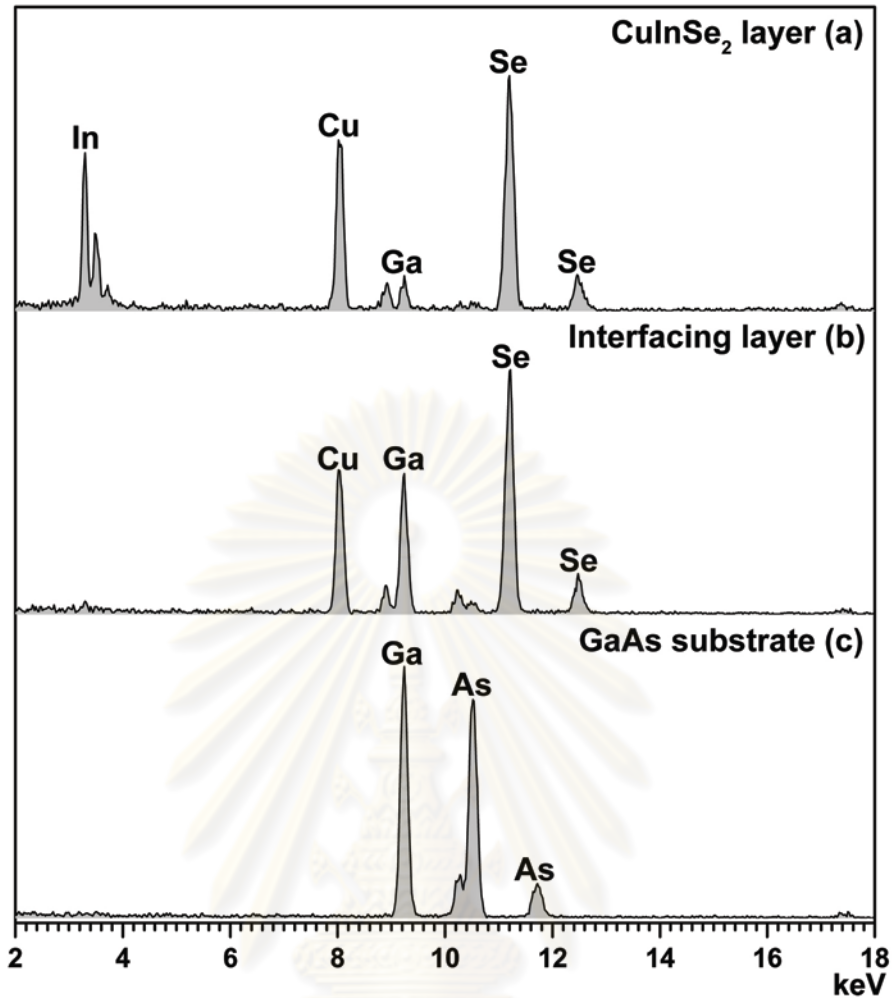
Figure 4.30: EDS spectra of Cu-rich CIS films after etching with KCN.

4.1.2.5 Growth model of Cu-rich CuInSe$_2$ epitaxial films

From the entire results and discussion, I propose the growth model of the Cu-rich CIS epitaxial films as the following. When the fluxes of Cu, In and Se constituents reach to the hot surface of GaAs substrate, the formation of CIS epitaxial films will be occurred simultaneously with the excess Cu$_{2-x}$Se epitaxial compounds. The excess Cu$_{2-x}$Se compounds can reside both on the top surface and inside the CIS layer. Because of the imperfection of GaAs surface from the thermal heating, the Ga-atoms near the surface can diffuse up into the growing films during the deposition process that result in the occurrence of Kirkendall voids [61]. The detection of Ga peak of EDS spectrum in CIS layer is the important evidence that verifies the diffusion of Ga-atoms from the substrate. The excess Cu$_{2-x}$Se compound in the growing films can be combined with the diffusive Ga-atoms to form as the CGS layer

dwelling at the area of substrate's surface as the interface layer between the growing film and the substrate. The thickness of this layer is limited by the substrate temperature and deposition time. The growth model of the Cu-rich CIS epitaxial films is depicted in Fig. 4.31. The CIS epitaxial films that are formed under the excess Cu condition show the perfect crystallographic structure which is confirmed by the exciton detection. The key parameter of this growth is the excess $Cu_{2-x}Se$ compounds that play the different role due to the substrate temperature. The lateral growth mode as the important mechanism in strain relief during the deposition is also dependent upon the excess $Cu_{2-x}Se$ compounds.
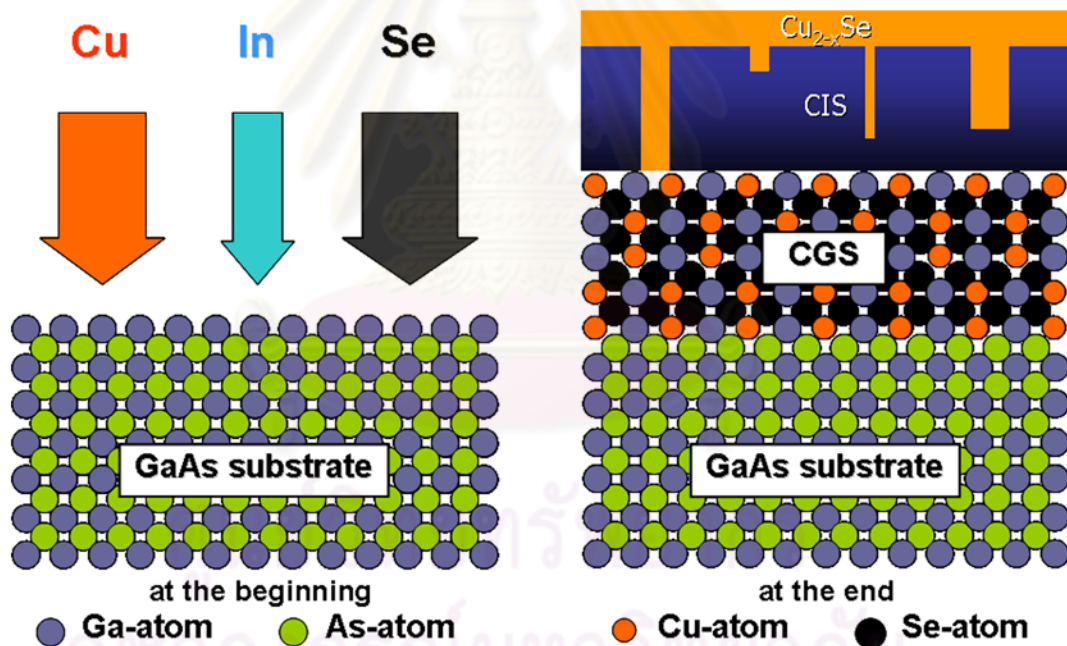
Figure 4.31: Growth model of Cu-rich CIS epitaxial films.

4.2 Results and Discussion of the CuInSe$_2$ Epitaxial Films Grown by Two-stage Growth Process

The two-stage CuInSe$_2$ epitaxial films are grown on GaAs (001) substrate by starting with the composition y ~ 1.6 in the first stage of the deposition process. The substrate temperature is kept constant at 600°C throughout the deposition time. The deposition time in the first stage (t$_1$) is 3 hours in all samples. After that, the shutter of Cu-source is shut off and remaining only In- and Se-sources. The deposition process of each sample is stopped at the composition y ~ 1.6, 1.3, 1.1, 1.0 and 0.9 that are calculated using Eq. 3.9. Figure 4.32 shows the pyrometer signal of the two-stage growth process. It can be seen that the signal in the first stage is similar to the single-stage Cu-rich films. When the Cu-source is not applied, the temperature of the film suddenly drops due to the decrease from the radiation reflection of the Cu-source. In the second stage, the transition of the composition will change from the Cu-rich to the Cu-poor film that causes the change in the emissivity. This effect can be observed by the increase of the pyrometer signal. The increasing signal will appear until the composition of the films is completely transformed to the Cu-poor. The pyrometer signal will display the sharp knee and the flat plateau. RHEED apparatus is used to examine the deposition process to guarantee the epitaxial growth of all samples. All as-grown films are characterized for their crystallographic structure, the surface morphology and optical properties to study the evolution of the growth.
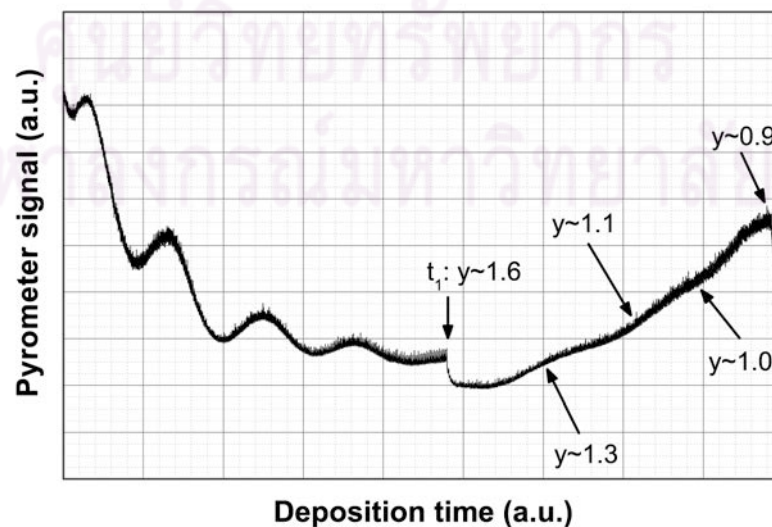
Figure 4.32: Pyrometer signal of two-stage CIS epitaxial films.

At the end of the deposition process, RHEED examination shows the streaky patterns in all samples implying the high quality epitaxial films. Figure 4.33 shows the evolution of the crystallographic structure of the two-stage CIS epitaxial films that obtained from the XRD measurement. It can be seen that the mixed phases between CIS (008) and $Cu_{2-x}Se$ (004) in the Cu-rich films gradually decreases after the excess $Cu_{2-x}Se$ compounds are incorporated with In atoms in the second stage of the deposition and convert to the CIS compound. The evidences that indicated the CIS formation are the reduction of the $Cu_{2-x}Se$ (004) peak and the beginning of the well-resolved peak of CIS (008) at 2θ around 64.16°. The sharper line width of the CIS (008) peak is related to the disappearance of $Cu_{2-x}Se$ (004) peak. The excess $Cu_{2-x}Se$ is perhaps one of the causes that perturbs the crystallographic structure of the CIS epitaxial films. Moreover, it can also be found that the CGS interface layer exists in all samples except the sample that evolves to the Cu-poor phase. Besides, the shift of the CIS (008) peak from 2θ around 64.16° to 64.25° is also observed. The AFM images in Fig. 4.34 reveal the evolution of surface morphology of the two-stage CIS epitaxial films. It shows that the undulations that occur from the Cu-rich condition in the first of the deposition process are the foundation pattern of the surface evolution. The numerous protrusions of the excess $Cu_{2-x}Se$ compound on the surface that can be detected in the Cu-rich CIS films are hardly observed when the composition of the films (y) is below 1.1. The disappearance of the protrusions is due to the CIS formation in the second stage. This result agrees with the reduction of $Cu_{2-x}Se$ (004) peak in XRD spectra. Furthermore, it can be found that the size of the undulation pattern that refers to the grain size is larger and leave the bigger holes when the composition changes to the Cu-poor phase. The results of optical reflectance as shown in Fig. 4.35 show the similar behavior as the XRD and the AFM results. The reduction of the metallic behavior of $Cu_{2-x}Se$ surface is again observed when the composition of the grown films evolves from the Cu-rich to the Cu-poor. The effect of metallic behavior disappears and shows the strong oscillations in the reflectance spectra after the composition of the films (y) is below 1.1. This phenomenon is consistent with the disappearance of protrusions in the AFM images. The reflectance oscillations stop at the energy of about 1.04 eV of the CIS compound except the Cu-poor CIS films whose oscillations stop at the energy of about 1.07 eV. This observation presumably involves the shift of CIS (008) peak in XRD result.
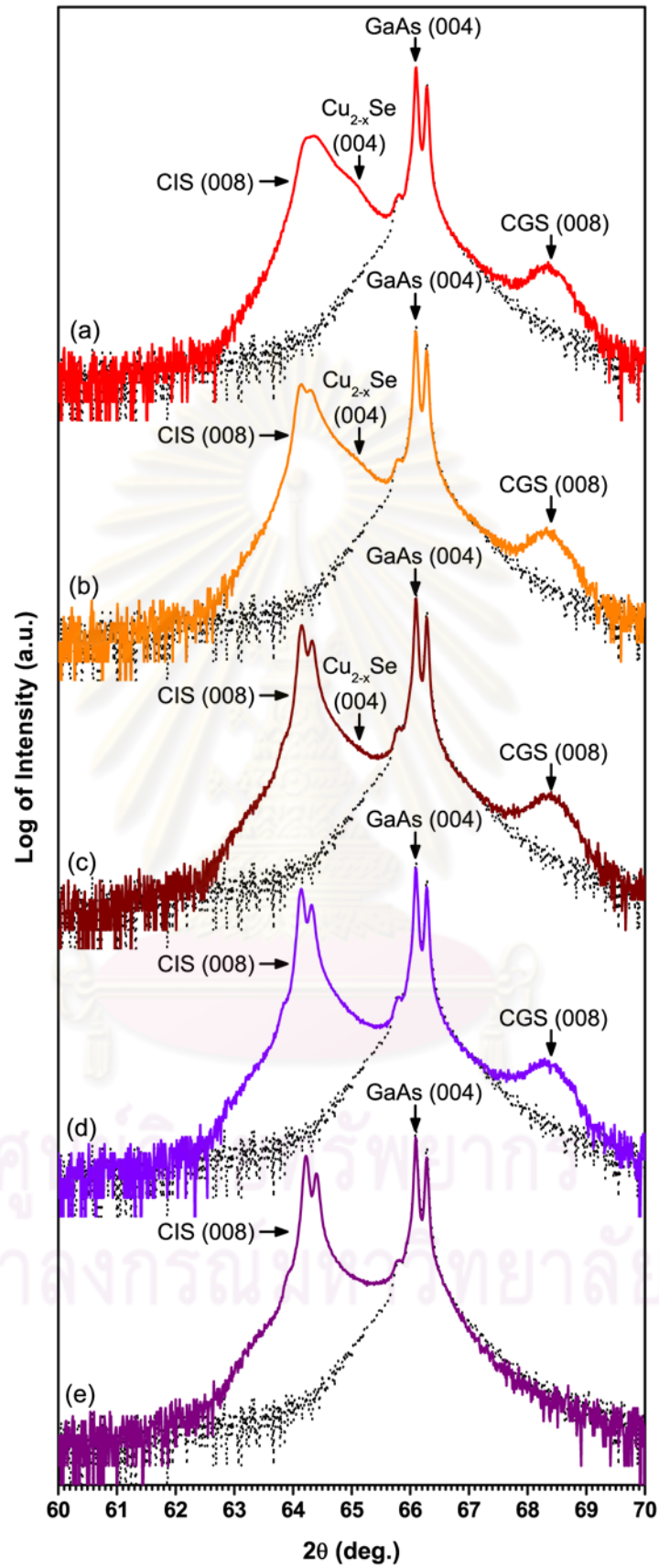
Figure 4.33: XRD spectra of two-stage CIS epitaxial films of the composition: (a) y ~ 1.6, (b) y ~ 1.6 → 1.3, (c) y ~ 1.6 → 1.1, (d) y ~ 1.6 → 1.0 and (e) y ~ 1.6 → 0.9.
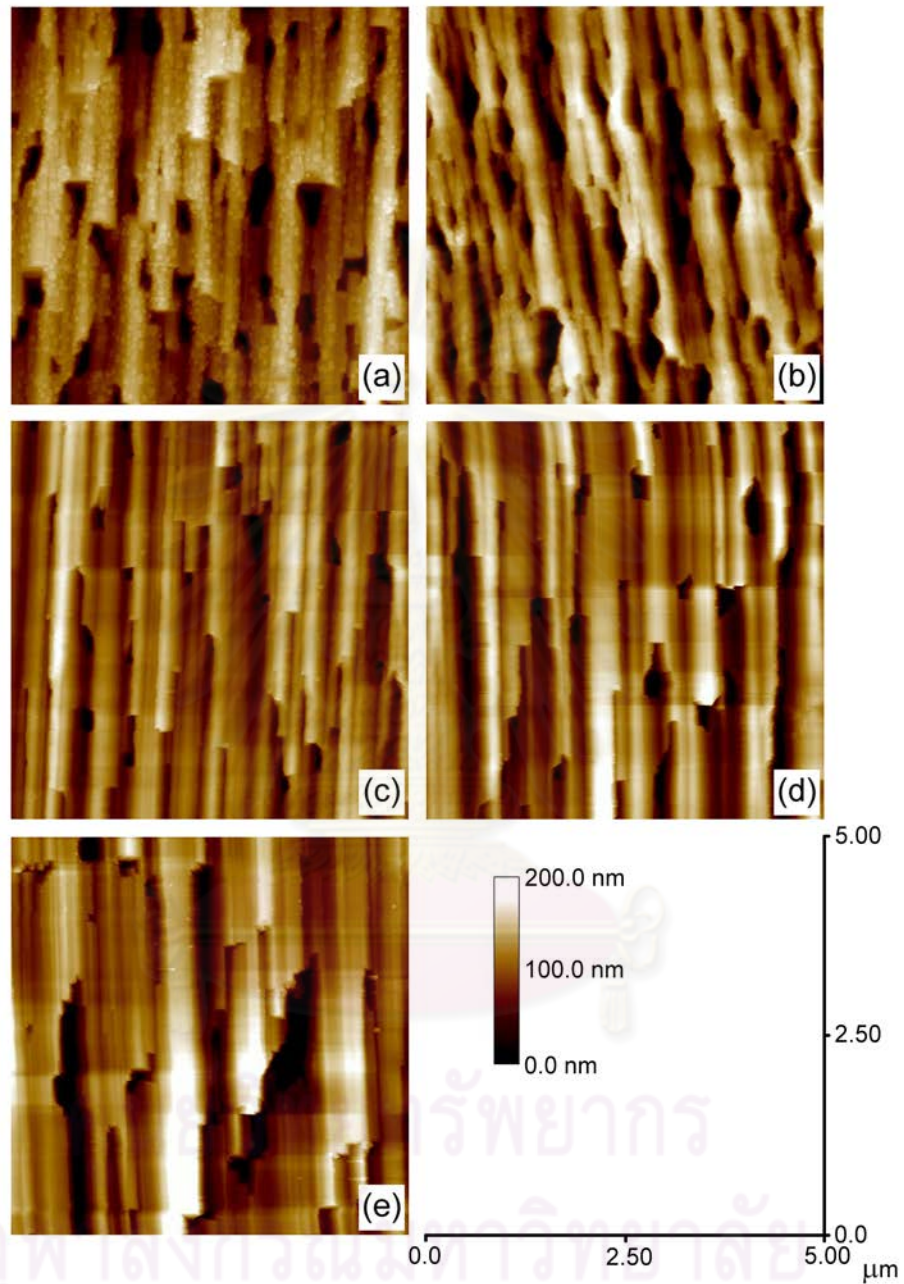
Figure 4.34: AFM images (5μm x 5μm) of two-stage CIS epitaxial films of the composition: (a) y ~ 1.6, (b) y ~ 1.6 → 1.3, (c) y ~ 1.6 → 1.1, (d) y ~ 1.6 → 1.0 and (e) y ~ 1.6 → 0.9.
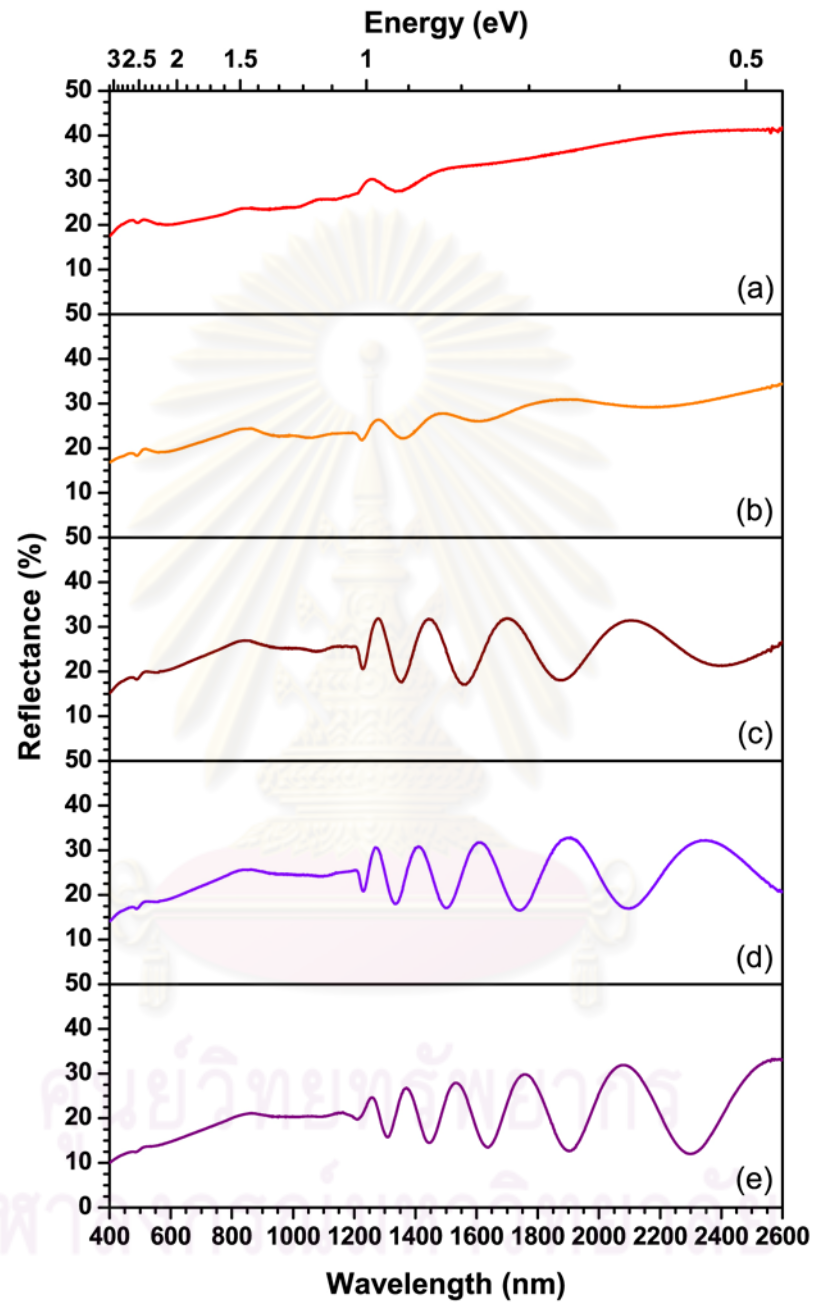
Figure 4.35: Optical reflectance spectra of two-stage CIS epitaxial films of the composition: (a) y ~ 1.6, (b) y ~ 1.6 → 1.3, (c) y ~ 1.6 → 1.1, (d) y ~ 1.6 → 1.0 and (e) y ~ 1.6 → 0.9.

The evolution of the intrinsic properties is observed by the PL measurement whose spectra are shown in Fig. 4.36. It can be summarized briefly that the excess $Cu_{2-x}Se$ in the Cu-rich CIS epitaxial films can support the perfect crystal which can be accounted by exciton detection. When the composition of the films becomes the Cu-poor, it demonstrates many defects that are regularly found in the Cu-poor films [17].
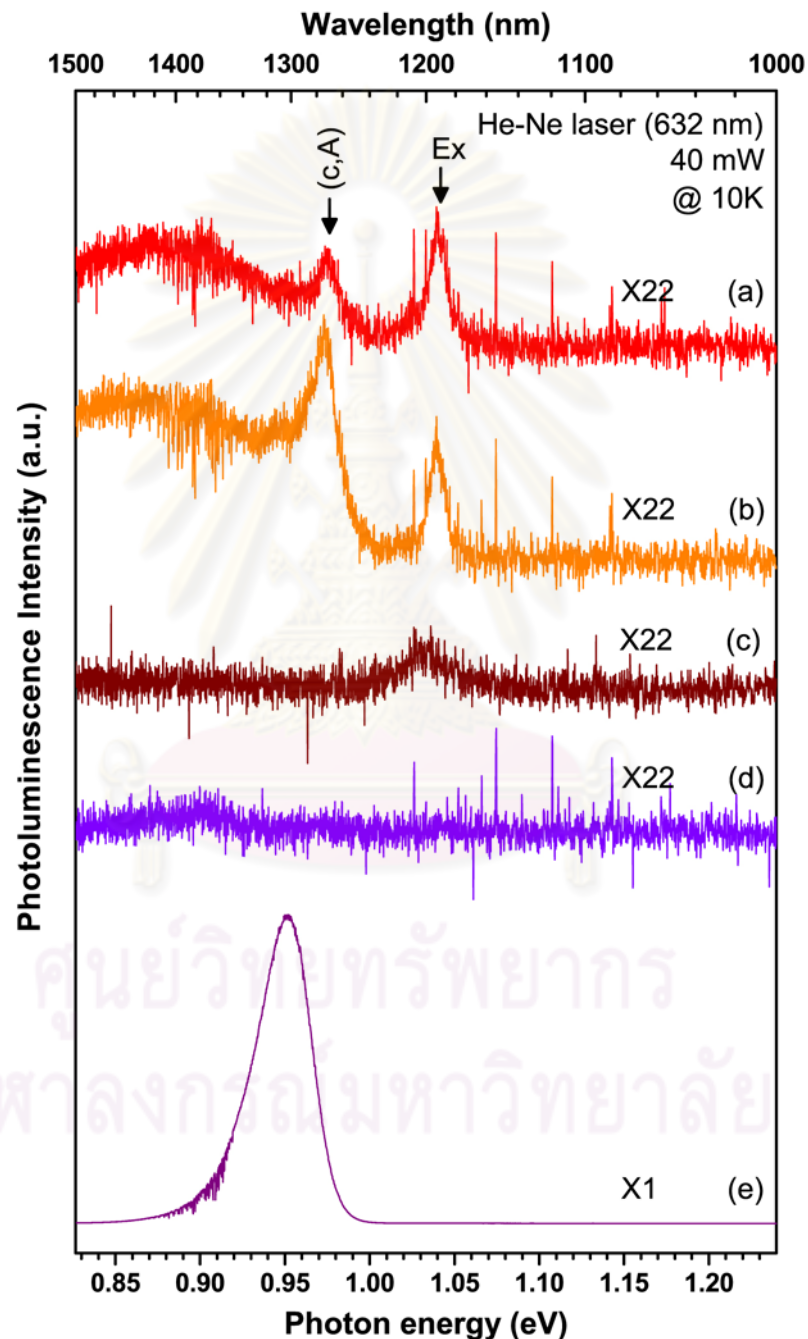
Figure 4.36: Photoluminescence spectra of two-stage CIS epitaxial films of the composition: (a) y ~ 1.6, (b) y ~ 1.6 → 1.3, (c) y ~ 1.6 → 1.1, (d) y ~ 1.6 → 1.0 and (e) y ~ 1.6 → 0.9 at 10 K.

4.3 Results and Discussion of the CuInSe₂ Epitaxial Films Grown by Modified Two-stage Growth Process

The modified 2-stage growth process technique is applied in the growth of CuInSe$_2$ epitaxial films on GaAs (001) substrate. The substrate temperature is also kept at 600°C during the deposition time that is the same as other growth processes. The composition of the growing films in the first stage of deposition is set at $y_1 \sim 1.6$ for 30 minutes (t_1). After that, the temperature of the In-source is ramped up in the second stage of deposition using the ramping rate $\upsilon = 0.0001$ s^{-1} to obtain $y \sim 1$ at the end of the deposition process. The ramping rate of this deposition process is calculated from Eq. 3.15 by setting the total deposition time T = 3 hours. The pyrometer signal of the modified two-stage growth process is shown in Fig. 4.37. The characteristic of signal is similar to the single-stage of the near stoichiometric films except the amplitude of the interference fringes related to the quality of the front and the back surface of the growing films is higher. The decrease of the signal in the first period is due to the radiation of the Cu-rich films. When the rate of the In-source is increased, the composition of the growing film evolves from the Cu-rich to near stoichiometric films resulting in the change of the emissivity of the film. By this reason, the tendency of increasing pyrometer signal in the next period is observed. During the deposition process, the epitaxial films are observed by RHEED which exhibits the streaky patterns at the end of the deposition process. This indicates that the films obtained by this growth process are relatively flat due to the lateral growth at high deposition temperature.
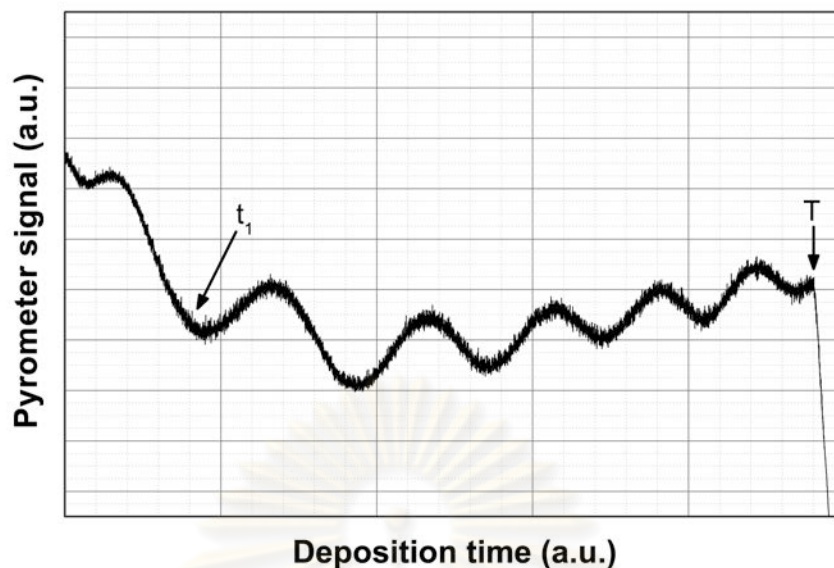
Figure 4.37: Pyrometer signal of modified two-stage CIS epitaxial films.

The XRD spectrum of the modified two-stage near stoichiometric CIS epitaxial films in Fig. 4.38(d) shows the well-resolved peak of CIS (008) at 2θ around 64.28° which indicates the good crystallographic structure. The characteristic of this XRD spectrum is similar to the XRD spectrum of the two-stage Cu-poor CIS epitaxial film as shown in Fig. 4.38(c) unlike the XRD spectrum of the single-stage near stoichiometric film in Fig. 4.38(a) or the two-stage near stoichiometric film in Fig. 4.38(b). It can also be mentioned that the formation of CGS interface layer in this growth technique is not observed even though it is evolved from the Cu-rich condition. The AFM image in Fig. 4.39 exhibits the homogeneous surface and undulations originated from the Cu-rich surface. In addition, many big and deep holes that are observed in the normal two-stage films can be reduced significantly. It is worth to note here that the optical reflectance shows much larger amplitude of interference fringes when compared to the previously mentioned growth process. Figure 4.40 presents the comparison of the optical reflectance spectra of the single-stage near stoichiometric films (green line), the two-stage near stoichiometric films (violet line) and the modified two-stage near stoichiometric films (pink line). This high oscillation agrees with the result of the pyrometer signal and that can be referred to the good surface morphology. The larger amplitude in the reflectance spectra below the gap also infers less defect states in the gap of the CIS. When investigating the

optical reflectance results carefully, there is a difference at the end of the oscillations which may also be associated with the shift of CIS (008) peak in the XRD results. The oscillations of the single-stage and the normal two-stage films stop at the energy around 1.04 eV while the oscillations of modified two-stage film stop at the energy around 1.07 eV. The optical reflectance result of the modified two-stage film cannot be used to identify preliminary that the grown film as CIS but rather the CIGS compound with minute amount of Ga atoms. Furthermore, the small oscillation which is the secondary oscillation connecting to the big oscillation which is the primary oscillation are observed. With the observation of diffusion of Ga atoms into the CIS layer shown in the EDS spectra of the previous section, it is speculated that the Ga is the main cause perturbing the crystallographic structure of the grown films that results in the optical reflectance and the shift of CIS (008) peak. Although the films that are grown by the modified two-stage growth process give the good crystallographic quality films and better surface morphology, there are many defect complexes in the films that exhibit in the PL measurement shown in Fig. 4.41(c). These defect complexes could be arisen from the distortion of crystallographic structure indicated by the great shift of the CIS (008) peak. The results of PL measurements in Fig. 4.41 suggest the fact that the crystallographic structure of both the near stoichiometric and the Cu-poor CIS epitaxial films are full of defects. From these results, it can be concluded that the evolution of both two-stage films are different in detail of growth mechanism after In and the excess $Cu_{2-x}Se$ incorporation although it evolves from the Cu-rich condition in the first stage of the deposition process which plays the important role to obtain the near perfect crystal and undulation pattern.
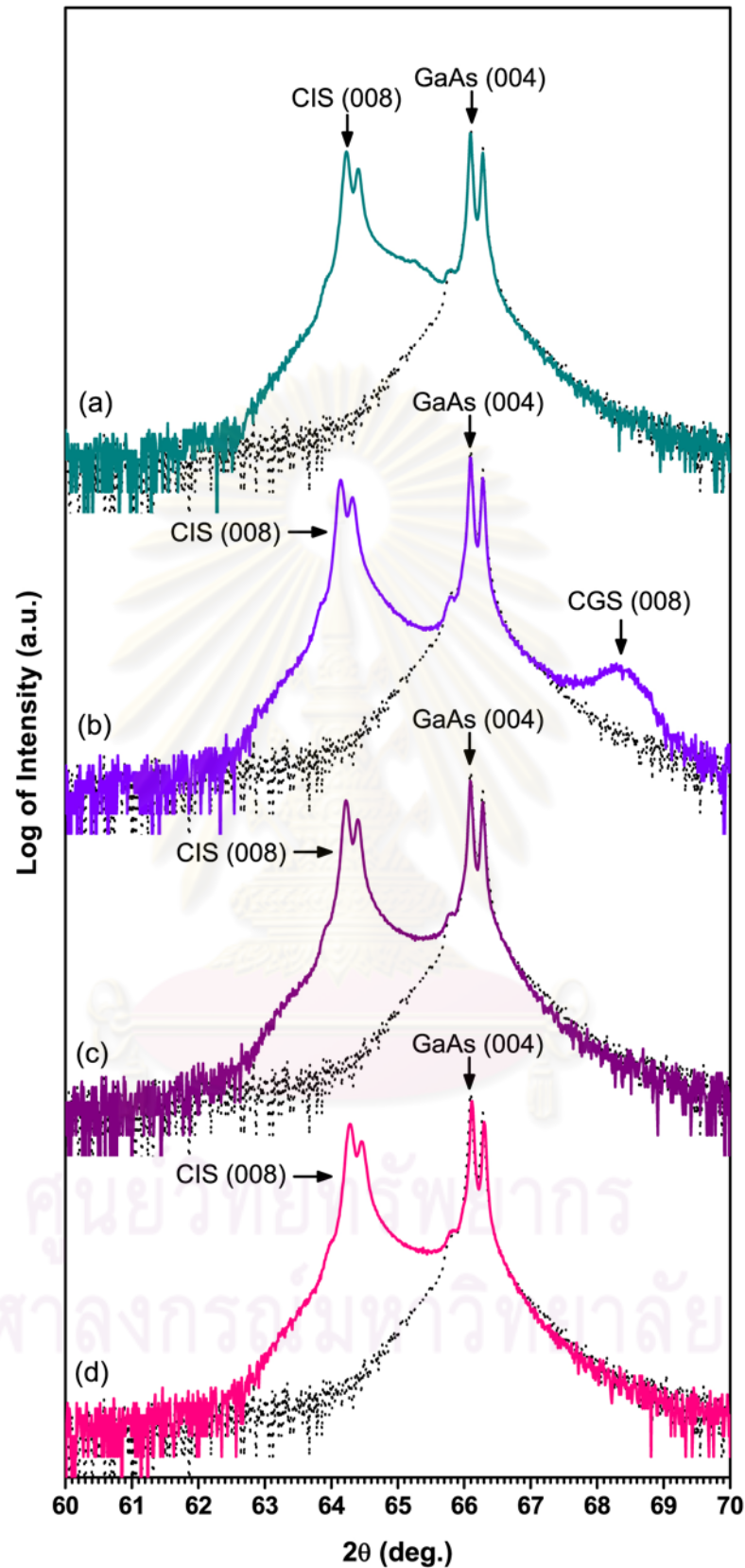
Figure 4.38: XRD spectra of CIS epitaxial films of (a) single-stage near stoichiometric, (b) two-stage near stoichiometric, (c) two-stage Cu-poor (y ~ 0.9) and (d) modified two-stage near stoichiometric, compared with GaAs substrate.
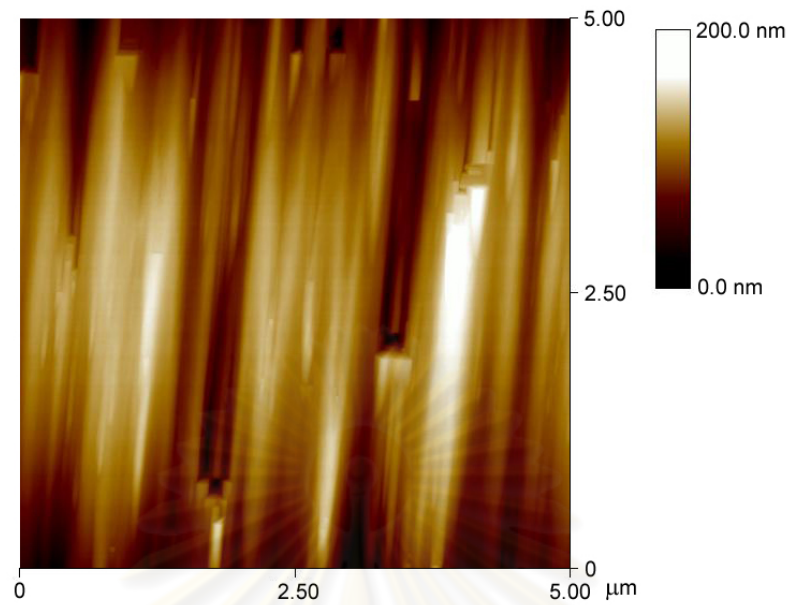
Figure 4.39: AFM image of modified two-stage near stoichiometric CIS epitaxial films.
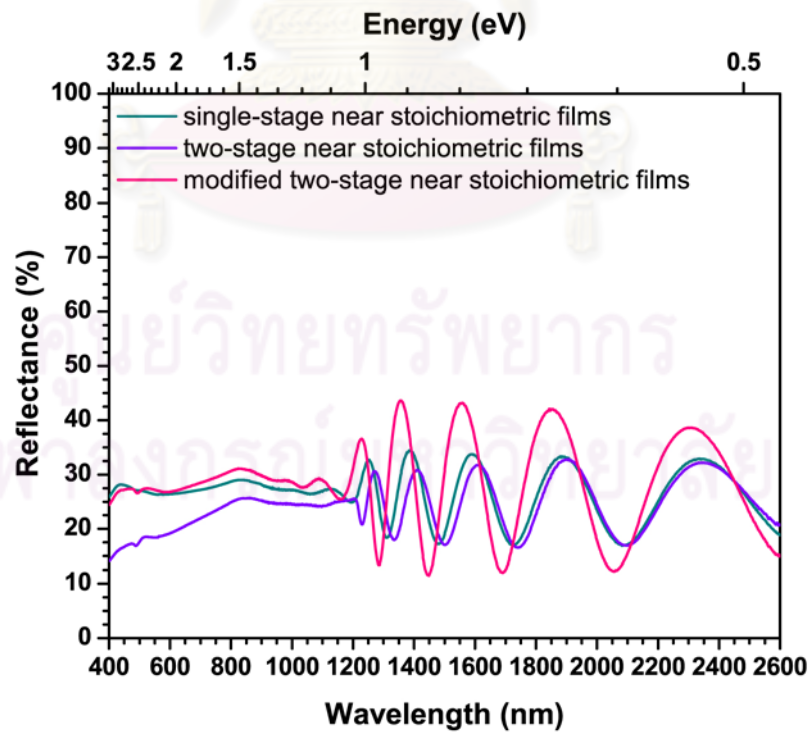
Figure 4.40: Optical reflectance spectra of modified two-stage near stoichiometric epitaxial films compared with single-stage films and normal two-stage films.
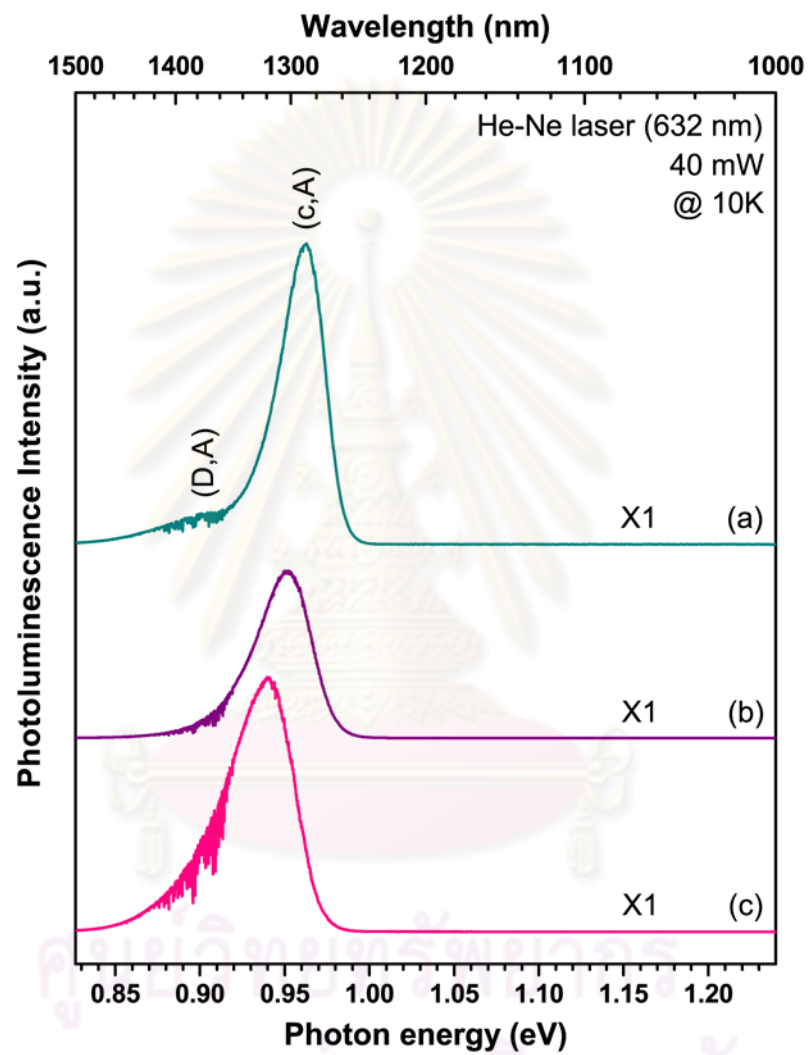
Figure 4.41: Photoluminescence spectra of (a) single-stage CIS epitaxial films, (b) two-stage CIS epitaxial films and (c) modified two-stage CIS epitaxial films at 10 K.

4.4 The Summary of the Growth Processes

All the MBE growth processes previously described can be used to grow the CIS epitaxial films which can be confirmed by the *in-situ* monitoring RHEED patterns. Table 4.2 summarizes the details of crystallographic structure of the epitaxial CIS films grown by the different growth processes. It can be concluded that the crystallographic structure is very sensitive to the method of growth process. The growth process that gives the lowest distortion of the crystallographic structure is the single-stage Cu-rich and etched with KCN aqueous solution. By this method, the near perfect crystal of CIS epitaxial films can be obtained which is accounted by the exciton detection. For the two-stage growth process, the distortion of crystallographic structure is stronger when the composition of the films converts to the near stoichiometric film and even more for the Cu-poor film. However, all the films show the well-resolved XRD spectral lines between Cu-$K_{\alpha1}$ and Cu-$K_{\alpha2}$ indicating the high quality of crystallographic structure of epitaxial films. The modified two-stage growth process can improve the surface morphology of the film but the mechanism of this growth takes the most distortion in the crystallographic structure that can generate defect complexes in the film.

Table 4.2: The position of XRD spectrum and c-axis of CIS (008) in various samples.

CIS Sample	2θ	c-axis (Å)
bulk	64.08°	11.615
single-stage near stoichiometric epitaxial films	64.23°	11.590
single-stage KCN-etched Cu-rich epitaxial films	64.12°	11.609
two-stage near stoichiometric epitaxial films	64.16°	11.602
two-stage Cu-poor (y~0.9) epitaxial films	64.24°	11.589
modified two-stage near stoichiometric epitaxial films	64.28°	11.583

Chapter V

Conclusions and Suggestions

In this dissertation, the growth of CuInSe$_2$ (CIS) epitaxial thin films on GaAs (001) substrates using molecular beam epitaxy technique has been successfully achieved without using pseudosubstrates or buffer layers. Reflection high energy electron diffraction (RHEED) apparatus and *in-situ* monitoring systems, e.g. the pyrometer signal and the output power of the temperature controller, applied during the deposition process are the powerful tools for obtaining high quality CIS films with reproducibility. The RHEED patterns exhibit the streaky patterns in both the Cu-rich films and the near stoichiometric films. As long as the structure belongs to the chalcopyrite phase, the streaky patterns can be observed which can be accounted as a high quality structure. Unlike the Cu-poor films, the structure of the films demonstrates as the sphalerite phase or ordered defect compound which exhibits lower quality structure resulting in the spotty RHEED patterns. The key parameters and the growth conditions which play the important roles in the growth mechanism for obtaining the high quality epitaxial CIS films are the phase of the excess Cu-Se compounds and the substrate temperature growing under the Cu-rich conditions. In this work, the phase of Cu-Se compounds should be Cu$_{2-x}$Se and substrate temperature should be more than 500°C. The CIS epitaxial films that are fabricated using these parameters and growth conditions can give a good crystallographic structure such that the excitonic emission can be observed. The growth model of the Cu-rich CIS films can be drawn. The films that are grown from the different deposition techniques and compositions give the difference in the physical properties due to the mechanisms of the growth that can be summarized as followed:

o The surface morphology of the near stoichiometric films that are grown by the single-stage process shows the rectangular shape due to the side plane of crystallographic structure of CIS in (001) plane and step-like structures. The crystallographic structure demonstrates the high quality single crystal with well-resolved XRD spectral lines. The optical reflectance shows the oscillations in the range of energy below the band gap due to the interference

between the front and the back surface of the grown films. The XRD spectra of the single-stage near stoichiometric films before and after etching with the KCN solution are similar. The physical structure observed by SEM measurement shows the dense CIS epitaxial films suggesting that the high quality single crystal epilayers are obtained but the intrinsic property of the films explored by the PL measurement reveals the presence of a large number of defects especially the acceptor-type defects including a few donor-type defects.

o The single-stage Cu-rich CIS epitaxial films show the difference in the physical properties before and after etching with the KCN solution. The as-grown films exhibit the broadened XRD spectra that are the combination of crystallographic phases of the CIS (008) structure and the $Cu_{2-x}Se$ (004) structure while the well-resolved peaks of CIS (008) indicating the high quality single crystal is the dominant structure after the KCN etching process. The surface morphology before etching process exhibits many rectangular shaped protrusions along with the undulations. The protrusions are the excess $Cu_{2-x}Se$ compounds which can reside both on the top surface that act as the metallic-like epilayer and inside the CIS layer that leave the holes or voids after etching the CIS films with KCN solution. After the etching process, the metallic reflection disappears and the full oscillations in the reflectance spectra are recovered. Although the physical structure of cross-section SEM image shows many deep holes of the excess $Cu_{2-x}Se$ like grain boundary but the existence of the excess $Cu_{2-x}Se$ helps to form the high quality crystallinity resulting in the exciton detection which can be used to determine the band gap energy of the CIS epitaxial films, i.e. $E_g = 1.045$ eV (at 10 K). The peculiar spectrum in the XRD result is due to the presence of the $CuGaSe_2$ (CGS) at the interface of the CIS films and the GaAs substrate. This interface layer is occurred by the incorporation of the excess $Cu_{2-x}Se$ with the diffusiving Ga atoms from the GaAs surface. The substrate temperature is the most important key for the quality of the films due to the function of the excess $Cu_{2-x}Se$.

o The two-stage films show streaky RHEED patterns which are considered to have the high quality film surface. The composition of the films starts with the Cu-rich condition to ensure high quality precursor which is confirmed by the exciton detection. The mechanism of the growth evolves from the Cu-rich

composition passing through the slightly Cu-rich, near stoichiometric and then Cu-poor composition, respectively. This evolution is possible by the incorporation of In atoms with the excess $Cu_{2-x}Se$. The well-resolved spectrum of the CIS (008) and the decrease of $Cu_{2-x}Se$ (004) are the good evidence which support the incorporation of In. The change in the optical reflection from the metallic surface to the semiconducting compound is in a good agreement with the evolution of the composition of the films. The undulated surface is the specific pattern found in the Cu-rich films remains throughout the evolution of the films. The mechanism of In-incorporation and Cu-deficiency in the second stage of the growth is the main cause of the change of the intrinsic property. The number of defects, especially acceptor-type defects, is increasingly generated when the composition of the growing films converts to the Cu-poor condition. This mechanism is the important evidence for the fabrication of the photovoltaic devices. Normally, the physical properties of CIS or CIGS should be p-type semiconductor more than intrinsic semiconductor, so the composition of the grown films should be slightly Cu-poor condition rather than the Cu-rich or stoichiometric condition.

o The modified two-stage process that is proposed to improve the Cu deficiency in the normal two-stage process is performed. The high quality epitaxial structure is obtained and confirmed by the streaky RHEED patterns. The higher amplitude of the interference fringes in the optical reflectance spectra and the homogeneous surface morphology are the signs for the physical quality enhancement. The crystallographic structure of the near stoichiometric composition is different from the normal two-stage near stoichiometric films but similar to the normal two-stage Cu-poor films. The Ga diffusion from the substrate could be the cause in the shift of the CIS (008) structure rather than the effect of strain. Although this process can enhance the extrinsic quality of the films, the intrinsic property of the films is somewhat the opposite, i.e. many defect complexes are induced inside the grown films.

As a result of findings in this research, I would suggest and recommend further investigations:

1. For a better understanding in the shift of the CIS (008) peak and the disappearance of $CuGaSe_2$ interface layer as well as the evolution of the composition of the two-stage films in both normal process and modified process, the effect of Ga diffusion from the substrate and the composition verification should be characterized by electron probe micro-analysis (EPMA) or secondary ion mass spectrometry (SIMS).

2. For an understanding of the strain effect in the epitaxial films, the high resolution X-ray diffractometer in reciprocal space mapping technique should be examined to analyze this problem.

References

[1] Shah, A. Y., Torres, P., Tscharner, R., Wyrsch, N., and Keppner, H. Photovoltaic Technology: The Case for Thin Film Solar Cells. Science 285 (1999): 692-698.

[2] Repins, I., et al. 19·9%-efficient ZnO/CdS/CuInGaSe$_2$ solar cell with 81·2% fill factor. Prog. Photovoltaics 16 (2008): 235-239.

[3] Luque, A., and Hegedus, S. Handbook of Photovoltaic Science and Engineering. West Sussex, England: John Wiley & Sons Inc. 2005.

[4] Chen, W. S., and Mickelsen, R. A. High Photocurrent polycrystalline thin film CdS/CuInSe$_2$ solar cell. Appl. Phys. Lett. 36(5) (1980): 371-373.

[5] Baldus, A., and Benz, K. W. Melt and metallic solution crystal growth of CuInSe$_2$. J. Cryst. Growth 130 (1993): 37-44.

[6] Shioda, R., Okada, Y., Oyanagi, H., Niki, S., Yamada, A., and Makita, Y. Characterization of molecular beam epitaxy grown CuInSe$_2$ on GaAs(001). J. Cryst. Growth 150 (1995): 1196-1200.

[7] Niki, S., et al. Molecular beam epitaxial growth and characterization of CuInSe$_2$ and CuGaSe$_2$ for device applications. J. Cryst. Growth 237–239 (2002): 1993-1999.

[8] Igarashi, O. Epitaxial growth of CuInSe$_2$ single crystal by halogen transport method. J. Cryst. Growth 130 (1993): 343-356.

[9] Yang, L. -Chung, Mao, H. Z., Rockett, A., Shafarman, W. N., and Birkmire, R. W. The growth by the hybrid sputtering and evaporation method and micro-structural studies of CuInSe$_2$ films. Sol. Energy Mater. Sol. Cells 36 (1995): 445-455.

[10] Rega, N., Siebentritt, S., Beckers, I., Beckmann, J., Albert, J., and Lux-Steiner, M. MOVPE of epitaxial CuInSe$_2$ on GaAs. J. Cryst. Growth 248 (2003): 169-174.

[11] Akl, A. A., and Afify, H. H. Growth, microstructure, optical and electrical properties of sprayed CuInSe$_2$ polycrystalline films. Mater. Res. Bull. 43 (2008): 1539-1548.

[12] Abou-Elfotouh, F., Dunlavy, D. J., and Coutts, T. J. Intrinsic defect states in CuInSe$_2$ single crystals. Solar Cells 27 (1986): 237-246.

[13] Jaffe, J. E., and Zunger, A. Theory of the Band-Gap Anomaly in ABC$_2$ Chalcopyrite Semiconductors. Phys. Rev. B 29 (1984): 1882-1906.

[14] Schumann, B., Tempel, A., and Kühn, G. Epitaxial Layers of CuInSe$_2$. Solar Cells 16 (1986): 43-63.

[15] Niki, S., et al. Photoluminescence properties of CuInSe$_2$ grown by molecular beam epitaxy. Sol. Energy Mater. Sol. Cells 35 (1994): 141-147.

[16] Niki, S., et al. Sharp Optical Emission from CuInSe$_2$ Thin Films Grown by Molecular Beam Epitaxy. Jpn. J. Appl. Phys. 33 (1994): L500-L502.

[17] Niki, S., et al. Heteroepitaxy and characterization of CuInSe$_2$ on GaAs(001). J. Cryst. Growth 150 (1995): 1201-1205.

[18] Niki, S., et al. Excitonic emissions from CuInSe$_2$ on GaAs(001) grown by molecular beam epitaxy. Appl. Phys. Lett. 67(9) (1995): 1289-1291.

[19] Niki, S., et al. High quality CuInSe$_2$ films grown on pseudo-lattice-matched substrates by molecular beam epitaxy. Appl. Phys. Lett. 69(5) (1996): 647-649.

[20] Chichibu, S. Room-temperature near-band-edge photoluminescence from CuInSe$_2$ heteroepitaxial layers grown by metalorganic vapor phase epitaxy. Appl. Phys. Lett. 70(14) (1997): 1840-1842.

[21] Chichibu, S., Shioda, T., Irie, T., and Nakanishi, H. Improved optical properties of CuInSe$_2$ thin films prepared by alternate-feeding physical vapor deposition. J. Appl. Phys. 81(1) (1998): 522-525.

[22] Fons, P., Niki, S., Yamada, A., and Oyanagi, H. Direct observation of the Cu$_{2-x}$Se phase of Cu-rich epitaxial CuInSe$_2$ grown on GaAs (001). J. Appl. Phys. 84(12) (1998): 6926-6928.

[23] Niki, S., et al. Effects of the surface Cu$_{2-x}$Se phase on the growth and properties of CuInSe$_2$ films. Appl. Phys. Lett. 74(11) (1999): 1630-1632.

[24] Stanbery, B. J., and et al. Epitaxial growth and characterization of CuInSe$_2$ crystallographic polytypes. J. Appl. Phys. 91(6) (2002): 3598-3604.

[25] Rega, N., Siebentritt, S., Beckers, I. E., Beckmann, J., Albert, J., and Lux-Steiner, M. Defect spectra in epitaxial CuInSe$_2$ grown by MOVPE. Thin Solid Films 431-432 (2003): 186-189.

[26] Yoon, S., et al. Effect of a Cu–Se secondary phase on the epitaxial growth of CuInSe$_2$ on (100) GaAs. J. Cryst. Growth 281 (2005): 209-219.

[27] Yang, L. -C. Sputtered epitaxial chalcopyrite CuInSe$_2$ films grown on GaAs substrates. J. Cryst. Growth 294 (2006): 202-208.

[28] Jaffe, J. E., and Zunger, A. Electronic structure of the ternary chalcopyrite semiconductors CuAlS$_2$, CuGaS$_2$, CuInS$_2$, CuAlSe$_2$, CuGaSe$_2$ and CuInSe$_2$. Phys. Rev. B 28(10) (1983): 5822-5847.

[29] Jaffe, J. E., and Zunger, A. Anion displacements and the band-gap anomaly in ternary ABC$_2$ chalcopyrite semiconductors. Phys. Rev. B 27(8) (1983): 5176-5179.

[30] Chang, C. H., Davydov, A., Stanbery, B. J., and Anderson, T. J. Thermodynamic Assessment of the Cu-In-Se System and Application to Thin Film Photovoltaics. Proc. 25th PVSC. (1996): 849-852.

[31] Fearheiley, M. L.. The Phase Relations in The Cu,In,Se System and The Growth of CuInSe$_2$ Single Crystals. Solar Cells 16 (1986): 91-100.

[32] Rockett, A., et al. Structure and chemistry of CuInSe$_2$ for solar cell technology: current understanding and recommendations. <u>Thin Solid Films</u> 237 (1994): 1-11.

[33] Klenk, R., Walter, T., Schock, H. W., and Cahen, D. A model for the successful growth of polycrystalline films of CuInSe2 by multisource physical vacuum evaporation. <u>Adv. Mater.</u> 5 (1993): 114-119.

[34] Rincón, C., Bellabara, C., González, J., and Sánchez Pérez, G. Optical Properties and Characterizations of CuInSe$_2$. <u>Solar Cells</u> 16 (1986): 335-349.

[35] Danilkin, S. A., Skomorokhov, A. N., Hoser, A., Fuess, H., Rajevac, V., and Bickulova, N. N. Crystal structure and lattice dynamics of superionic copper selenide Cu$_{2-\delta}$Se. <u>J. Alloys Comp.</u> 361 (2003): 57-61.

[36] Milat, O., Vučić, Z., and Ruščić, B. Superstructural ordering in low-temperature phase of superionic Cu$_2$Se. <u>Solid State Ionics</u> 23 (1987): 37-47.

[37] Oliveira, M., McMullan, R. K., and Wuensch, B. J. Single crystal neutron diffraction analysis of the cation distribution in the high-temperature phases α-Cu$_{2-x}$S, α-Cu$_{2-x}$Se and α-Ag$_2$Se. <u>Solid State Ionics</u> 28–30 (1988): 1332-1337.

[38] Yamamoto, K., and Kashida, S. X-ray study of the average structures of Cu$_2$Se and Cu$_{1.8}$S in the room temperature and the high temperature phases. <u>J. Solid State Chem.</u> 93 (1991): 202-211.

[39] Machado, K. D., et al. Structural study of Cu$_{2-x}$Se alloys produced by mechanical alloying. <u>Acta Cryst. B</u> 60 (2004): 282-286.

[40] Dimmler, B., and Schock, H. W. Scalability and Pilot Operation in Solar Cells of CuInSe$_2$ and their Alloys. <u>Prog. Photovolt. Res. Appl.</u> 6 (1998): 193-199.

[41] Bernardini, G. P., and Catani, A. The Cu-Se System. <u>Mineral. Deposita (Berl.)</u> 3 (1968): 375-380.

[42] Cho, A. Y. Film Deposition Techniques. J. Vac. Sci. Technol. 8 (1970): S31-S38.

[43] Cho, A. Y. GaAs Epitaxy by a Molecular Beam Method: Observation of Surface Structure on (001) Face. J. App. Phys. 42(5) (1971): 2074-2081.

[44] Vassent, J. L., Marty, A., Gilles, B., and Chatillon, C. Angular Distribution of Molecular Beams and Homogeneous Layer Growth: Optimization of Geometrical Parameters in Molecular Beam Epitaxy. Vacuum. 64 (2002): 65-85.

[45] Arnau, A. Piezoelectric Transducers and Applications. Valencia, Spain: 2nd edition Springer. 2008.

[46] Vossen, J. L., and Kern, W. Thin Film Processes. San Diago, U.S.A: Academic Press. 1978.

[47] Nishitani, M., Negami, T., and Wada, T. Composition Monitoring Method in $CuInSe_2$ Thin Film Preparation. Thin Solid Films 258 (1995): 313-316.

[48] Panita Chinvetkitvanich. Molecular Beam Deposition and Characterization of Wide-Band-Gap $Cu(In,Ga)Se_2$ for Thin Film Solar Cells. Doctoral dissertation, Department of Physics Faculty of Science Chulalongkorn University, 2006.

[49] Goldstein, J., et al. Scanning Electron Microscopy and X-Ray Microanalysis. 3rd Edition. New York, U.S.A.: Springer, 2003.

[50] Niki, S., et al. Effects of strain on the growth and properties of $CuInSe_2$ epitaxial films. J. Cryst. Growth 175/176 (1997): 1051-1056.

[51] Yu, P. W. Radiative recombination in melt-grown and Cd-implanted $CuInSe_2$. J. Appl. Phys. 47(2) (1976): 677-684.

[52] Joint Committee on Powder Diffraction Standards (JCPDS), 40-1487.

[53] Joint Committee on Powder Diffraction Standards (JCPDS), 6-680.

[54] Hashimoto, Y., Kohara, N., Negami, T., Nishitani, M., and Wada, T. Surface Characterization of Chemically Treated Cu(In,Ga)Se$_2$ Thin Films. Jpn. J. Appl. Phys. Part 1 35 (1996): 4760-4764.

[55] Joint Committee on Powder Diffraction Standards (JCPDS), 35-1100.

[56] S. Niki, et al. Anion vacancies in CuInSe$_2$. Thin Solid Films 387 (2001): 129-134.

[57] Zhang, S. B., Wei, Su-Huai, and Zunger, A. Stabilization of Ternary Compounds via Ordered Arrays of Defect Pairs. Phys. Rev. Lett. 78(21) (1997): 4059-4062.

[58] Guillemoles, J. -F., Rau, U., Kronik, L., Schock, H. -W., and Cahen, D. Cu(In,Ga)Se$_2$ Solar Cells: Device Stability Based on Chemical Flexibility. Adv. Mater. 11 (1999): 957-961.

[59] Chatraphorn, S., et al. Photoluminescence of a High Quality CuInSe$_2$ Single Crystal. Jpn. J. Appl. Phys. 37 (1998): L269-L271.

[60] Arthibenyakul, B., Chityuttakan, C., and Chatraphorn, S. The Presence of CuGaSe$_2$ Interface Layer in the Growth of Cu-rich CuInSe$_2$/GaAs(001) Epitaxial Films. J. Cryst. Growth 316 (2011): 97-100.

[61] Schroeder, D. J., Berry, G. D., and Rockett, A. A. Gallium diffusion and diffusivity in CuInSe$_2$ epitaxial layers. Appl. Phys. Lett. 69(26) (1996): 4068-4070.

APPENDICES

APPENDIX A

List of Symbols and Abbreviations

Symbols

a	Lattice parameter
a.u.	Arbitrary unit
c	Lattice parameter
Cu_i	Copper interstitial: Cu-interstitial
Cu_{In}	Copper substitution to Indium site
Cu_{Se}	Copper substitution to Selenium site
E_a	Activation energy
E_g	Energy band gap
E_x	Near-band-edge exciton, exciton energy
eV	Energy unit: electron volt
h	Miller index
$h\upsilon$	Photon energy
In_{Cu}	Indium substitution to Copper site
In_i	Indium interstitial: In-interstitial
In_{Se}	Indium substitution to Selenium site
k	Miller index
K	Temperature unit: Kelvin
k_B	Boltzmann constant
l	Miller index
M	Mass per mole
n	Refractive index
N_A	Avogadro's number
Se_{Cu}	Selenium substitution to Copper site
Se_i	Selenium interstitial: Se-interstitial
Se_{In}	Selenium substitution to Indium site
Torr	Pressure unit
T_{pyro}	Temperature of Pyrometer

u	Displacement parameter
V_{Cu}	Copper vacancy: Cu-vacancy
V_{In}	Indium vacancy: In-vacancy
V_{Se}	Selenium vacancy: Se-vacancy
W	Power unit: watt
y	Films composition: [Cu]/[In]
y > 1	Cu-rich
y ~ 1	Near stoichiometric
y < 1	Cu-poor, In-rich
α	Molar density: $\rho*M^{-1}$
ε	Emissivity of the grey body
η	Distortion parameter
θ	Bragg angle
κ	Mean free path of the particle
λ	Wavelength
ρ	Density
σ	Stefan–Boltzmann constant
υ	Ramping rate
φ	Collision diameter of the molecule
Δm	Molecularity deviation
ΔS	Stoichiometry deviation
(c,A)	Conduction band to acceptor transition
(D,A)	Donor to acceptor transition
(D,v)	Donor to valence band transition
[ ]	The number of atom: N
Å	Angstrom: $(10^{-10}$ m)
°C	Temperature unit: degree Celsius

Abbreviations

1-stage	Single stage
2-stage	Two stage
AFM	Atomic force microscopy
AF-PVD	Alternate-feeding physical vapor deposition
BEI	Back scatter image
CGS	Copper gallium diselenide: $CuGaSe_2$
CH	Chalcopyrite
CIS	Copper indium diselenide: $CuInSe_2$
CIGS	Copper indium gallium diselenide: $Cu(In_{1-x}Ga_x)Se_2$
Cu	Copper element
DI	De-ionized
EDS	Energy dispersive X-ray spectroscopy
EPD	End point detection
EPMA	Electron probe micro-analysis
FWHM	Full width at half maximum
GaAs	Gallium arsenide
H_2O	Water
H_2O_2	Hydrogen peroxide
H_2SO_4	Sulfuric acid
HAADF	High angle annular dark field
In	Indium element
JCPDS	Joint Council for Powder Diffraction Studies
K-cell	Knudsen effusion cell
KCN	Potassium cyanide
LPE	Liquid phase epitaxy
MBD	Molecular beam deposition
MBE	Molecular beam epotaxy
MEE	Migration-enhanced epitaxy
Mo	Molybdenum
MOVPE	Metalorganic vapor phase epitaxy
NIR	Near infra-red

ODC	Ordered defect compound
OP	Output power
QCM	Quartz crystal thickness monitor
P	Pressure
PBN	Pyrolytic boron nitride
PID	Proportion-integral-deviation
PL	Photoluminescence
PV	Photovoltaic
PZT	Piezoelectric transducer
RHEED	Reflection high energy electron diffraction
Se	Selenium element
SEM	Scanning electron microscopy
T	Temperature
TCE	Trichloroethylene
TEM	Transmission electron microscopy
UHV	Ultra-high vacuum
UV	Ultra-violet
VIS	Visible
VPE	Vapor phase epitaxy
XRD	X-Ray diffraction
ZB	Zincblende

APPENDIX B

List of Publications

[1]   B. Arthibenyakul, C. Chityuttakan, P. Chinvetkitvanich, K. Yoodee, Somphong Chatraphorn and Sojiphong Chatraphorn, The growth of $CuInSe_2$ epitaxial thin films from a Cu-Se precursor. Thai Journal of Physics (SPC 2008) Series 3 (2008) : 1-4.

[2]   B. Arthibenyakul, C. Chityuttakan, K. Yoodee and S. Chatraphorn, Formation of $CuGaSe_2$ interfacing layer in the epitaxial growth of Cu-rich $CuInSe_2$ thin films. Thai Journal of Physics (SPC 2009) Series 4 (2009) : 16-19.

[3]   B. Arthibenyakul, C. Chityuttakan, K. Yoodee and S. Chatraphorn, Photoluminescence of 1-stage and 2-stage $CuInSe_2$ Epitaxial Films Grown by Molecular Beam Epitaxy. Thai Journal of Physics (SPC 2010) Series 5 (2010) : 361-364.

[4]   B. Arthibenyakul, C. Chityuttakan and S. Chatraphorn, The Presence of $CuGaSe_2$ Interface Layer in the Growth of Cu-rich $CuInSe_2$/GaAs(001) Epitaxial Films. J. Cryst. Growth 316 (2011) : 97-100.

ศูนย์วิทยทรัพยากร
จุฬาลงกรณ์มหาวิทยาลัย

Biography

Mr. Bancha Arthibenyakul was born on November 27th, 1980 in Bangkok, Thailand. He received the scholarship for study in science program from Development and Promotion of Science and Technology talents project (DPST) in 1996. He received the Bachelor degree of Science (Second Class Honors) in Physics from Chulalongkorn University, Bangkok Thailand in 2003.

Conference Presentations:

2005 31st Congress on Science and Technology of Thailand, Suranaree University of Technology, Nakhon Ratchasima, Thailand, 18 - 20 October 2005.

2006 32nd Congress on Science and Technology of Thailand, Queen Sirikit National Convention Center, Bangkok, Thailand, 10 - 12 October 2006.

2007 Siam Physics Congress 2007, Rose Garden Riverside Hotel, Nakhon Pathom, Thailand, 22 - 24 March 2007.

2008 Siam Physics Congress 2008, Mandarin Golden Valley Resort and Spa and Greenery Resort, Nakhon Ratchasima, Thailand, 20 - 22 March 2008.

   34th Congress on Science and Technology of Thailand, Queen Sirikit National Convention Center, Bangkok, Thailand, 31 October – 2 November 2008.

   4th Mathematic and Physical Science Graduate Congress, National University of Singapore, Singapore, 17 – 19 December 2008.

2009 Siam Physics Congress 2009, Methavalai Hotel Chaam, Petchburi, Thailand, 19 - 21 March 2009.

2010 Siam Physics Congress 2010, River Kwai Village Hotel, Kanchanaburi, Thailand, 25 - 27 March 2010.

   6th Mathematic and Physical Science Graduate Congress, University of Malaya, Malaysia, 13 – 15 December 2010.